Received: 26 February 2024 | Revised: 18 April 2024 | Accepted: 6 May 2024

DOI: 10.1002/ar.25505

RESEARCH ARTICLE

The Anatomical Record WILEY

A new semi-fossorial thescelosaurine dinosaur from the Cenomanian-age Mussentuchit Member of the Cedar Mountain Formation, Utah

Haviv M. Avrahami[1,2] | **Peter J. Makovicky**[3] | **Ryan T. Tucker**[4] | **Lindsay E. Zanno**[1,2]

[1]North Carolina State University, Raleigh, North Carolina, USA

[2]North Carolina Museum of Natural Sciences, Raleigh, North Carolina, USA

[3]Department of Earth and Environmental Sciences, University of Minnesota, Minneapolis, Minnesota, USA

[4]Department of Earth Sciences, Stellenbosch University, Stellenbosch, South Africa

Correspondence
Haviv M. Avrahami, North Carolina State University, Raleigh, North Carolina, USA.
Email: avrahamihm@gmail.com

Funding information
North Carolina Fossil Club; Canyonlands Natural History Association; Paleontological Society; Jurassic Foundation; National Science Foundation

Abstract

Thescelosaurines are a group of early diverging, ornithischian dinosaurs notable for their conservative bauplans and mosaic of primitive features. Although abundant within the latest Cretaceous ecosystems of North America, their record is poor to absent in earlier assemblages, leaving a large gap in our understanding of their evolution, origins, and ecological roles. Here we report a new small bodied thescelosaurine—*Fona herzogae* gen. et sp. nov.—from the Mussentuchit Member of the Cedar Mountain Formation, Utah, USA. *Fona herzogae* is represented by multiple individuals, representing one of the most comprehensive skeletal assemblages of a small bodied, early diverging ornithischian described from North America to date. Phylogenetic analysis recovers *Fona* as the earliest member of Thescelosaurinae, minimally containing *Oryctodromeus*, and all three species of *Thescelosaurus*, revealing the clade was well-established in North America by as early as the Cenomanian, and distinct from, yet continental cohabitants with, their sister clade, Orodrominae. To date, orodromines and thescelosaurines have not been found together within a single North American ecosystem, suggesting different habitat preferences or competitive exclusion. Osteological observations reveal extensive intraspecific variation across cranial and postcranial elements, and a number of anatomical similarities with *Oryctodromeus*, suggesting a shared semi-fossorial lifestyle.

KEYWORDS

Cretaceous, Dinosaur, Fossorial, Ornithischian, Thescelosaurine

1 | INTRODUCTION

Thescelosaurines were a group of small to medium-sized, plant-eating dinosaurs that inhabited North America during the Late Cretaceous (Norman, Sues, et al., 2004). Members of the clade are characterized by bipedal locomotion, an elongated rostrum bearing a keratinous rhamphotheca, leaf-shaped cheek teeth and semi-conical

premaxillary teeth (Boyd, 2014), shortened forelimbs (Senter & Mackey, 2023), ribcages overlain with ossified plates (Boyd et al., 2011), and neurosensory systems adapted for low-to-the ground posture and possible semi-fossorial behavior (Button & Zanno, 2023). More broadly, thescelosaurines preserve a primitive bauplan reminiscent of the earliest ornithischian lineages (Baron, 2019; Baron et al., 2017; Sereno, 1997; Weishampel, 2004) and are important for polarizing evolutionary transitions such as resting or burial posture (Yang et al., 2020), dietary transitions (Allison et al., 2019; Barrett et al., 2011; Becerra et al., 2022; Salgado et al., 2017), respiratory adaptations (Bourke et al., 2014; Radermacher et al., 2021), burrowing behavior (Varricchio et al., 2007), body size evolution (Norman, 2004; Norman, Sues, et al., 2004; Norman, Witmer, & Weishampel, 2004; O'Gorman & Hone, 2012), and biogeographic radiations (Barrett et al., 2014). Despite their evolutionary significance and their abundance in Maastrichtian ecosystems of North America, thescelosaurines remain poorly understood. To date, Thescelosaurinae is species-poor, consistently composed only of three unique species of *Thescelosaurus* (*Th. neglectus*, *Th. assiniboiensis*, and *Th. garbanii*), a collection of material referable to the genus level (Boyd et al., 2009; Brown et al., 2011), and frequently, the genus *Parksosaurus* (e.g., Sues et al., 2023).

As a clade, thescelosaurines were spatiotemporally constrained to the latest Cretaceous of North America, but their close relationship to orodromines, known from the Early Cretaceous, leaves a large knowledge gap in our understanding of their biogeographic origins and evolutionary relationships. Thescelosaurines, along with Orodrominae, form the two consistently stable and well-supported internal subclades of Thescelosauridae; however, beyond this, the composition of Thescelosauridae is variable, with some studies including a collection of other small-bodied early diverging ornithischians (hereafter SBEDOs). Although several of these species are well-preserved in terms of anatomical completeness, ontogenetic series, and specimen quantity (e.g., *Haya* and *Jeholosaurus*), these specimens are often preserved in articulation, preventing comprehensive documentation of elements from multiple views and limiting the number of phylogenetically informative characters that can be established and verified. This deficiency contributes to the phylogenetic instability within Thescelosauridae and among close relatives.

Here, we describe *Fona herzogae*, a new species of possibly semi-fossorial thescelosaurine dinosaur, from the Mussentuchit Member of the Cedar Mountain Formation, based on one of the largest articulated and disarticulated skeletal collections of a single SBEDO. This collection allows us to document and figure elements in previously underrepresented views. Our description of *Fona herzogae* aids in understanding the evolution of early diverging ornithischians; allows for better comparison of neornithischian interrelationships and investigations into fossorial behavior; and expands the growing list of known dinosaurian taxa that compose the faunas of the mid-Cretaceous of North America.

1.1 | Geological setting

Higher subduction rates during the Albian-Cenomanian transition resulted in an intensified volcanism across the westerly lying Cordilleran Arc triggering a rejuvenation of shortening across the Sevier fold-and-thrust-belt (Currie, 2002; DeCelles & Coogan, 2006; Laskowski et al., 2013). Due to this tectonic activity in the west, the north–south trending foredeep migrated eastward, accommodating both unroofed thrust sediments and voluminous amounts of volcanilithic detritus (Tucker et al., Accepted; Currie, 2002; DeCelles & Coogan, 2006; Laskowski et al., 2013). Remnants of this dynamic setting are scattered across the Western Interior (WI), which include the penecontemporaneous deposits of the Mussentuchit Member of the Cedar Mountain Formation (Utah) to the central WI, along with the Wayan Formation of Idaho and Vaughn Member of the Blackleaf Formation in Montana (Tucker et al., Accepted; Kirkland et al., 2016; Krumenacker, 2019).

The Mussentuchit Member is the youngest Cedar Mountain Formation member ($99.674 + 0.439/-0.197$ to $98.905 + 0.158/-0.183$ Myr) and represents a $\sim$ 800 k window into the world of Laramidia's eastern shores just prior to the Greenhorn cycle in the Western Interior Seaway (WIS) (Tucker et al., 2022; Tucker et al., 2023). Sedimentary successions of the Mussentuchit Member predominantly consist of smectitic mudrocks, thin-bedded sandstones, and four laterally extensive bedded ashes (MAZ1–MAZ4) (Tucker et al., 2023) (Figure 1). Most recently, the Mussentuchit Member has been interpreted to reflect a mix of orogen-transverse (Sevier highlands) and orogen-parallel accumulation of basinal sediments (Tucker et al., Accepted). We envision a similar setting for the Wayan-Vaughn Member; however, this has yet to be confirmed. Despite both the Mussentuchit and Wayan-Vaughn depocenters being located within the foredeep, the northerly lying Wayan-Vaughn depocenter is ascribed as a more arid environment composition (Krumenacker, 2019). In contrast, the more southerly Mussentuchit depocenter has been interpreted as humid (Suarez et al., 2012; Tucker et al., 2022), possibly resulting in each Member preserving similar, yet distinct, species compositions (Avrahami et al., 2022; Krumenacker, 2019).

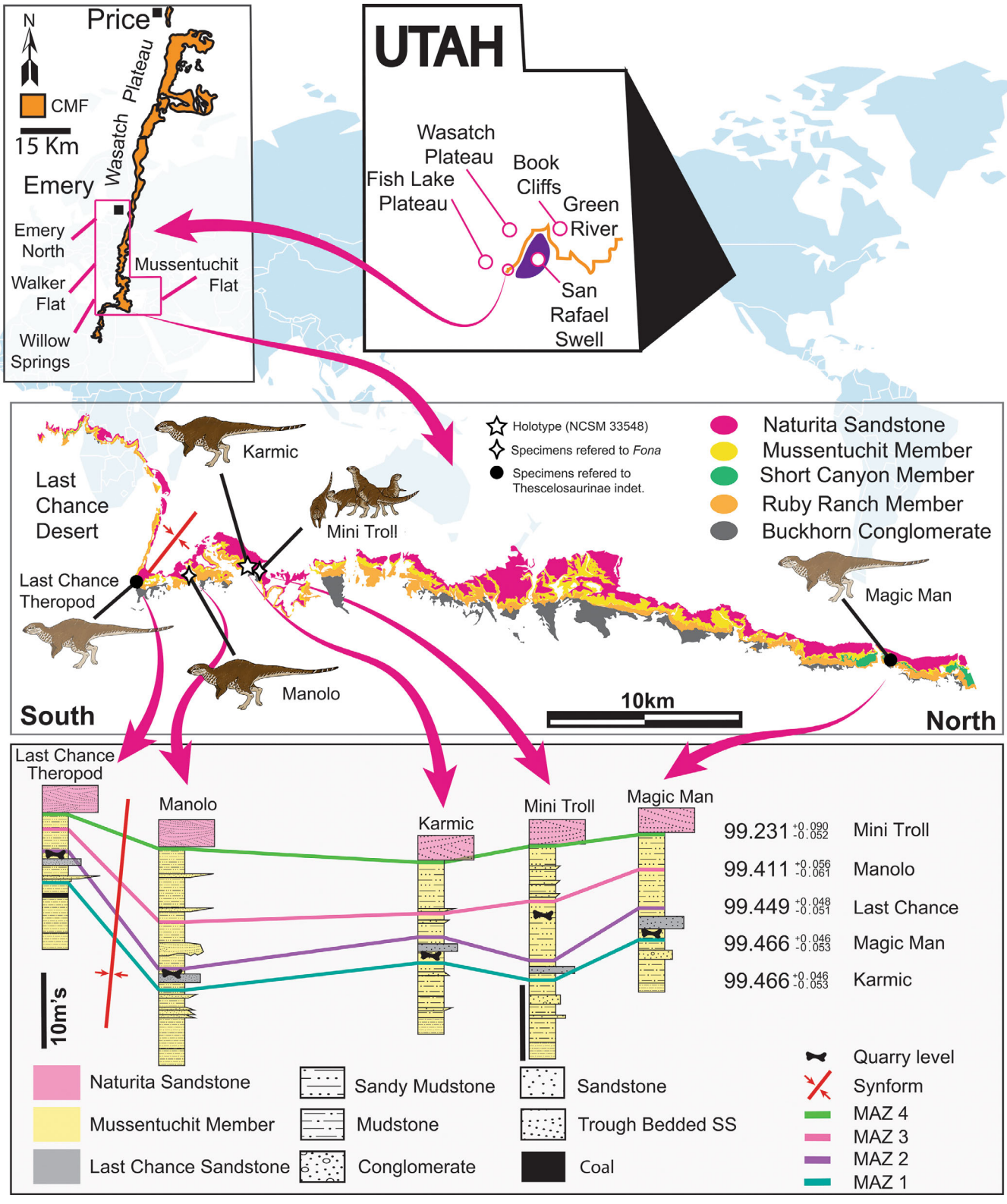

FIGURE 1 Index map and stratigraphic section. Bayesian age-stratigraphic model for key fossil sites in the Mussentuchit Member using a composite stratigraphic framework and depositional ages for MAZ1–4 (Tucker et al., 2023) and the modified Bchron Bayesian age-stratigraphic model (Trayler et al., 2020). Posterior ages and uncertainties for stratigraphic positions are interpreted from the median, and 95% highest-density intervals of the model runs. Model runs were truncated above using a 95.6 Ma age for the overlying Naturita Sandstone (Tucker et al., 2022, 2023). Figure modified from Tucker et al., 2023.

2 | MATERIALS AND METHODS

2.1 | Institutional abbreviations

AMNH: American Museum of Natural; BMNHC: Beijing Museum of Natural History, Beijing, China; BYU: Earth Sciences Museum, Brigham Young University, Provo, Utah; CMN: Canadian Museum of Nature, Ottawa, Canada; DMNS: Denver Museum of Nature & Science, Denver, Colorado; FMNH: Field Museum of Natural History, Chicago, Illinois; IMNH: Idaho Museum of Natural History, Pocatello, Idaho; MPC-D: Institute of Geology, Mongolian Academy of Sciences, Ulaan Baatar, Mongolia; ROM: Royal Ontario Museum, Toronto, Ontario, Canada; MCZ: Museum of Comparative Zoology, Cambridge, Massachusetts; MOR: Museum of the Rockies, Bozeman, Montana; NCSM: North Carolina Science Museum, Raleigh, North Carolina; NCSU AIF: North Carolina State University Analytical Instrumentation Facility, Raleigh, North Carolina; NMNH: Smithsonian National Museum of Natural History; NHMU: Natural History Museum of Utah, Salt Lake City, Utah; NHMUK: Natural History Museum, London, England; NMZ: Naturhistorisches Museum der Universität Zürich, Switzerland; OMNH: Sam Noble Oklahoma Museum of Natural History, Norman, Oklahoma; SMA: Sauriermuseum Aathal, Aathal, Switzerland; SMU: Southern Methodist University, Dallas, Texas; STMN: Shandong Tianyu Museum of Nature, Pingyi, China; TMP: Royal Tyrrell Museum, Drumheller, Alberta; UGS: Utah Geological Survey, Salt Lake City, Utah; YPM: Yale Peabody Museum of Natural History, New Haven, Connecticut.

2.2 | Morphometrics

In order to compare the shape of the scapulae of *Fona* with other early-diverging ornithischians, we updated the morphometric dataset from Fearon and Varricchio (2015) by adding in *Fona*, along with several other early diverging ornithischians measured from published figures or 3D scans (Data S1). After log-transforming the data, a principal component analysis was performed in PAST version 4.0.4 (Hammer et al., 2001) and the figure was created using Adobe Illustrator CC 2015.

2.3 | Phylogenetic analyses

2.3.1 | Matrices

To reconstruct interrelationships among early diverging ornithischians and identify the evolutionary relationships of *Fona*, we performed a series of phylogenetic analyses utilizing a new matrix derived from the compilation of datasets from several recent studies. Zanno, Gates, et al. (2023) is the most recent version of the Boyd (2015) matrix (77 taxa and 255 characters) and was selected as the seed matrix onto which all others were merged because its taxon list contains the highest number of thescelosaurids. To this updated Boyd (2015) matrix, we incorporated characters from three other matrices (Dieudonné et al., 2021; Han et al., 2018; Poole, 2015) and subsequent derivatives of these datasets (e.g., Cruzado-Caballero et al., 2019; Poole, 2023; Rozadilla et al., 2019), to provide resolution of early diverging ornithischian interrelationships. Some similar characters between matrices were incompatible for merging, due to slight variations in wording or discrepancies between state binning sizes/ranges. In these cases, we retained the character that best reflected variation across SBEDOs. Additionally, characters that suffer from the logical fallacies identified by Simões et al. (2017) to such a degree that evaluation or reproducibility was hindered were removed. Lastly, invariant characters were also removed (see details below), resulting in a matrix composed of 411 characters.

The character codings for all SBEDOs were revaluated either from literature, published 3D scans, or in person when possible. If a character coded for an outgroup (non-SBEDO) taxon conflicted between merged matrices and could not be verified independently, the code was either converted to unknown or, converted to the state represented in the majority of merged matrices. These specific changes can be found as comments with detailed justifications appended to individual spreadsheet cells in the supplemental file (Data S2).

Lastly, we added the following taxa to the matrix: *Changmiania* was added from Yang et al. (2020), *Diluvicursor* from Herne et al. (2018), *Minimocursor* was added and recoded from Manitkoon, Deesri, Khalloufi, et al. (2023), and several taxa were added or updated directly from the literature, including *Sanxiasaurus* (Li et al., 2019), *Leaellynasaura* (Rich et al., 2010; Sharp et al., 2017), and *Yueosaurus* (Zheng et al., 2012). *Sanjuansaurus* was removed due to low skeletal completeness and patristic distance from the ingroup.

2.3.2 | Bayesian analyses

We ran a series of time-calibrated and non-time-calibrated Bayesian analyses. Bayesian methods can outperform parsimony in terms of improved accuracy and precision towards the true topology under certain conditions (Puttick et al., 2019). They are particularly optimal when handling matrices composed of 50–200 taxa

(Vernygora et al., 2020), 100–500 characters (Wiens & Morrill, 2011), high amounts of missing data, and high levels of homoplasy (Puttick et al., 2019), and they may provide more reliable quantification of the confidence of estimated relationships in the form of the posterior probability at the nodes. Although certain recent studies suggest that these benefits might be limited to simulated datasets (Goloboff et al., 2019) or suggest that Bayesian inference could exhibit lower precision compared to Maximum Parsimony (Schrago et al., 2018), a definitive consensus is yet to be established. Other recent investigations highlight that Bayesian methods consistently yield a topology from morphological data that aligns more closely with the molecular topology and underscore the enhanced performance of Bayesian methods when applied to real morphological data (e.g., Barbosa et al., 2024; Dalmasso et al., 2022).

Analyses using Bayesian inference were parameterized in the program BEAUti 2.7.6 and run using the associated software Beast 2.7.6 (Bouckaert et al., 2019). Nexus files were formatted in Mesquite to be compatible with BEAUti, requiring all invariant characters to be removed. Additionally, Beast can only handle either/or polymorphic states coded as with slash "/" not simultaneous polymorphisms coded with a "&". Therefore, all "&" were converted to a slash. Next, in BEAUti, the dataset was converted into .xml files that are readable by Beast (Data S3). For Beast to incorporate discrete morphological data, a series of supported packages were installed to BEAUti from its built-in package manager. These include BEASTLabs 2.0.2, cladeage (CA) 2.1.0, Morphological Models (MM) 1.2.1, Model_Selection 1.6.2, Nested Sampling (NS) 1.2.1, Optimized Relaxed Clock (ORC) 1.1.2, and sampled ancestor (SA) 2.1.1.

Six partitions were automatically created based on character state quantity, and each partition was flagged to allow the tree likelihood to use ambiguities as equally likely values for the tips. All partitions use the Lewis MK substitution model with a gamma category count of four to allow for rate heterogeneity. The clock model was set to the optimized relaxed clock. The Yule model was used for the Non-time-calibrated analyses, whereas the Fossilized Birth-Death model was used in the time-calibrated analysis. *Marasuchus* was used as the outgroup.

All analyses were run with an MCMC chain length of ~100 million, storing every 5000 trees. Convergence was evaluated using Tracer 1.7.1 (Rambaut et al., 2018). The maximum clade credibility tree (MCC) was created using the associated program TreeAnnotator 2.6.3 with default settings. Tree data was formatted and visualized using *FigTree* 1.4.4 and Adobe Illustrator.

2.3.3 | Parsimony analyses

The parsimony analysis was run in TNT version 1.6 (Goloboff & Morales, 2023). An invariant character was added to the first column to maintain numerical consistency between TNT and Mesquite. After the matrix was imported, "Max. trees" was set to 99,999 and RAM was set to 500 Mb. *Marasuchus* was set as the outgroup taxon and characters 23, 35, 41, 128, 160, 172, 176, 239, 252, 257, 264, and 265, were set to ordered/additive. A traditional search was performed with the TBR algorithm, setting using 1000 replicates and saving 1000 trees per replication, leaving all other settings as default. The final tree score was 1823. Lastly, a strict consensus tree and a 50% majority rule tree were calculated using the default settings from all trees. The topology of these analyses is presented in (Data S4).

2.4 | Osteological figures

The majority of figures presented in this study are based on associated disarticulated materials from multiple specimens from the Mini Troll locality (Figures 2, 3, and 4). This is because skull elements from the Mini Troll locality are generally better preserved, and underwent preparation, analyses, and documentation prior to the discovery and preparation of NCSM 33548. All osteology figures were produced in orthographic view using the open-source software Blender. Three-dimensional models were created using the iPhone application Metascan (Avrahami, Lindsey, & Herzog, 2023), as well as an Artec Space Spider Industrial 3D scanner. The majority of osteological figures are presented as 3D models rather than photographs. This was done because the surface texture of most bones is uniformly black and shiny, making it difficult to highlight subtle features with minimal relief using traditional photographic techniques. Lighting techniques in Blender do not suffer from these limitations, and all forms of perspective distortion and focal length blur are eliminated.

3 | SYSTEMATIC PALEONTOLOGY

DINOSAURIA Owen (1842).

ORNITHISCHIA Seeley (1887).

NEORNITHISCHIA Cooper, 1985 (sensu Butler et al., 2008).

ORNITHOPODA Marsh, 1881 (sensu Butler et al., 2008).

THESCELOSAURIDAE (Sternberg, 1937).

THESCELOSAURINAE (Sternberg, 1940).

THESCELOSAURINAE indet.

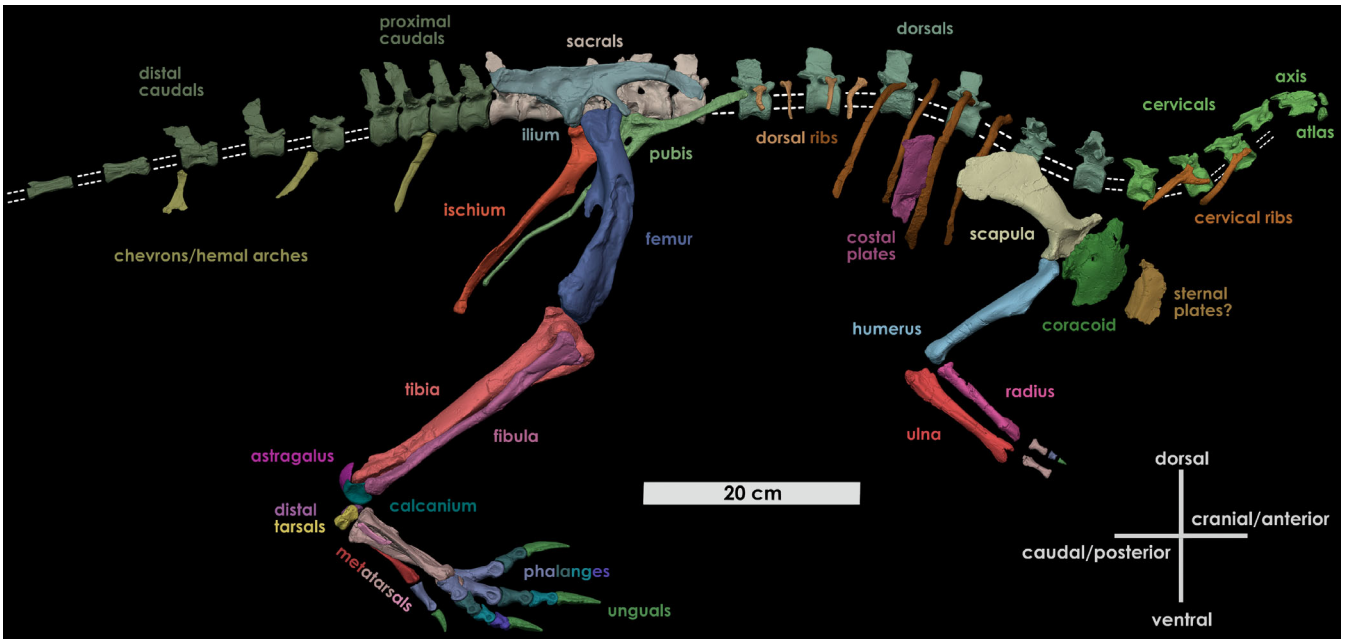

FIGURE 2 Postcranial skeletal reconstruction. Postcranial 3D reconstruction of select disarticulated elements from the Mini Troll locality. The exact number of cervical, dorsal, and caudal vertebrae and ribs are unknown, illustrated by the white dotted lines. Portions of the manus are also incomplete.

3.1 | Referred materials

Over a decade of fieldwork in the Mussentuchit Member has produced a rich record of thescelosaurine specimens including isolated and concentrated remains. Here we adopt an apomorphy-based framework for referrals. Specimens not preserving any autapomorphic features of *Fona herzogae* are referred to Thescelosaurinae indet. only if they preserve traits we recognize herein as diagnostic for this taxon. To date, these include thescelosaurine materials housed at the NCSM from the Last Chance Theropod (NCPALEOUT21) and Magic Man (UT-21-07-23-Z1) localities. The thescelosaurine materials from Last Chance Theropod (NCSM 33547, 36187, 36137, 36192, and 36281) are among the smallest recovered and may represent a single individual. Elements from Magic Man (NCSM 36190, 36191, and 36272) represent the largest thescelosaurine partial individual recovered to date, but this specimen has not yet been completely excavated. Additional specimens likely to represent thescelosaurines, but lacking currently recognized diagnostic features are mentioned in the remarks.

3.2 | Occurrence

Indeterminate thescelosaurine materials have been recovered from throughout the (lower and upper) Mussentuchit Member, upper Cedar Mountain Formation, Utah, USA. Magic Man [UT-21-07-23-Z1] (lower Mussentuchit between MAZ1 and Last Chance Sandstone $99.466 + 0.046/-0.053$ Ma) is the stratigraphically lowest locality preserving a partial skeleton. Last Chance Theropod (NCPALEOUT21) ($99.449 + 0.048/-0.051$) is stratigraphically bound between MAZ1 and MAZ2 and located directly above the Last Chance Sandstone (Tucker et al., Accepted), the boundary between the upper and lower Mussentuchit Member (Figure 1 and Data S5).

3.3 | Remarks

Individuals from Last Chance Theropod and Magic Man are referred to Thescelosaurinae based on several features of the scapulae. NCSM 36272 from the Magic Man locality possesses a sharp scapular spine across the lateral surface of the acromion process and a small medial tubercle at the base of the scapular neck—a feature present in *Oryctodromeus*, *Thescelosaurus neglectus* (USNM V 7760), yet absent in *Othnielosaurus* (SMA 0010), and *Orodromeus* (MOR 623 and 294), and similar but distinct from the more elongated structures in *Iani smithi* (Zanno, Gates, et al., 2023). A first pedal phalanx from the individual preserved at Last Chance Theropod (NCSM 36281) possesses a shallow depression on the ventral surface that is offset medially near the proximal articular facet, as in *Oryctodromeus*

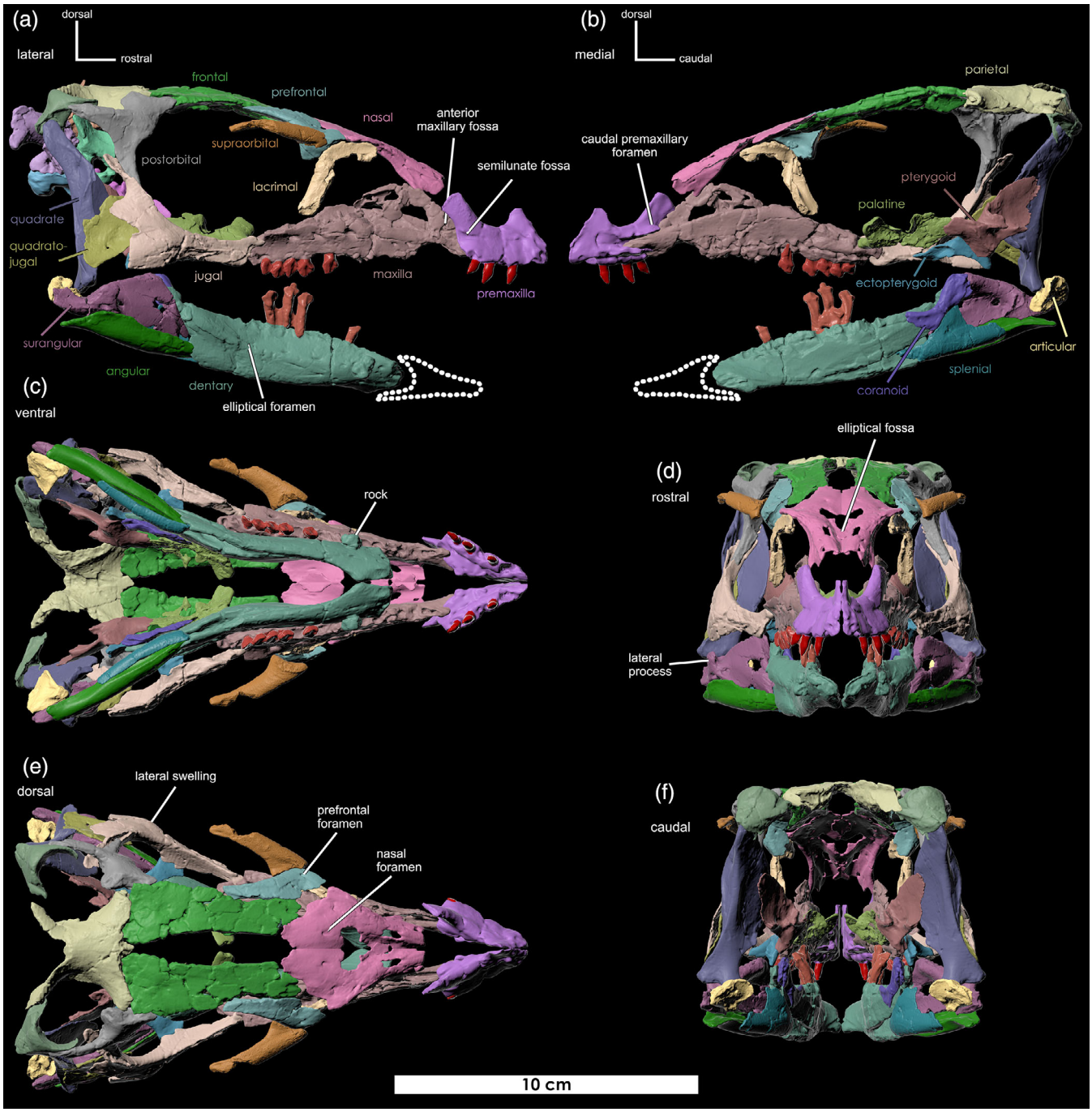

FIGURE 3 Reconstructed skull. Cranial reconstruction derived from elements recovered from the Mini Troll, Karmic, and Manolo localities in (a) lateral, (b) medial, (c) ventral, (d) rostral, (e) dorsal, and (f) caudal views. Dashed lines represent the missing predentary. All non-midline elements are duplicated and mirrored elements in lateral view are denoted with an asterisk here. *premaxilla (FMNH PR 4581), maxilla (NCSM 36143), nasal (NCSM 36144), *jugal (NCSM 33548), quadratojugal (NCSM 36160), *postorbital (NCSM 36149), quadrate (NCSM 36159), squamosal (NCSM 36164), parietal (NCSM 36148), *frontal (NCSM 36136), prefrontal (NCSM 36151), *lacrimal (NCSM 36172), *supraorbital (NCSM 36147), *pterygoid (NCSM 36158), *palatine (NCSM 33548), ectopterygoid (NCSM 36132), *dentary (NCSM 36131), coronoid (NCSM 33548), surangular (NCSM 36166), angular (NCSM 36126), splenial (NCSM 36162), articular (NCSM 33548). Elements of the braincase are shown only in A and specimen numbers are provided in the Figure 8 caption.

(MOR 1642). A partially articulated tail of a large individual collected by the FMNH in 2012 (FMNH PR 5102) likely pertains to *Fona* given its general morphology but possesses no currently recognized diagnostic features of *Fona* or Thescelosaurinae.

Fona n. gen.

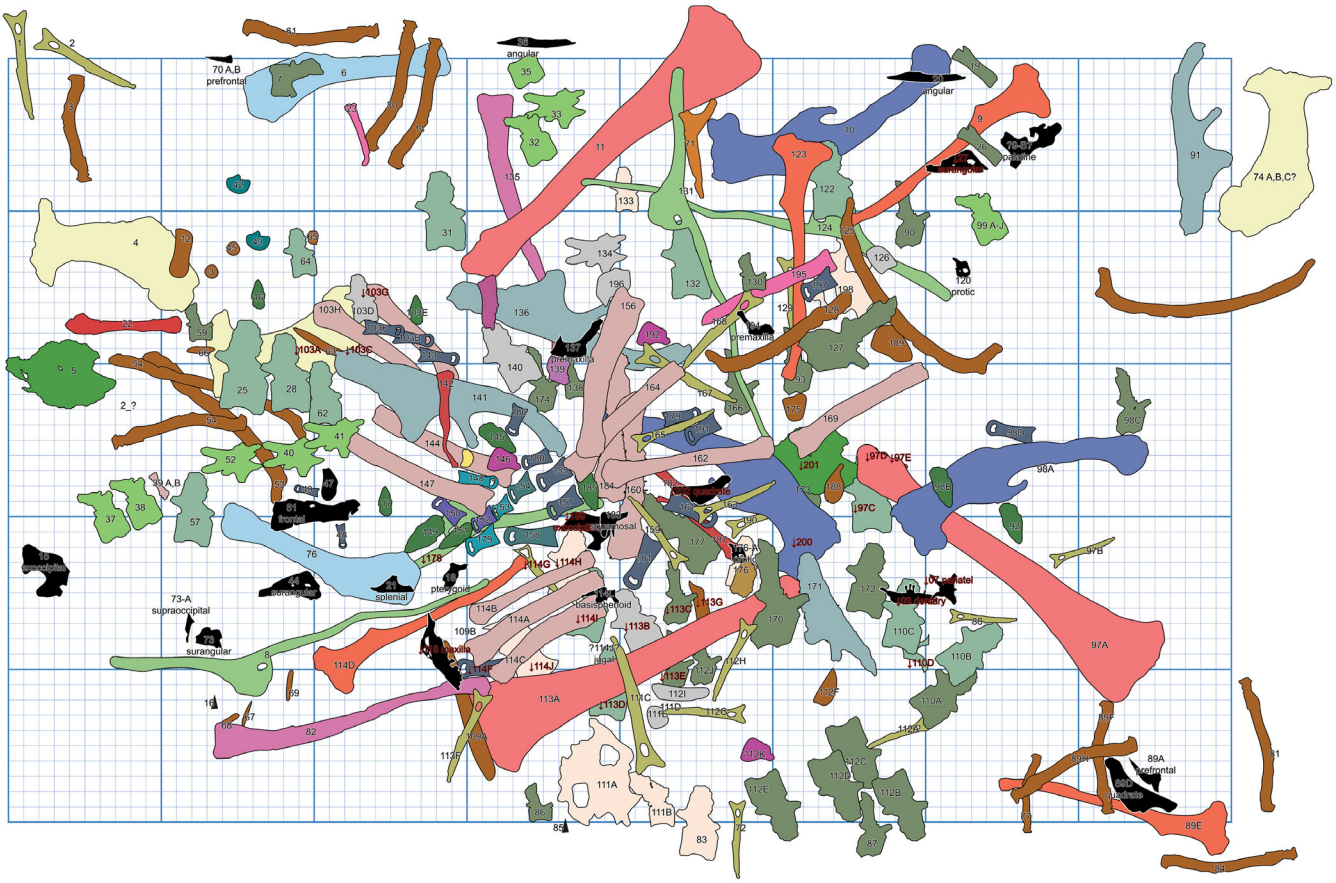

FIGURE 4 Distribution of in situ bones from the Mini Troll locality. Quarry map of jacket MM15-MT-37 showing the distribution and relative locations of skeletal elements belonging to the two best-represented individuals from the Mini Troll locality. Hex color codes and bone silhouettes correspond to those in Figure 1. Gray bones are those that remain unidentified or underprepared. Numbers on elements represent a preparation ID. Numbers outlined in red and denoted with a ↓ were underlying those outlined in white. Cranial elements are black and not to scale. The scale of the map and bones is not exact, as the map was reconstructed using multiple photographs from different angles at different times during the preparation process. Not all bones mapped. NCSM specimen numbers corresponding to field numbers can be found in Data S7.

3.4 | Etymology

Fona (/Foat'NAH/) from the Austronesian language Fino' CHamoru. The ancestral maga'håga of the CHamoru people is Fo'na whose name can be translated as 'the origin'. With her brother Pontan, whose name can be translated as 'a ripe coconut', they became the first paramount female and male chiefs (the ancestral maga'låhi of the CHamoru people), ancestrally venerated according to CHamoru tradition (Borja-Quichocho-Calvo, 2021; Cruz, 2022). According to oral history and legend, when Pontan's spirit began to perish and die, Fo'na discovers her powers and uses them to craft parts of Pontan's body into the pieces of the universe. His eyes were turned into the sun and moon, his eyebrows became the rainbows, his back the earth, his chest the sky, his blood the ocean, and from his stomach and penis the mountains and the sacred Creation Point stone pillar were born (Duhaylonsod & Cepeda, 2022). Fo'na had such sorrow from the loss of her brother that her tears flowed down his body to form the currents of the sea, and in reverence to her brother's dream, she decided to bring life to the universe, throwing herself into the earth where her body turned to stone. From her fossilized body sprang forth the first people at Fuha Rock, imbued with her good spirit (Cepeda, 2021; Cunningham, 1992; Perez, 2019; Perez, 2021). This ancestral story of the CHamoru people mirrors the life and death of the thescelosaurine dinosaurs at the Mini Troll locality, as there were at least two subadult individuals that may have been male and female, or perhaps siblings. Additionally, their bodies fell into the earth where they too fossilized. This naming, rooted in the story of Pontan's sacrifice and Fo'na's love for her brother, highlights the CHamoru values of inafa'måolek (to make good for all), geftåo (the need for compassion, selflessness, and familial bonds)

(Duhaylonsod & Cepeda, 2022), the importance of the equality shared between women and men (Naholowa'a, 2018), and ongoing efforts to decolonize paleontology (Monarrez et al., 2021).

3.5 | Diagnosis

As for the type species.

Fona herzogae sp. nov.

3.6 | Etymology

The specific epithet honors Lisa Herzog (discoverer of the Mini Troll locality) for her unparalleled dedication to the paleontology program at the NCSM and the collection, care, and conservation of fossil specimens worldwide.

3.7 | Holotype

NCSM 33548, a single partially articulated, nearly complete skeleton.

3.8 | Referred materials

Two subequally sized individuals, along with sparse juvenile material (including a third, slightly smaller, right metatarsal II and a juvenile femur) (NCSM 33545, 36125–36136, 36138–36186, 36188, 36189, 36193–36271, 36274–36280, 36282–36287) from the Mini Troll locality (NCPALEO16). FMNH PR 4581 comprises most of a skeleton missing a number of cranial elements, the entire pelvic girdle, and metatarsals.

3.9 | Occurrence

NCSM 33548 was recovered from the Karmic Orodromine locality (UT-16-07-22-Z1), lower Mussentuchit Member, upper Cedar Mountain Formation, Emery County, Utah, USA (Figure 1). Stratigraphic occurrence is between MAZ1 and Last Chance Sandstone (99.466 + 0.046/−0.053 Ma; Tucker et al., 2023) making it the only locality definitively preserving *F. herzogae* from the lower Mussentuchit unit to date. Mini Troll (NCPALEOUT16) is the geologically youngest locality, emplaced below MAZ3, with an age of 99.231 + 0.090/−0.052 Ma. FMNH PR 4581 was preserved at the Manolo site (UT130831), (99.411 + 0.056/−0.061 Ma) above MAZ2 in the upper Mussentuchit (Figure 1).

Age data is based on a Bayesian age stratigraphic model (Trayler et al., 2020) of the member originally detailed in Tucker et al. (2023). Materials referable to *Fona* span the lower to upper Mussentuchit Member of the Cedar Mountain Formation, a range of, at minimum, 235,000 kyr. UT-16-07-22-Z1 and NCPALEOUT16 are located on land administered by the US Bureau of Land Management, respectively; exact locality information is restricted by federal statute and is available to qualified researchers via the NCSM.

4 | DIAGNOSIS

Fona herzogae is a small-bodied, early diverging ornithischian with the following unique combination of characters (autapomorphies are denoted with an asterisk) (Figure 5) *(1) a rostral maxillary fossa located caudal to the first tooth position (unknown in *Oryctodromeus* and possibly shared by *Isaberrysaura* and *Haya*); *(2) an otoccipital that bears a dorsoventrally elongate fossa on the medial surface of the occipital condyle located directly caudal to the medial opening of CN XII; *(3) a rostrocaudally oriented ventral canal on the prootic; *(4) The dorsal margin of the axis neural spine is parallel with the dorsal suture of the centrum, forming an angle of essentially ∼0°. *(5) Ischial shaft has bulbous thickening along the dorsal margin directly distal to the obturator process (prominent on both ischia of at least two individuals and weakly present on only the right of another.) (6) base of the prepubic process bears a prominent lateral swelling (possibly present but significantly reduced in *Oryctodromeus* and *Th. neglectus*). (7) the caudoventral prong of the jugal's caudal process underlaps a groove along the ventral margin of the quadratojugal (shared by *Th. neglectus*, likely *Changmiania*, and possibly at least one specimen of *Jeholosaurus* [STMN 23–17]). (8) dentary teeth with vertical wear facets on the labial surface that terminate abruptly near the crown base to form a mesiodistally inclined shelf (shared by *Oryctodromeus*). (9) A low, round tuberosity on the medial side of the scapula located directly opposite to the glenoid ridge (shared with *Oryctodromeus* and possibly *Iani smithi*). Standard skeletal measurements of NCSM 33548 are provided in Table 1. Characters 7–9 serve as important synapomorphies that help place *Fona* within Thescelosaurinae.

5 | DESCRIPTION

5.1 | General preservation

The preserved position of NCSM 33548 indicates that it was buried with its chest facing stratigraphic bottom and

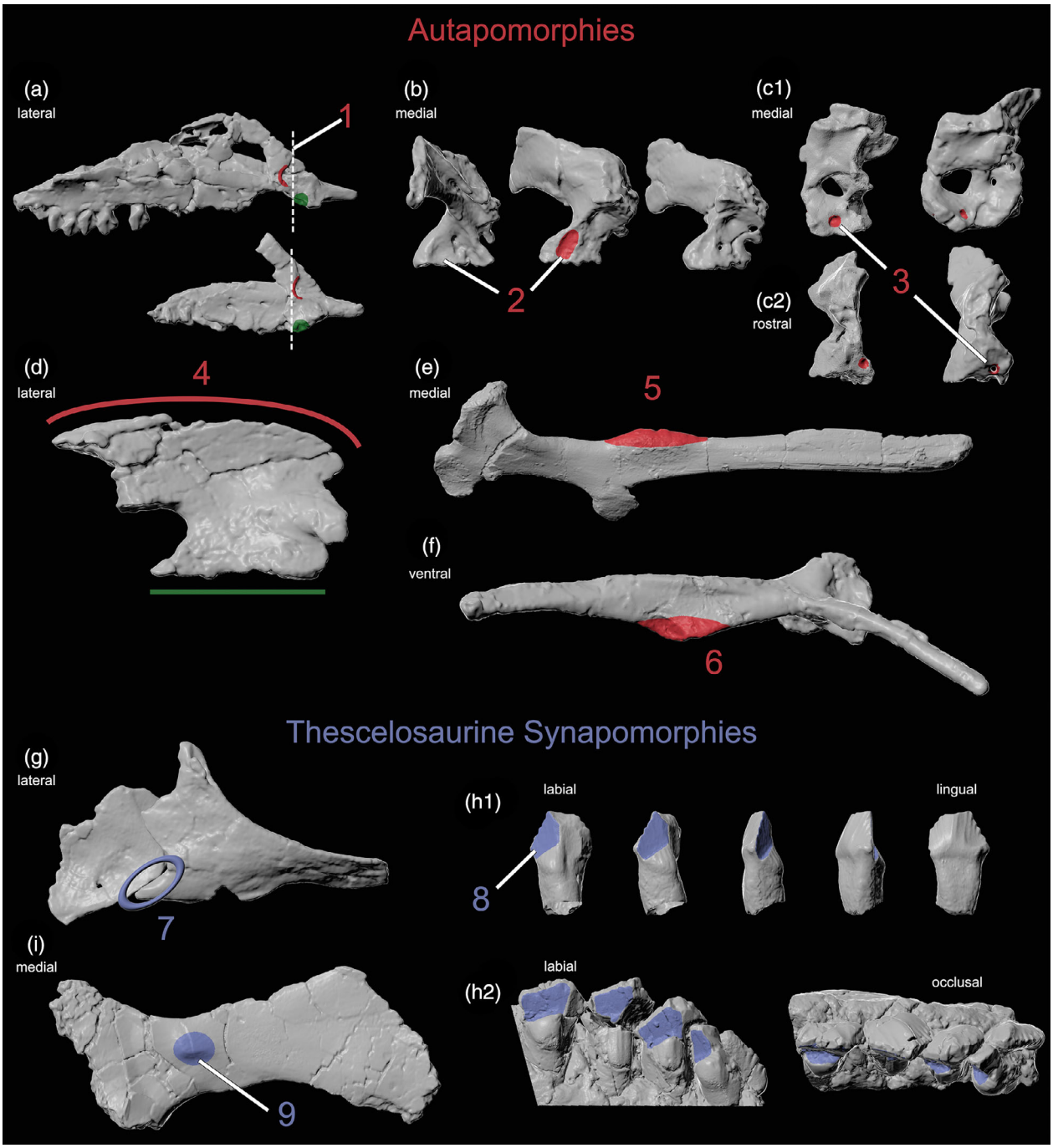

FIGURE 5 Diagnostic features of *Fona herzogae*. (a) two maxillae in lateral view highlighting the unique position of the rostral maxillary fossa; NCSM 36143 (top), NCSM 36142 (bottom). (b) Three otoccipitals in caudal view highlight the unique fossa on the medial surface of the occipital condyle. From left to right NCSM 33548, 36135, 36133. (c) Two prootica in medial (c^1) and cranial (c^2) views highlight the unique ventral canal; NCSM 33548 (left), NCSM 36156 (right). The 3D mesh of NCSM 36156 was modified to highlight the perforation of foramina. (d) Axis (NCSM 36203) in lateral view highlights the dorsal margin's unique horizontal orientation. (e) Ischium (NCSM 36261) in medial view highlights the shaft's unique dorsal inflation. (f) Pubis (NCSM 36259) in ventral view highlights the prepubic process's unique lateral inflation. (g) Quadratojugal (NCSM 36160) to jugal (NCSM 36138) articulation in lateral view, shared with *T. neglectus* and possibly other SBEDOs. (h) Dentary teeth highlighting unique wear patterns that may be shared with *Oryctodromeus*. (h^1) is a single erupted tooth (FMNH PR 4581) represented in rotation from the labial surface (left) to the lingual surface (right). (h^2) are four in-place erupted teeth of NCSM 36130 in labial view (left), and occlusal view (right). (i) Scapula (FMNH PR 4581) in medial view highlighting medial tubercle shared with *Oryctodromeus*, *Th. neglectus* (USNM V 7760) and possibly some iguanodontians. Autapomorphies are denoted in red, with comparative features denoted in green. Notable synapomorphies with *Oryctodromeus* or *Thescelosaurus are* denoted in blue. Elements not to scale. All elements are from the Mini Troll locality unless specified otherwise.

TABLE 1 Skeletal measurements of *Fona herzogae* (NCSM 33548).

Element	Measurement	Value (mm)
Scapula (right)	Dorsoventral length from suture with coracoid to distal end of blade	153.5
Scapula (right)	Craniocaudal width at narrowest point of neck	29.4
Scapula (right)	Craniocaudal width of dorsal blade	79.8
Scapula (right)	Dorsoventral diameter of glenoid fossa	24.6
Coracoid (right)	Dorsoventral height from suture with scapula to ventral margin	56.3
Coracoid (right)	Craniocaudal length from acromium process to ventral edge of the glenoid fossa	73.8
Sternal (left)	Craniocaudal length of element	70.2
Sternal (right)	Craniocaudal length of element	82.6
Humerus (left)	Proximodistal length of element	145.7
Humerus (left)	Craniocaudal width of element at midshaft	22.2
Humerus (left)	Craniocaudal width of element at proximal end	41.9
Humerus (left)	Craniocaudal width of element at distal end	24.3
Humerus (right)	Proximodistal length of element	151.3
Humerus (right)	Thickness from caudal margin to cranial tip of deltopectoral crest	21.9
Ulna (right)	Proximodistal length of element	106.8
Radius (left)	Proximodistal length of element	106.7
Radius (right)	Proximodistal length of element	108.8
MC-II? (right)	Proximodistal length of element	18.6
MC-III? (right)	Proximodistal length of element	24.2
Tibia (left)	Proximodistal length of element	235.1
Fibula (left)	Proximodistal length of element	236.5
Fibula (left)	Circumference at midshaft	30.9
Fibula (left)	Craniocaudal width of element at proximal end	30.0
Femur (right)	Proximodistal length of element	209.0
Femur (right)	Circumference proximal to 4th trochanter	85.9 *crushed
Femur (right)	Circumference distal to 4th trochanter	82.4 *crushed
Femur (left)	Length of 4th trocanter from tip to proximal junction with shaft	36.2
MT-II (left)	Proximodistal length of element	100.9
MT-III (left)	Proximodistal length of element	100.5
MT-IV (left)	Proximodistal length of element	84.1
MT-V (left)	Mediolateral width of element	6.1
P-4-1 (left)	Proximodistal length of element	27.3
P-4-2 (left)	Proximodistal length of element	15.7
P-4-3 (left)	Proximodistal length of element	13.7
P-4-4 (left)	Proximodistal length of element	11.7
P-4-5 (left)	Proximodistal length of element	31.3
Ischium (left)	Length between obturator process and distal end	145.9
Pubis (paired)	Length from symphysis to distal ends	106.4
Pubis (right)	Proximodistal length of post-pubic process	213.0
Dentary (left)	Rostrocaudal length from dorsal tip of coronoid process to predentary articulation	89.4
Dentary (left)	Rostrocaudal length of tooth row	73.1
Postorbital (left)	Maximum rostrocaudal length of dorsal margin	39.9
Postorbital (left)	Mediolateral width of orbital margin	8.6

(Continues)

TABLE 1 (Continued)

Element	Measurement	Value (mm)
Postorbital (right)	Mediolateral width of orbital margin	7.5
Frontal (left)	Transverse width measured from frontal suture caudal to prefrontal groove	11.5
Frontal (left)	Maximum dorsoventral thickness of frontal sutural surface	3.6
Frontal (right)	Transverse width measured from frontal suture caudal to prefrontal groove	12.5
Frontal (right)	Maximum dorsoventral thickness of frontal sutural surface	3.7
Jugal (left)	Rostrocaudal length of ectopterygoid facet	17.6
Jugal (left)	Transverse thickness of element measured at the rostral margin of ectopterygoid	9.1
Jugal (right)	Rostrocaudal length of ectopterygoid facet	14.8
Jugal (right)	Transverse thickness of element measured at the rostral margin of ectopterygoid	9.9

with its forelimbs splayed out laterally. Moving caudally, the dorsal column twists about its axis such that the right side of the pelvis faces stratigraphically upwards. Elements of the left side of the body were buried deeper, which may explain their superior preservation. The articulated left pes is contracted and tucked close to its pelvis, whereas the partially disarticulated right foot is extended further from the body (Figure 6).

5.2 | Cranial skeleton

5.2.1 | General remarks

Here, we provide a general description of skull elements. Comprehensive descriptions are pending in a dedicated detailed cranial osteology (Avrahami et al., in prep).

5.2.2 | Premaxilla

The premaxilla bears a dentigerous main body and caudal and dorsal processes that articulate with the maxilla and nasal. All premaxillae of *Fona* are unfused, in contrast to the fused premaxilla of *Th. neglectus* (Boyd, 2014), *Changchunsaurus* (Jin et al., 2010), *Oryctodromeus* (Krumenacker, 2017), and *Zephyrosaurus* (Sues, 1980). They lack the rugose, mediolaterally expanded shelf that characterizes the rostral tip of the premaxillae in *Hypsilophodon* (Galton, 1974; Huxley, 1870), *Jeholosaurus* (Barrett & Han, 2009), *Changchunsaurus* (Jin et al., 2010), *Th. neglectus* (Boyd, 2014), and *Zephyrosaurus* (Sues, 1980) (Figure 3a). A semilunate fossa located along the premaxillary-maxillary boundary is present in several SBEDOs and is intraspecifically and contralaterally variable in *Fona*. It is prominent on FMNH PR 4581, very reduced on NCSM 36152, and absent on NCSM 36153. It also appears to be absent in *Oryctodromeus*. In ventral view, *Fona* has five premaxillary tooth positions. The caudal process of the premaxilla projects caudodorsally to overlap a facet on the lateral surface of the nasal and likely did not contact the lacrimal unlike *Jeholosaurus* (Barrett & Han, 2009), although the full rostral extent of the lacrimal is unknown. The premaxilla of *Fona* houses four foramina, three of which are located rostrally, and are known to be widely distributed across early diverging ornithischians (e.g., Boyd, 2014; Rozadilla et al., 2019; Sereno, 1991). A fourth foramen, herein termed the caudal premaxillary foramen is located at the junction between the base of the caudal process and the medially directed dorsal projection (Figure 3b). It is present in all *Fona* premaxillae and likely represents an opening for the ophthalmic branch of the trigeminal nerve V (Barker et al., 2017). CT scans reveal it is present in *Th. neglectus*. It does not appear to be present in the fused premaxilla of *Oryctodromeus* (MOR 1636). However, it may be obscured by matrix, poor preservation, or consolidants, or it may be lost during ontogeny.

5.2.3 | Maxilla

The maxilla is an elongate, dentigerous bone that articulates with the premaxilla and jugal, and possibly the lacrimal and elements of the palate. The cumulative *Fona* materials include three maxillae, all of which are partially complete. NCSM 36142 and NCSM 36143 preserve the rostral region from which the ascending process emerges and projects caudodorsally. At the base of this process is a semilunate fossa (rostral maxillary fossa) (Figure 3a). This fossa is present in *Th. neglectus* (Boyd, 2014), *Changchunsaurus* (Jin et al., 2010), *Haya* (Barta & Norell, 2021), *Hypsilophodon* (Galton, 1974), *Jeholosaurus* (Barrett & Han, 2009), *Orodromeus* (Scheetz, 1999), *Zephyrosaurus*

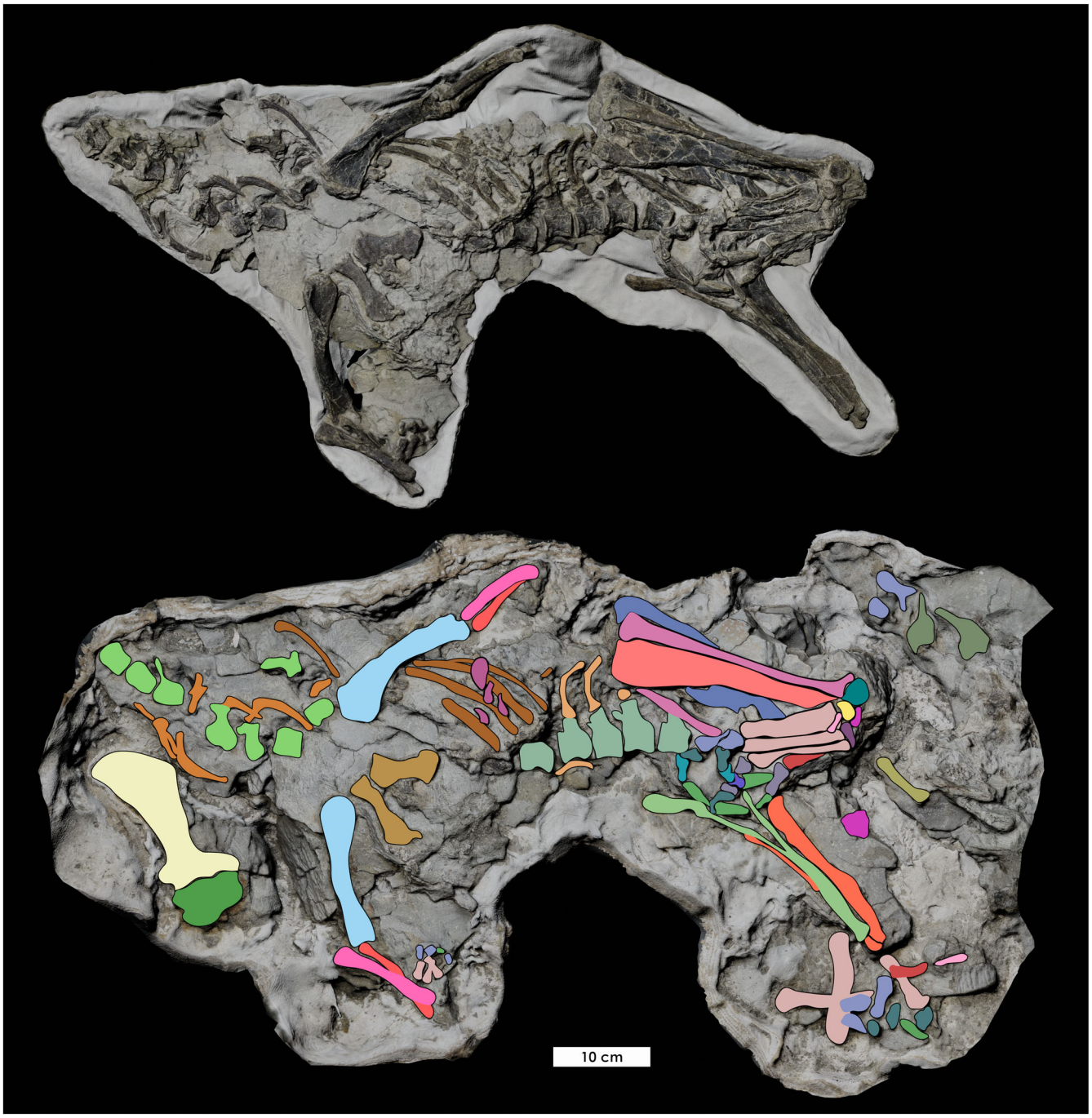

FIGURE 6 Articulated skeleton of *Fona herzogae* NCSM 33548. Jacket containing the mostly complete, articulated postcranial skeleton of NCSM 33548 from the Karmic locality, missing portions of the cervical and caudal series. (top) 3D scan of the skeleton after full preparation. (bottom) 3D scan of the skeleton during an earlier stage of preparation with bones highlighted. The figured view represents the side facing stratigraphic bottom.

(Sues, 1980), *Changmiania* (Yang et al., 2020), *Galleonosaurus* (Herne et al., 2019), and possibly *Isaberrysaura* (Salgado et al., 2017). In *Fona*, the caudal margin of the rostral maxillary fossa occurs caudal to the first tooth position (Figure 5a), whereas, in all other early diverging ornithischians that exhibit the fossa, except for possibly *Isaberrysaura* (Salgado et al., 2017) and possibly a single specimen of *Haya* (MPC-D 100/3181), it occurs rostral to the first tooth position.

The condition of the rostral maxillary fossa in *Oryctodromeus* (MOR 1642) is unknown because the rostral end of the maxilla is poorly preserved. However, a second smaller juvenile *Oryctodromeus* maxilla (MOR 1636) preserves a small depression in this region that is

partially obscured by matrix. If this depression is the rostral maxillary fossa, it would share the condition with *Fona*. However, in both *Fona* and *Haya*, a foramen pierces through this fossa caudomedially, which is absent on MOR 1636.

The rostral tip of the maxilla is defined by a rostral process that inserts between the medial projections of the premaxilla. It is likely shared by all thescelosaurids that preserve a maxilla (Boyd, 2014), as well as *Talenkauen* (Rozadilla et al., 2019), but is possibly absent in *Haya* (Barta & Norell, 2021).

5.2.4 | Nasals

The nasal of *Fona* is a thin, plate-like bone that articulates with the premaxilla, frontal, prefrontal, and lacrimal. We identify MOR 1642 as the nasals of *Oryctodromeus*. They are similar to those of *Fona* in that they are unfused along the internasal suture, a condition shared by *Haya* (Barta & Norell, 2021). Additionally, both *Fona* and *Oryctodromeus* exhibit the elliptical fossa along the sagittal midline of the nasals, as occurs in most ornithopods, as well as some early diverging ceratopsians (Han et al., 2016; Xu et al., 2002) and early diverging stegosaurs (Sereno & Zhimin, 1992). However, this fossa is less pronounced in *Fona* (Figure 3d) as well as *Th. neglectus* (contra Boyd, 2014). The exact contact between the lacrimal and maxilla remains unclear as these elements are partially damaged or incomplete in the area of articulation with the nasal. A single foramen is located near the mediolaterally widest portion of the nasal, as in *Haya* (Makovicky et al., 2011). This is in contrast to the condition in *Jeholosaurus* (Barrett & Han, 2009) and *Th. neglectus* (Boyd, 2014) in which a row or series of foramina are located more laterally.

5.2.5 | Jugal

The jugals are triradiate-shaped bones with processes to articulate with the postorbital and maxilla and facets for articulation with the quadratojugal, ectopterygoid, and lacrimal. The jugals of *Fona* are similar to the preserved portions of the jugal in *Oryctodromeus* (MOR 1642). Their lateral surfaces bear moderately laterally convex areas covered in rugose texture that are variably present across specimens (Figure 3a). This swelling and rugosity occur with increasing prominence in larger specimens of *Fona*, being completely absent in the smallest jugal (Figure 5g). Similar thickened protuberances and nodular ornamentation occur in *Changchunsaurus* (Jin et al., 2010), *Oryctodromeus* (Krumenacker, 2017), and some specimens of *Jeholosaurus* (Barrett & Han, 2009), but these features are completely absent in *Haya* (Barta & Norell, 2021; Makovicky et al., 2011), *Dysalotosaurus* (Hübner & Rauhut, 2010), and *Th. neglectus* (Boyd, 2014). This condition is distinct from the prominent caudally projecting process present in orodromines such as *Orodromeus* (MOR 294) and *Zephyrosaurus* (MCZ 4392 and YPM 56695), which are possibly homologous with a similar structure in *Heterodontosaurus* (Norman et al., 2011; Sereno, 2012). It should be noted that a recently published SBEDO, *Minimocursor*, was reported to share this important feature. However, based on our interpretation of figure 5c in Manitkoon, Deesri, Khalloufi, et al. (2023) the jugal of PRC 150 was imaged in medial view, rather than lateral, with the ectopterygoid and maxillary contacts of the rostral process misinterpreted as a caudal boss. This is further supported by the fossa located along the caudal process, which likely represents the articulation with the lateral surface of the quadratojugal. The caudal process of the *Fona* jugal is a dorsoventrally broad, sheet-like structure that is bifurcated into separate, mediolaterally flattened projections, that overlap the rostral portion of the lateral surface of the quadratojugal.

5.2.6 | Quadratojugal

The quadratojugal of *Fona* is a plate-like bone that articulates with the jugal and quadrate. It has a complex connection with the jugal that was previously considered a possible autapomorphy of *Th. neglectus* (Boyd, 2014). In most SBEDOs, no portion of the jugal contacts the ventral margin or medial surface of the quadratojugal. However, in *Fona*, *Th. neglectus* (Boyd, 2014), *Changmiania* (Yang et al., 2020), and likely at least one specimen of *Jeholosaurus* (STMN 23–17), the ventral projection of the caudal process of the jugal contacts the ventromedial surface of the quadratojugal (Figure 5g). More specifically, the dorsal margin of the projection slots into a small groove located along the ventral edge of the quadratojugal. This is dissimilar to the condition present in the early diverging iguanodontian *Zalmoxes* in which the jugal houses a recess for the rostral margin of the quadratojugal (Weishampel et al., 2003). The quadratojugal bears a single small foramen, a condition shared by many SBEDOs.

5.2.7 | Postorbital

The postorbital is a triradiate bone that articulates with the frontal, parietal, squamosal, jugal, and laterosphenoid. The caudal process of the postorbital that articulates with the squamosal is not bifid as in *Th. neglectus*

and possibly some specimens of *Haya* (Barta & Norell, 2021; Boyd, 2014). The lateral surface of the caudal process is dorsoventrally convex, in contrast to the concave condition of *Th. neglectus* (Boyd, 2014) and possibly *Changchunsaurus* (Jin et al., 2010; Zan et al., 2005) (Figure 3a). The laterosphenoid socket is located at the caudodorsal corner of the rostral process, caudal to the orbital margin, and lateral to the parietal contact. This socket continues laterally onto the caudomedial corner of the frontal, a condition shared by a variety of SBEDOs. The lateral surface also bears a rostrally inflected protuberance, as occurs in a number of SBEDOs (Norman, 2004). It is extensively rugose on NCSM 33548 (Figure 7a), as in *Th. neglectus*, and possibly served as the attachment site for a caudal supraorbital.

5.2.8 | Quadrate

The quadrate of *Fona* is dorsoventrally elongate and characterized by pterygoid and jugal wings, which project rostrally from the main shaft (Figure 3f). In lateral view, the dorsal third of the quadrate is caudally inflected such that the dorsal articulation with the squamosal is located caudal to the plane of the quadrate ventral condyles. A possible paraquadratic foramen is present across the lateral surface near the jugal wing in a number of SBEDOs such as *Th. neglectus*, *Haya*, *Parksosaurus* (Boyd, 2014; Makovicky et al., 2011), and some early diverging iguanodontians and ankylopollexians (Norman, 2004). This foramen seems absent in all *Fona* quadrates. However, on a single specimen (NCSM 36159) there is a deep concavity on the rostral surface of the main shaft, in between the pterygoid and jugal wings, which may represent the paraquadratic foramen. The medial surface of the pterygoid wing has a subtle dorsoventrally elongate fossa, as occurs in *Oryctodromeus* (Krumenacker, 2017) and *Th. neglectus* (Boyd, 2014).

5.2.9 | Squamosal

The squamosal of *Fona* is crescentic in dorsal view (Figure 3e). The rostral process that contacts the postorbital has a strong rostromedial curvature, which is shared by *Oryctodromeus*, *Orodromeus*, but appears more rostrocaudally straight in *Hypsilophodon* (NHMUK R197), *Haya* (Barta & Norell, 2021), *Th. neglectus* (Boyd, 2014), and especially *Changmiania*, in which the rostral process is rostrally elongated and straight due to the elongation of the dorsal margin of the infratemporal fenestra (Yang et al., 2020). The prequadratic process is present but incomplete.

5.2.10 | Parietal

The parietal is an hourglass-shaped bone in dorsal view that articulates with the supraoccipital, squamosal, postorbital, and frontal. Two parietals are preserved representing *Fona* (NCSM 36148) and (FMNH PR 4581), both of which lack a pronounced sagittal crest (Figure 3e), a condition shared only by *Lesothosaurus* (Porro et al., 2015), *Changmiania* (Yang et al., 2020), and *Orodromeus* (MOR 1136). Unfortunately, a parietal is not preserved for *Oryctodromeus*.

The contact with the frontals is formed by an interdigitating suture, which bows caudally in dorsal view. This is in contrast to the condition in *Changmiania*, and *Lesothosaurus*, in which the contact is mediolaterally straight (Porro et al., 2015; Yang et al., 2020). The parietal contacts the postorbital at its rostrolateral corner via a deep pocket into which the postorbital slots, a condition shared by *Dysalotosaurus* (Sobral et al., 2012). The median process is a small tab-like projection that emerges rostrally from the midline. It is plow-shaped, contacting only the ventral surface of the frontal where it inserts into a small groove at the caudomedial corner. This condition, in which the process is only exposed in ventral view, is shared by *Th. neglectus* (Boyd, 2014) and *Te. tilletti* (Thomas, 2015: figure 21), and possibly the fully articulated skulls of *Haya* (Barta & Norell, 2021). In contrast, a dorsally exposed median process is present in *Dysalotosaurus* (Sobral et al., 2012), and possibly some specimens of *Hypsilophodon* (Galton, 1974). The caudolateral corner of the parietal forms a mediolaterally thin process that curves around the caudomedial border of the supratemporal fenestra to contact the squamosal. The contact with the squamosal consists of a short triangular joint surface, in which the rostrolateral face of the caudolateral process slots into a triangular depression on the squamosal medial process. This condition is similar in *Haya*. However, the caudolateral process in *Haya* exhibits a drooping, pendant shape with broader dorsoventral margins, and the contact with the squamosal occurs along the ventral tip of the process (Barta & Norell, 2021). These conditions are dissimilar to *Th. neglectus* in which the caudolateral process extends much further ventrally and appears to wrap around the medial process of the squamosal (Boyd, 2014). There is no sign of a parietal contact for the laterosphenoid, as occurs in *Hypsilophodon* (Galton, 1974), *Zephyrosaurus* (Sues, 1980), and *Te. tilletti* (Thomas, 2015). A subtle, caudally projecting tab is present along the caudal margin at the midline, as in *Th. neglectus* (Boyd, 2014) and *Dysalotosaurus* (Sobral et al., 2012).

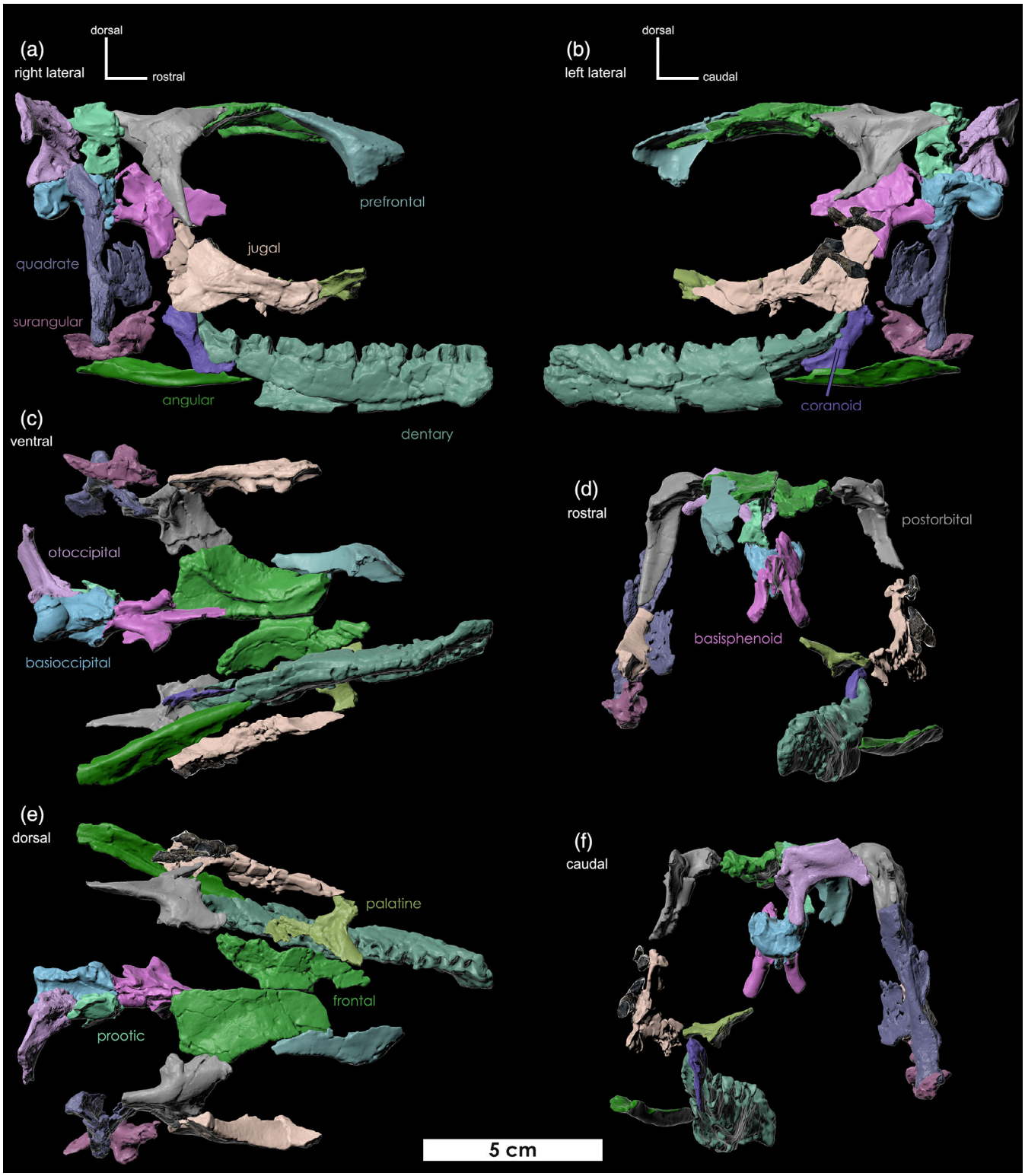

FIGURE 7 Reconstructed skull of *Fona herzogae* NCSM 33548. Cranial reconstruction limited to only the holotype specimen from the Karmic locality in (a) right lateral, (b) left lateral, (c) ventral, (d) rostral, (e) dorsal, and (f) caudal views. Several disarticulated dentary and maxillary teeth are cemented to the left jugal.

5.2.11 | Frontal

The frontal is a flat, rectangular bone that articulates with the prefrontal, nasal, parietal, and postorbital. The paired frontals of *Oryctodromeus* (MOR 1642) have midline depressions on their dorsal surfaces, which seems to correspond to a slight bulging of the orbital margin laterally. This depression is present to a lesser extent in

Orodromeus (MOR 1136). *Fona* is represented by several frontals from multiple localities. NCSM 36136 lacks this condition, whereas it is present in FMNH PR 4581 and NCSM 33548 (Figure 7e), suggesting this feature may be intraspecifically variable. This depression is also absent in *Thescelosaurus*. The paired frontals of *Oryctodromeus* are more robust dorsoventrally than most examples of *Fona*. The facet for the dorsal head of the laterosphenoid is located ventromedial to the postorbital contact, at the caudal termination point of the crista cranii (Figure 8). It continues onto the postorbital as in many SBEDOs such as *Agilisaurus*, *Jeholosaurus*, *Lesothosaurus*, *Thescelosaurus*, and *Zephyrosaurus* (Barrett et al., 2005; Barrett & Han, 2009; Boyd, 2014; Sereno, 1991; Sues, 1980).

5.2.12 | Prefrontal

The prefrontal is a wedge-shaped bone that articulates with the frontal, nasal, supraorbital, and lacrimal. The rostral process of the prefrontal in *Fona* is a dorsoventrally thin sheet of bone that tapers to a pointed triangular tip (Figure 3e). Its rostromedial edge would have bordered the caudolateral margin of the nasal and would likely have been positioned dorsal to the lacrimal, as in most early diverging ornithischians (Boyd et al., 2009; Norman, Sues, et al., 2004; Norman, Witmer, & Weishampel, 2004). This is in contrast to *Parksosaurus*, in which the triangular tip of the prefrontal dives rostroventrally to insert between the lacrimal and the dorsal process of the maxilla, nearly preventing contact between the two (Boyd et al., 2009; Galton, 1973). Barta and Norell (2021) notes a slight contact between the maxilla and the prefrontal in *Haya*, which appears to be absent in *Fona*, as inferred by the apparent lack of a sutural surface on the dorsolateral portion of the prefrontal. There are no rugosities present for the supraorbital, in contrast to those of *Th. neglectus* (Boyd et al., 2009). The prefrontal foramen is present and on NCSM 36151 it is located dorsally, slightly medial to the supraorbital contact (Figure 3e). This foramen was previously reported as one of the five autapomorphies of *Thescelosaurus* (Boyd et al., 2009), but also occurs in at least one specimen of *Haya* (MPC-D 100/3181) (Barta & Norell, 2021). On NCSM 33548 there are at least five foramina located across the craniolateral corner of the dorsal surface.

5.2.13 | Lacrimal

The lacrimal (NCSM 36172) is an angled, "L"-shaped bone with a strongly arched dorsal margin (Figure 3a,b). Although its precise alignment with the maxilla, ectopterygoid, jugal, prefrontal, nasals, and premaxilla remains uncertain due to damage, it is more similar to *Hypsilophodon* (NHMUK PV R 2477 and R 197) in morphology and configuration, than to *Th. neglectus* (NCSM 15728). In lateral view, the dorsal margin of the vertex, which likely contacted the prefrontal, is evenly rounded as in *Hypsilophodon* (NHMUK PV R2477), in contrast to the sharper angle and a rounded dorsolateral boss on the lacrimal of *Th. neglectus* (NCSM 15728). The medial surface of the rostral portion bears a distinct shallow groove to likely facilitate an overlapping contact with the lateral rim of the prefrontal and nasal, as opposed to *Th. neglectus* in which the nasal overlaps the lateral surface of the lacrimal. There is a prominent lacrimal duct, which faces entirely medially, in contrast to the more caudally facing opening in *Th. neglectus* (NCSM 15728).

5.2.14 | Supraorbital

The rostral supraorbital is a rostrocaudally elongate, slightly curved, rod-like bone that tapers caudally, and bears a strong resemblance to that of *Th. neglectus* (NCSM 15728). It is slightly dorsoventrally flattened, bows slightly dorsolaterally, and bears a tear-drop-shaped, cross-section along its length, with the thin medial surface forming a rounded margin, in contrast to the sharply edged margin of *Th. neglectus*. Rostrally, the rostral supraorbital is mediolaterally widest and characterized by a small, medially projecting process, and a second small, rostrolaterally projecting process (Figure 3e). These two projections formed a contact with the lateral surface of the prefrontal. The ventral surface of the lateral projection is slightly rugose and may have formed a contact with the lacrimal.

5.2.15 | Supraoccipital

The supraoccipital is a blocky midline bone that articulates with the otoccipital, prootic, and parietal. In caudal view, the caudodorsal surface lacks the prominent midline nuchal crest present in many early diverging ornithischians. However, there is a slightly raised, rostrocaudally oriented ridge extending along the midline (Figure 8f), a condition shared with *Th. neglectus* (Boyd, 2014), *Th. assiniboiensis* (Brown et al., 2011), and *Haya* (Barta & Norell, 2021). The presence and/or prominence of this feature also seems to be ontogenetically variable in *Orodromeus* (Poole, 2015: character 77). A lack of a nuchal crest was also reported in *Changmiania* (Yang et al., 2020). There are two subtle concave depressions located lateral to the median ridge, a condition present in many SBEDOs. In contrast to *Th. neglectus* and *Dysalotosaurus* (Boyd, 2014; Brown et al., 2011; Sobral et al., 2012), there is no sign of a groove or canal for the vena capitis

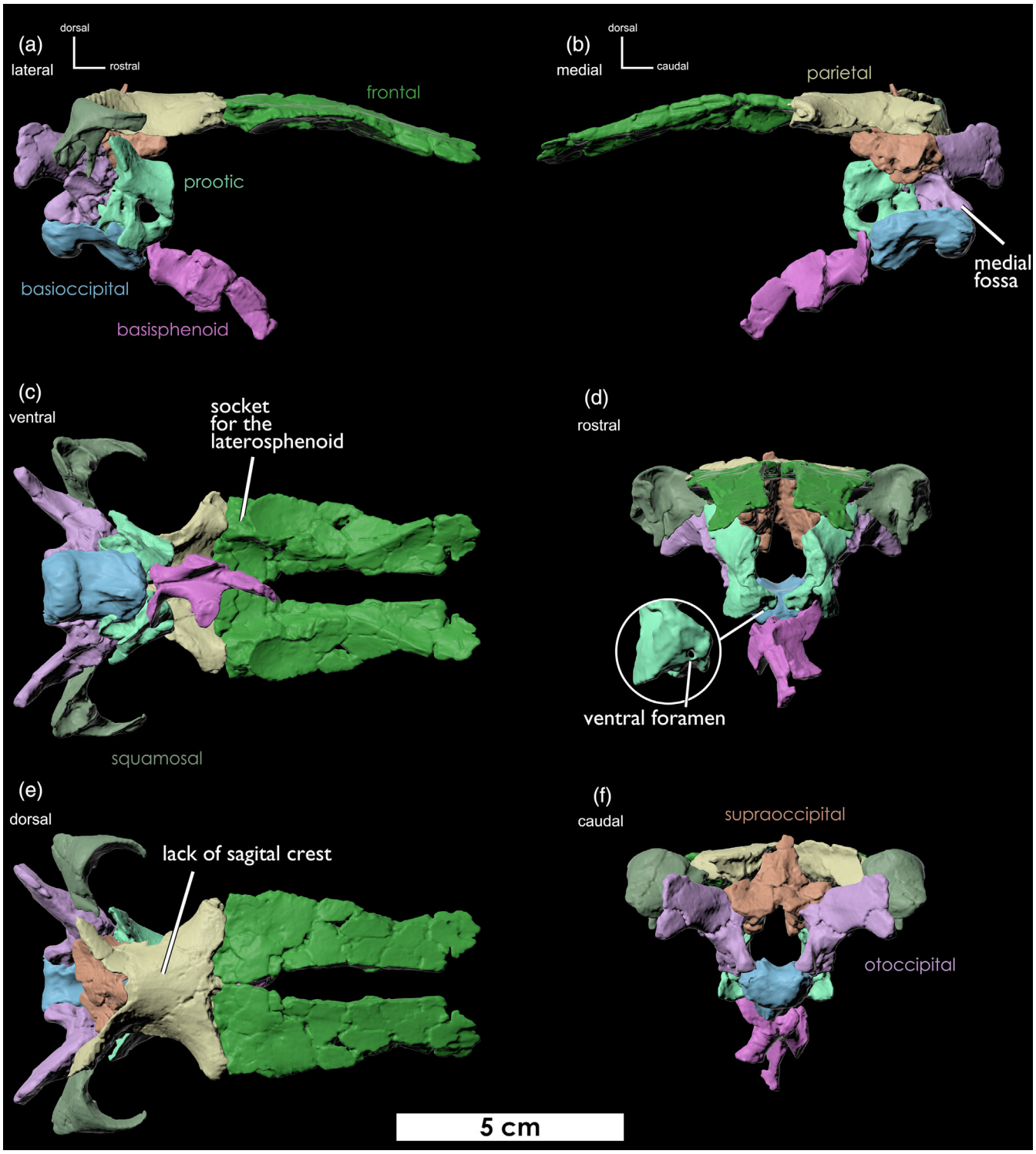

FIGURE 8 Reconstructed braincase of *Fona herzogae*. Reconstruction of the braincase derived from elements belonging to multiple individuals from several localities in (a) lateral, (b) medial, (c) ventral, (d) rostral, (e) dorsal, and (f) caudal views. All non-midline elements are duplicated and mirrored elements in lateral view are denoted with an asterisk here. Parietal (NCSM 36148), *frontal (NCSM 36136), supraoccipital (NCSM 36165), *otoccipital (NCSM 36133), prootic (NCSM 36156), basisphenoid (NCSM 36129), basioccipital (FMNH PR 4581).

dorsalis within or near these concavities. There are no foramina across the dorsal surface in contrast to *Th. neglectus* and *Th. assiniboiensis* (Boyd, 2014; Brown et al., 2011). The caudoventral margin contributes to the dorsal rim of the foramen magnum. This condition occurs in most SBEDOs except for *Thescelosaurus*,

Dryosaurus, *Dysalotosaurus*, and some iguanodontians (e.g., *Tenontosaurus*) in which the contribution is significantly reduced or completely absent (Sobral et al., 2012; Thomas, 2015).

5.2.16 | Otoccipital

The paraoccipital process of the otoccipital has a pendant/hatchet shape (Figure 8f), as in *Th. neglectus* (Boyd, 2014), *Zephyrosaurus* (Sues, 1980), *Haya* (Barta & Norell, 2021), *Orodromeus* (MOR 403) and *Oryctodromeus* (Varricchio et al., 2007). The central portion of the caudal surface of the paroccipital process bears a subtle bulge extending dorsolaterally, which may correspond with the border of a broad depression located near the dorsolateral margin of the foramen magnum in *Haya*, thought to represent the insertion site for *m. rectus capitis posterior* (Barta & Norell, 2021). As in *Th. neglectus*, the lateral surface of the process also lacks the prominent striations present in *Haya* (Barta & Norell, 2021). In medial view, there is a dorsoventrally elongate fossa on the medial surface of the occipital condyle that is present on five separate otoccipitals from the Mini Troll, Karmic, and Manolo localities. This fossa is located directly caudal to the medial opening of CN XII (Figure 8b) and is not present in *Orodromeus*, *Oryctodromeus*, or *Th. neglectus*. However, it may be present in *Th. assiniboiensis*.

5.2.17 | Prootic

The prootic is a mediolaterally compressed, quadrangular bone that articulates with the otoccipital, basisphenoid, laterosphenoid, and supraoccipital. *Fona* is represented by five prootic elements. All four right prootica (NCSM 36155, 36156, 36157 and NCSM 33548) form fully enclosed foramen for the trigeminal nerve (CN V) and the middle cerebral vein, in contrast to *Th. assiniboiensis* (Brown et al., 2011), *Orodromeus*, *Parksosaurus*, and *Hypsilophodon* (NHMUK R 2477; Galton, 1989), in which the laterosphenoid participates in the rostral margin of the foramina. There is a canal located in the rostroventral region of the prootic, which pierces through the prootic as it travels caudally, and somewhat medially, through the dorsum sellae (Figure 8d). In rostral view, the opening of this canal is positioned along the contact with the basisphenoid. This canal has not been described on the prootic before, and may represent a continuation of the carotid canal of the basisphenoid as on the hadrosaurine *Kerberosaurus manakini* (Bolotsky & Godefroit, 2004: figure 2a) and the saurolophine *Kundurosaurus nagornyi* (Godefroit et al., 2012: figure 11d).

5.2.18 | Basisphenoid/Parasphenoid

The basiphenoid is an elongate tetraradiate bone that articulates with the protic, basioccipital, and pterygoid. The basipterygoid processes of the basiphenoid (NCSM 33548, 36128, and 36129) are relatively longer than those in *Haya* (Barta & Norell, 2021) but not as elongate as *Te. tilletti* (Thomas, 2015). They are ovoid in cross-section, with the rostral margin tapering to a sharp edge, as in *Th. neglectus* (Boyd, 2014). The ventral surface of the basisphenoid bears a well-defined rostrocaudally oriented groove (Figure 8c), a condition shared with *Oryctodromeus* (Krumenacker, 2017, figure 5e). This groove is wider and less distinct in *Zephyrosaurus* (Sues, 1980) and absent in *Lesothosaurus* (Porro et al., 2015), *Haya* (Barta & Norell, 2021), *Orodromeus* (MOR 1136), *Th. neglectus*, and *Th. assiniboiensis* (Boyd, 2014; Brown et al., 2011). In *Dysalotosaurus* and *Hypsilophodon* there is no midline groove, and instead, there is a deep pit between the basipterygoid processes that may represent a remnant of an embryonic hypophyseal fenestra (Galton, 1974; Sobral et al., 2012).

5.2.19 | Basioccipital

The basioccipital articulates with the otoccipital, basisphenoid, and atlas of the axial skeleton. Two basioccipitals are preserved. NCSM 33548 is fused to the basisphenoid (Figure 7c), whereas FMNH PR 4581 is unfused (Figure 8c). In lateral view, the ventral margin is deeply concave, and in dorsal view, the lateral margins are slightly medially constricted. There is no midline ridge on the dorsal surface of the foramen magnum near the basisphenoid contact, in contrast to *Zephyrosaurus* (MCZ 4392 & YPM 56695), *Oryctodromeus* (only MOR 1642, and possibly *Th. neglectus*, and *Th. assiniboiensis*; Boyd, 2014; Brown et al., 2011).

A midline ventral keel is present near the basisphenoid contact, a condition shared by many SBEDOs. On NCSM 33548, the ventral extent of this keel is extensive, descending slightly below the ventral margin of the basisphenoid, whereas on FMNH PR 4581 it is nearly half the depth. A similar range of variation is present in *Zephyrosaurus*, suggesting this feature may be intraspecifically variable. This keel is not laterally bordered by two small knobs, in contrast to *Th. neglectus* (Boyd, 2014).

In ventral view, the shape of the occipital condyle's rostral margin is variable, being mediolaterally flat on FMNH PR 4581, whereas on NCSM 33548 it forms a prominent rostrally directed curve. A similar range of variation is present in *Zephyrosaurus*, suggesting this feature may be intraspecifically variable. *Oryctodromeus* (MOR 1642) bears two bilateral foramina near the

craniodorsal corner of the occipital condyle, which are absent on MOR 1636 as well as *Fona*.

5.2.20 | Pterygoid

The pterygoid is a complex, triradiate, sheet-like bone that articulates with the quadrate, basisphenoid, ectopterygoid, and palatine. It is mediolaterally thin and dorsoventrally wide (Figure 3b,f) but not as wide as in *Th. neglectus*, *Lesothosaurus* (Boyd, 2014; Porro et al., 2015), or *Oryctodromeus* (MOR 1642). There is no sign of the lateral pterygoid ridge across the lateral surface, as is present in *Th. neglectus* (Boyd, 2014). A distinct thumb-like process on the medial surface accepts the descending basipterygoid processes from the basisphenoid, and the lateral surface is weakly convex where it braces the subtle medial fossa of the quadrate.

5.2.21 | Palatine

In dorsal view, the palatine is a thin rectangular-shaped bone (Figure 7e). It is dorsoventrally flattened with a rostrocaudal length nearly double its mediolateral width. The palatines of *Haya* (Barta & Norell, 2021), *Iani* (Zanno, Gates, et al., 2023), and *Lesothosaurus* (Porro et al., 2015) are also longer than wide, in contrast to *Th. neglectus*, which has a length-to-width ratio closer to one (Boyd, 2014). The palatine is a thin sheet across its caudal aspect, which overlaps the pterygoid. The ventral surface of this lamina is smooth and flat, lacking the ventral prong in *Th. neglectus* (NCSM 15728). The rostrolaterally directed process is the most robust region of the element, forming a thickened and caudally hooked sutural surface that likely articulated with the lacrimal, jugal, and/or maxilla, although the precise alignment of elements in this region remains uncertain due to incomplete preservation. In contrast, the rostromedial process is much thinner dorsoventrally and may have contacted the contralateral palatine.

The ventral surface is characterized by a narrow, rostrocaudally oriented groove formed by two thin laminae running in parallel and located along the midline of the element. This groove is bordered laterally and medially by two broad and weakly concave surfaces. This is in contrast to the much larger, laterally positioned grooves that serve to embrace the maxilla in *Iani* and *Th. neglectus* (Boyd, 2014; Zanno, Gates, et al., 2023). A prominent caudolateral projection was noted in *Iani*, which emerges along the curved caudolateral margin between the pterygoid and maxillary process (Zanno, Gates, et al., 2023). Reprocessed CT scans of *Th. neglectus* reveal it to be a shared feature. It appears to be absent in *Fona*.

5.2.22 | Ectopterygoid

The ectopterygoid is an "L" shaped bone that articulates with the pterygoid, jugal, and palatine. The medial third of the ectopterygoid forms a main body that is broader dorsally and tapers ventrally (Figure 3). It has a mediolaterally concave caudal surface and a flat rostral surface that fits into a concave groove on the mandibular ramus of the pterygoid. The rostromedial corner does not have the postpalatine fenestra present in *Th. neglectus* (Boyd, 2014). Overall it is remarkably similar in morphology to the ectopterygoid of *Talenkauen* (Rozadilla et al., 2019), although it lacks the prominent dorsal lobe.

5.2.23 | Dentary

The dentary is an elongate dentigerous bone that articulates with the predentary, coronoid, splenial, surangular, and angular. The coronoid process of the dentary is not as dorsally inclined as in *Th. neglectus* (Boyd, 2014). Directly ventral to the tooth row on the medial surface is a row of closely spaced, rostrocaudally elongate, oval-shaped special foramina located below each of the 17 tooth positions. These foramina are also present in *Changchunsaurus* (Jin et al., 2010), *Haya* (Barta & Norell, 2021), *Hypsilophodon* (Galton, 1974), and a number of other ornithischians (Edmund, 1957). A larger, caudally placed foramen is present ventral to the twelfth tooth position (Figure 3a). This foramen is present in *Changchunsaurus* (Jin et al., 2010) and *Th. neglectus* (Boyd, 2014), but not *Haya* (Barta & Norell, 2021). The lateral surface of the dentary is rough and bears several elongate excavations and numerous small foramina, especially towards the rostral tip. In contrast to *Haya*, there are no distinctly paired mental foramina contained within a lateral groove near the rostral end (Barta & Norell, 2021).

5.2.24 | Coronoid

A single right coronoid is preserved from NCSM 33548 (Figure 7a,b). It is a mediolaterally compressed "L" shaped bone, independent from the rising coronoid process of the dentary, upon which it braces medially. It forms an angle of ~130°, as in *Th. neglectus* (Boyd, 2014). It has a rostral margin that becomes strongly inflected rostrally at the vertex, in contrast to *Hypsilophodon* in which this margin forms a much more consistent gradational curvature (Button et al., 2023). The rostral process is much shorter than *Th. neglectus* (Boyd, 2014) and *Hypsilophodon* (Button et al., 2023); however, this may be due to damage, as this portion of the element would have

been thin and delicate. Its medial surface is slightly concave, possibly to accept the dorsal process of the splenial, which contacts this region in *Th. neglectus* (Boyd, 2014). A single foramen occurs in this concavity near the rostral end of the preserved portion. The caudoventral corner of the coronoid lacks the short ventral process present in *Th. neglectus* (Boyd, 2014) and *Hypsilophodon* (Button et al., 2023). The dorsal process of the coronoid is rostrocaudally expanded, terminating in a sharp point at its apex as in *Hypsilophodon* (Button et al., 2023), but in contrast to the more lobate process of *Th. neglectus* (Boyd, 2014). The lateral surface of the dorsal process is marked by a moderately pronounced ridge oriented dorsoventrally and offset slightly from the rostral margin, which would have facilitated the contact with the rising coronoid process of the dentary. A similar surface is present in *Th. neglectus*, which appears to be formed by a more concave facet (Boyd, 2014, figure 16i). The caudal corner of the dorsal process bears a deep facet that likely received the dorsal corner of the surangular, as it does in *Hypsilophodon* (Button et al., 2023).

5.2.25 | Surangular

The surangular is a tripartite, sigmodal bone that articulates with the dentary, angular, coronoid, prearticular, and articular. The lateral process of the surangular is finger-like and emerges laterally from the surangular and then deflects dorsally, and somewhat rostrodorsally (Figure 3a,d). A similarly developed process is found on *Th. neglectus* (Boyd, 2014), *Haya* (Barta & Norell, 2021), *Talenkauen* (Rozadilla et al., 2019), and the early diverging iguanodontians *Te. tilletti* (Thomas, 2015) and *Zalmoxes robustus* (Weishampel et al., 2003). However, the process is most similar to the structure seen in *Th. neglectus*, being dorsoventrally taller rather than rostrocaudally wide. The lateral process is not as prominent in other SBEDOs such as *Orodromeus*, *Zephyrosaurus*, *Changchunsaurus*, *Haya*, or *Hypsilophodon* (Galton, 1974; Galton, 1997; Jin et al., 2010; Makovicky et al., 2011; Scheetz, 1999; Sues, 1980). Rather, these taxa possess a thickened bulbous boss located in the same region.

5.2.26 | Angular

The angular is a canoe-shaped bone that articulates with the surangular, articular, splenial, and dentary. Most of the ventral margin of the angular is strongly mediolaterally rounded and slightly rostrocaudally convex as in *Hypsilophodon* (Galton, 1974), *Jeholosaurus* (Barrett & Han, 2009), *Changchunsaurus* (Jin et al., 2010), and *Th. neglectus* (Boyd, 2014). This is in contrast to the condition in *Haya* (Barta & Norell, 2021) and *Changmiania* (Yang et al., 2020), in which the ventral surface is rostrocaudally concave. The caudal fifth of the angular's ventral margin becomes slightly concave, as in *Haya* (Barta & Norell, 2021). In dorsal or ventral view, the angular is mediolaterally narrowest rostrally and becomes gradually wider caudally, where it forms the floor of the retroarticular process. *Fona* lacks the lateral fossa seen in *Th. neglectus* (Boyd, 2014) (Figure 3a).

5.2.27 | Splenial

The splenial is a sheetlike bone. The caudal process of the splenial likely contacted the medial surfaces of the prearticular and angular, as in *Th. neglectus* (Boyd, 2014). The dorsal and ventral margins of this process run caudally in parallel and lack the bifurcation present in *Changchunsaurus*, *Archaeoceratops* (Jin et al., 2010), and possibly *Lesothosaurus* (Porro et al., 2015) (Figure 3b).

5.2.28 | Articular

The articular (Figure 3) is a roughly pyramidal bone and the most caudally located element of the mandible. A ventrolateral facet would have accepted the medial surface of the retroarticular process of the surangular, whereas the rostrodorsal surface would have contributed to the glenoid for the ventromedial condyle of the quadrate. The medial surface is broadly flat and smooth, and forms a slight concavity at its caudoventral corner, likely representing the contact for the lateral surface of the prearticular. A single foramen is present on the medial surface which likely connects with a similar sized foramen positioned directly opposite on the lateral surface.

5.2.29 | Dentition

Premaxillary teeth ($n = 5$) are subconical with a constriction at the root-crown transition. They have bulbous crown bases and recurved tips and some have faint, fine serrations. Both labial and lingual sides of the premaxillary teeth are covered by enamel but lack the apicobasal enamel striations seen in *Th. neglectus*.

A minimum of 18 maxillary tooth positions are present. This high tooth count is shared by *Hexinlusaurus*, *Thescelosaurus*, *Kulindadromaeus*, and *Isaberrysaura* (Barrett et al., 2005; Boyd, 2014; Godefroit et al., 2014; Salgado et al., 2017), as opposed to other early ornithischians that usually display 13–15 maxillary teeth (Barta & Norell, 2021).

Erupted maxillary teeth are labiolingually compressed and have a median ridge. Tooth crowns bear a maximum of 11 denticles, similar to the condition in *Haya* (Makovicky et al., 2011).

On NCSM 36130, distal dentary crowns 10–13 are fully erupted, well-preserved, and display an interesting wear pattern. Each crown has two vertical wear facets on the labial surface, in contrast to the continuous occlusal surface of the maxillary teeth. These facets are oriented apicobasally and converge at a midline eminence, indicating that the labial surface of each dentary crown likely occluded with the lingual surfaces of two maxillary crowns during mastication (Figure 5h). All wear facets are planar and oriented nearly vertically, forming a 180° angle with the long axis of the tooth. This is in contrast to the more concave facets that are angled at 70° in *Changchunsaurus* (Jin et al., 2010).

The distal wear facets of crowns 10 and 13, which show the best preservation, are limited to the apical half of the crown, whereas the mesial wear facet seems to continue basally. The distal wear facet terminates abruptly, forming a flat but angled shelf that slants apically towards the midline eminence, functionally similar to what is observed in some leptoceratopsids (Chinnery & Horner, 2007). Basal to this shelf, the remainder of the cingulum is minimally worn and appears as a bulbous swelling. A third possible mesiodistally flat wear facet runs apicobasally along the midline.

On NCSM 36131, the possible contralateral to NCSM 36130, the wear facets of erupted crowns eight—10 are more extensively worn and the basal shelf is reduced and rounded, suggesting that this condition may be transient. CT scans of an *Oryctodromeus* dentary (IMNH 44946) reveal a similar wear pattern may be present on the labial surface of at least one erupted tooth.

5.3 | Axial skeleton

5.3.1 | Atlas

The atlantal intercentrum of *Fona* is similar to other SBEDOs, having a crescentic outline in cranial view, a concave facet on the ventral surface, and a round cranioventral margin (Figure 9). This is in contrast to the heart-shaped atlantal intercentrum of *Oryctodromeus* (MOR 1642), which has a cranioventral margin that is concave, a condition shared with *Haya* and *Hypsilophodon* (Barta & Norell, 2021; Galton, 1974; Makovicky et al., 2011).

The unfused neural arches are irregularly "L" shaped bones in dorsal view. They differ in a number of ways from those of *Th. neglectus* (NCSM 15728) and *Oryctodromeus*. In *Th. neglectus* the caudal margin forms a strong concave profile, whereas in *Fona* and *Oryctodromeus* this margin is mostly straight. In *Oryctodromeus* and *Th. neglectus* the caudomedial corner of the neurapophysis is characterized by a distinct tab, which is absent in *Fona*.

5.3.2 | Axis

The axis of *Fona* (NCSM 36203) is unique in that the dorsal margin of the neural spine is oriented horizontally, relative to the long axis of the intercentrum suture (Figures 5 and 9). In all other SBEDOs, with the possible exception of one specimen of *Lesothosaurus* (Baron et al., 2017, Figure 2), the dorsal margin is inclined. This discrepancy is most profound when compared with *Oryctodromeus* (MOR 1642), in which this angle of inclination is approximately 38°.

5.3.3 | Cervical vertebrae

In lateral view, all cervicals are roughly as long as tall (Figure 9), a condition shared by most SBEDOs except for *Koreanosaurus*, and is also absent in several elasmarians, which have craniocaudally elongate cranial centra (Calvo et al., 2007; Huh et al., 2010; Novas et al., 2004; Rozadilla et al., 2019). The cranial articular surfaces of cervicals are flat to slightly convex and have heart-shaped articular facets. The caudal articular surfaces are concave and taller than wide, in contrast to a number of *Oryctodromeus* cervicals with mediolaterally expanded centra. As in *Haya* (Barta & Norell, 2021), some caudal cervical centra are wedge-shaped in lateral view, with ventral margins that are slightly longer than the dorsal margin. The lateral surfaces are each marked by a ridge that runs the length of the centrum, which bows dorsally and becomes more prominent at the cranial articular surface to form the parapophysis. The surfaces ventral to these ridges become broadly concave before merging at the ventral margin to form a sharp keel. A ventral keel is widespread among early diverging ornithischians (e.g., Butler et al., 2012). However, in *Fona*, this keel is often ventrally convex in lateral view and descends further ventrally than the ventral margins of the articular surfaces. None of the centra from the Mini Troll locality have a nutrient foramen, in contrast to *Koreanosaurus* and *Changchunsaurus* (Butler et al., 2011; Huh et al., 2010). However, one cervical centrum from the Manolo locality bears a foramen on its left and right lateral surfaces. Neural canals tend to be elliptical and dorsoventrally elongate, in contrast to the more D-shaped outlines of *Oryctodromeus* (Krumenacker, 2017). The neural arch is inclined caudally and becomes taller caudally. The neural spine is mediolaterally thin and short, and epipophyses

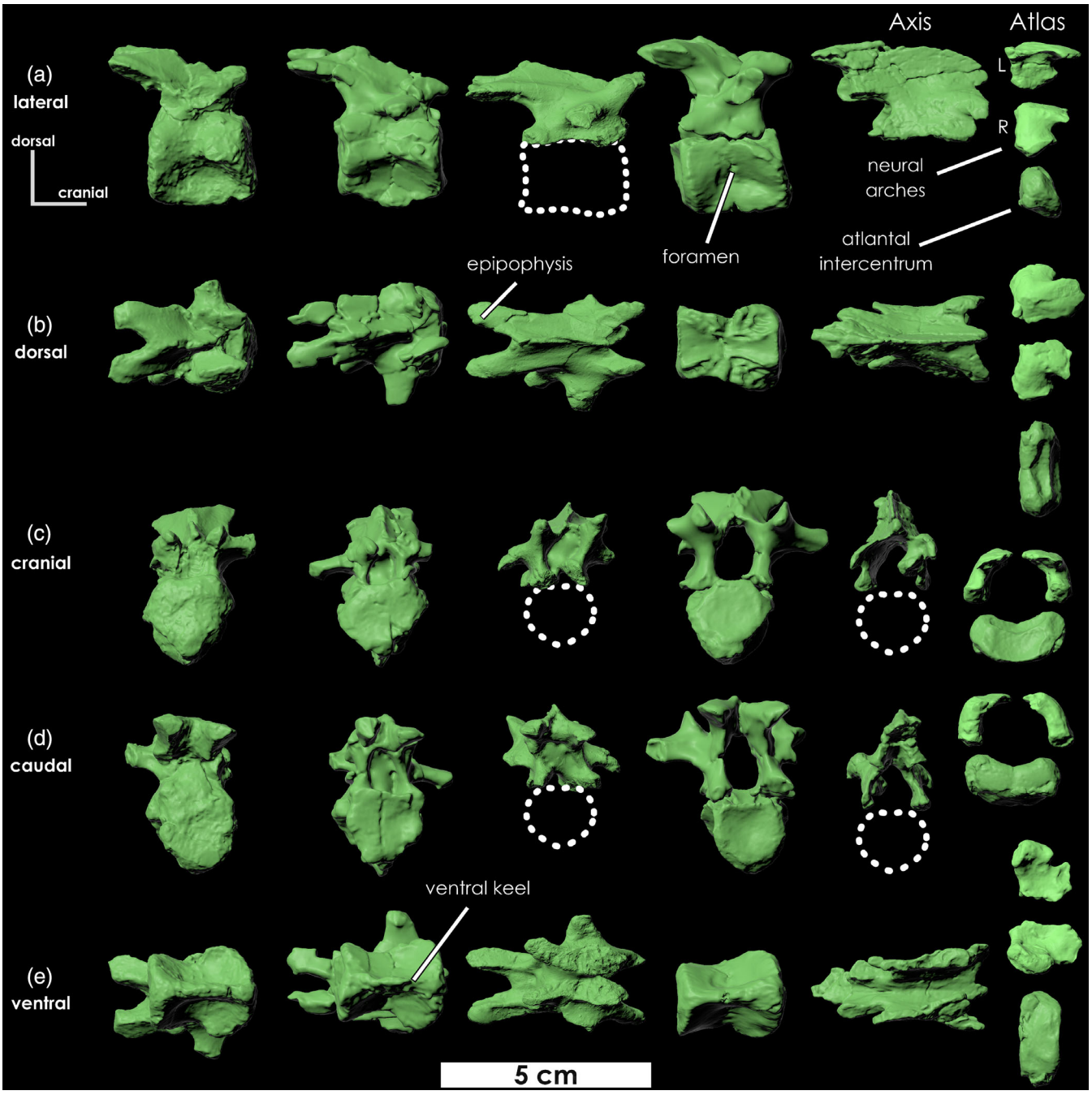

FIGURE 9 Cervical vertebrae of *Fona herzogae*. Well-preserved cervical vertebrae from the Mini Troll and Manolo localities in (a) lateral, (b) dorsal, (c) cranial, (d) caudal, and (e) ventral views. The exact cervical number is unknown. Cervical vertebrae from left to right: NCSM 36202, NCSM 36200, NCSM 36524, FMNH PR 4581, NCSM 36203. Left neural arch (NCSM 36197) is denoted with an "L", right neural arch (NCSM 36194) is denoted with an "R". The atlantal intercentrum is NCSM 36585. Dashed lines represent missing centrum.

are present on at least three cranial cervical vertebrae (FMNH PR 4581, NCSM 36200, and NCSM 36524), as in some elasmarians (Rozadilla et al., 2019) and heterodontosaurids (Sereno, 2012). The prezygapophyseal surfaces face dorsomedially and slightly cranially, whereas the postzygapophyseal surfaces face ventrolaterally and slightly caudally.

5.3.4 | Dorsal vertebrae

The centra of cranial dorsal vertebrae are slightly mediolaterally compressed and their ventral surface is marked by a subtle ventral keel, a condition shared by other SBEDOs (Figure 10). Middle and caudal dorsal vertebrae become mediolaterally wider and their ventral surfaces

are craniocaudally concave and smooth, in contrast to the ventral grooves in *Parksosaurus* (Sues et al., 2023). Approximately 20 dorsal centra are preserved from the Mini Troll locality and all are amphicoelous. Only two dorsal centra from the Mini Troll and Manolo localities have vascular foramen across their lateral surfaces. This is in contrast to *Parksosaurus* and *Changchunsaurus*, which have foramen on all dorsal centra (Butler et al., 2011; Sues et al., 2023). The ventral and lateral rims of articular surfaces are marked by numerous fine ridges, a condition shared by many SBEDOs (Barta & Norell, 2021). At least two dorsal centra preserve an elliptical foramen that pierces the floor of the neural canal (dorsal surface of the centrum). This foramen is also present in *Hypsilophodon* but is absent in *Parksosaurus* and *Thescelosaurus* spp. (Brown et al., 2011; Galton, 1974; Sues et al., 2023). The cranioventral margin of the cranial dorsal centra does not have the rugose swelling present in *Changchunsaurus* and *Jeholosaurus* (Butler et al., 2011; Han et al., 2012). In lateral view (Figure 10a), the sutural surface of several dorsal centra are defined by a short but sharp triangular dorsal projection that rises near the midpoint of the margin, a condition shared by *Iani* (Zanno, Gates, et al., 2023).

The dia- and parapophyses are distant from each other on the cranial dorsal vertebrae. The parapophyses steadily migrate up the transverse process, eventually merging near the caudal end of the series to form a single broad articular facet. Simultaneously, the angle formed between the transverse processes shifts from a generally steeper "V" shape in the cranial most dorsals to more laterally directed down the column, a condition shared by *Oryctodromeus* (Varricchio et al., 2007), but in contrast to *Koreanosaurus*, which has cranial dorsals that are not as dorsally inflected (Huh et al., 2010). Cranial dorsal transverse processes bear a laterally extending ridge on their ventral surfaces that bisects the processes into two gentle depressions, with the base of the caudal depressions forming deep infrapostzygapophyseal fossae. A similar ridge is present in *Jeholosaurus* (Han et al., 2012), but is absent in *Changchunsaurus* and *Haya*, which instead have a single shallow fossa (Barta & Norell, 2021; Butler et al., 2011).

The neural spines of the mid- to caudal dorsals are transversely compressed, sub-rectangular, and caudally inclined plates, with parallel cranial and caudal margins. In cranial view, the spine is mediolaterally thinner ventrally, becoming thicker towards the horizontal dorsal margin. The neural spine of the first dorsal is tall, constituting nearly two-thirds of the total vertebral height. The neural canals are ovoid and mediolaterally elongate, in contrast to the dorsoventrally elongate canals of *Haya* (Barta & Norell, 2021).

The cranial dorsals possess two deep fossae immediately above the neural canal, near the junctions between the neural spines and the zygapophyses. The cranial fossa between the prezygapophyses is triangular in outline whereas the caudal fossa between the postzygapophyses is a dorsoventrally elongate oval. The cranial fossa diminishes in prominence down the series, eventually becoming absent, whereas the caudal fossa seems to diminish only minimally and remains present on most dorsals, including the last.

In dorsal view, the mid-caudal dorsals of *Oryctodromeus* and *Orodromeus* have neural spines with hourglass-shaped cross-sections. In *Fona*, 10 of the 12 well-preserved mid-caudal dorsals have neural spines that taper cranially, producing an elongated triangular cross-section. However, the neural spines of at least two mid-caudal dorsals (NCSM 36210, 36209, and possibly 36204) are hourglass-shaped, excluding this feature as diagnostic, although it may be positionally or intraspecifically variable.

5.3.5 | Sacral vertebrae

The sacrum of *Fona* is composed of seven sacrals, herein considered any vertebrae in the series that possess at least one articular surface with an excavated sutural texture (Figure 11c,d). The first two vertebrae are sacralized dorsals, a condition shared by *Oryctodromeus* (Krumenacker, 2017), and *Orodromeus* (Scheetz, 1999). On NCSM 33548 sacrals two-six are fully fused. In contrast, the Mini Troll locality preserves two pairs of fused sacrals two and three, and a third fused pair of sacrals (possibly the fifth and sixth).

The ventral surface of the centra are marked by distinct craniocaudally elongated grooves that are more prominent at the cranial and caudal ends of the series but are absent on the fourth and seventh centra, and absent on the third of NCSM 33548 (Figure 12). Ventral grooves spanning across sacral centra are also present in *Oryctodromeus* (Krumenacker, 2017) and possibly *Hexinlusaurus* (He & Cai, 1984), but are absent in *Orodromeus* (Scheetz, 1999), which has a ridge in place of the groove on the second sacral, and a flat ventral surface on all subsequent sacral centra. A ventral ridge or keel is also present and positionally variable on several other SBEDOs such as *Haya* (Barta & Norell, 2021), *Changchunsaurus* (Butler et al., 2011), *Parksosaurus* (Sues et al., 2023), *Dysalotosaurus* (Hübner, 2018), *Sektensaurus* (Ibiricu et al., 2019), Isasicursor (Novas et al., 2019), and *Sanxiasaurus* (Li et al., 2019). A flat or slightly rounded condition characterizes the sacrals of *Jeholosaurus*, *Hypsilophodon*, and *Notohypsilophodon* (Galton, 1974; Han et al., 2012; Ibiricu et al., 2014). A single disarticulated first sacral of *Fona* from the Manolo locality (FMNH PR 4581)

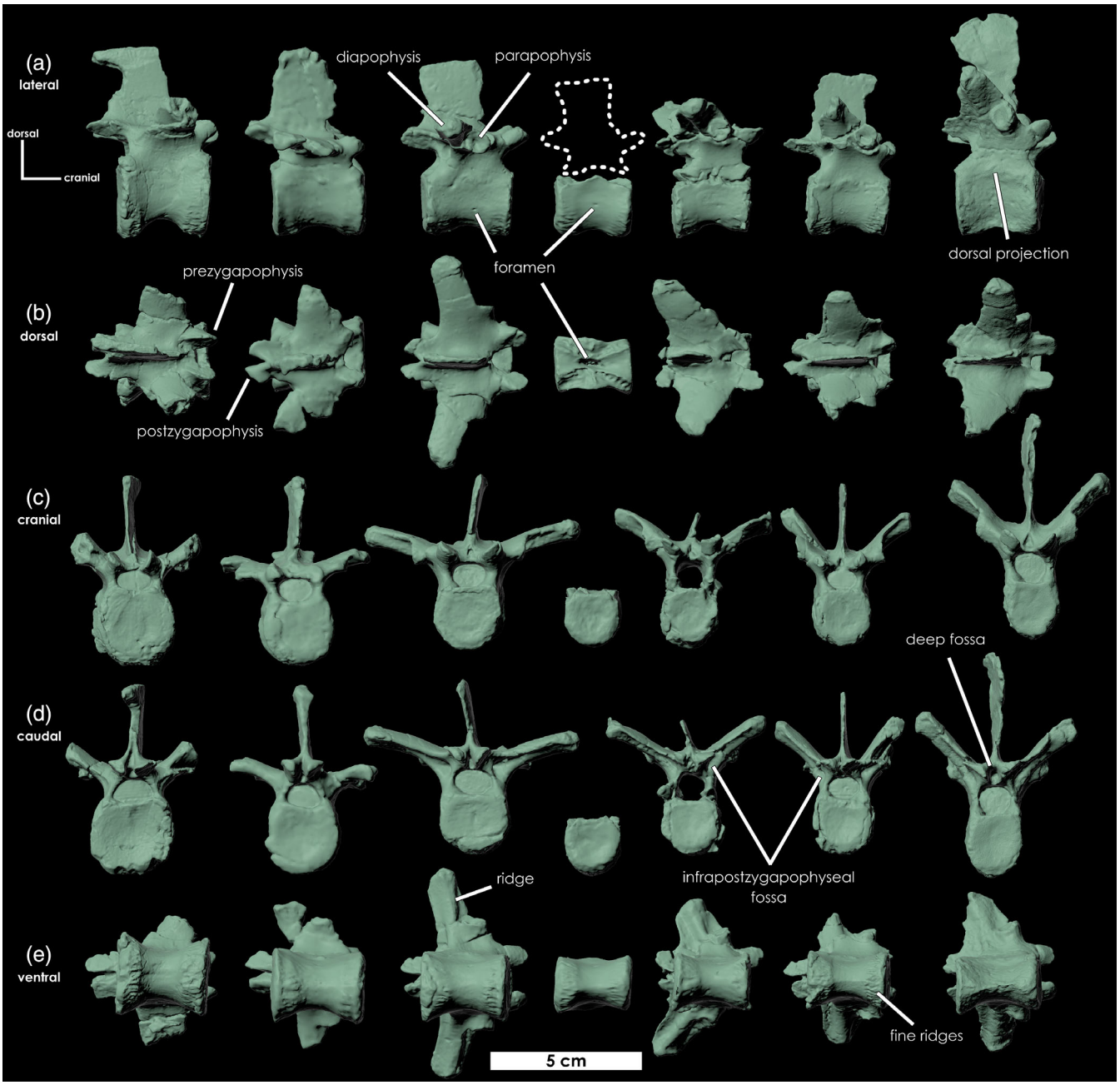

FIGURE 10 Dorsal vertebrae of *Fona herzogae*. Dorsal vertebrae from the Mini Troll and Manolo localities in (a) lateral, (b) dorsal, (c) cranial, (d) caudal, and (e) ventral views. The exact cervical number is unknown. From left to right: NCSM 36207, NCSM 36205, NCSM 36206, FMNH PR 4581, NCSM 36211, NCSM 36208, NCSM 36193. Dashed lines represent missing neural arch.

exhibits a ridge rather than a groove, suggesting this feature may be ontogenetically or intraspecifically variable.

In *Fona*, the neural canal from sacrals three to five (and perhaps the cranial half of six) becomes strongly mediolaterally compressed to form a "V" shape that deeply excavates the centrum. This condition is shared by most *Orodromeus* specimens across sacrals two through five, except for the cranial most sacral on MOR 238, which has a "U" shaped neural canal. In contrast, several isolated juvenile *Oryctodromeus* sacrals from MOR 1636 are "U"-shaped, as well as the fourth sacral of *Koreanosaurus* (Huh et al., 2010), suggesting that this feature may be ontogenetically or intraspecifically variable, or may vary by position throughout the sacral series between different species. The sacral neural spines are mediolaterally thin, craniocaudally broad, and approximately twice the height of the centrum.

The transverse processes of the first and second sacralized dorsals are not fused to associated dorsal ribs, in contrast to *Oryctodromeus* (Krumenacker, 2017).

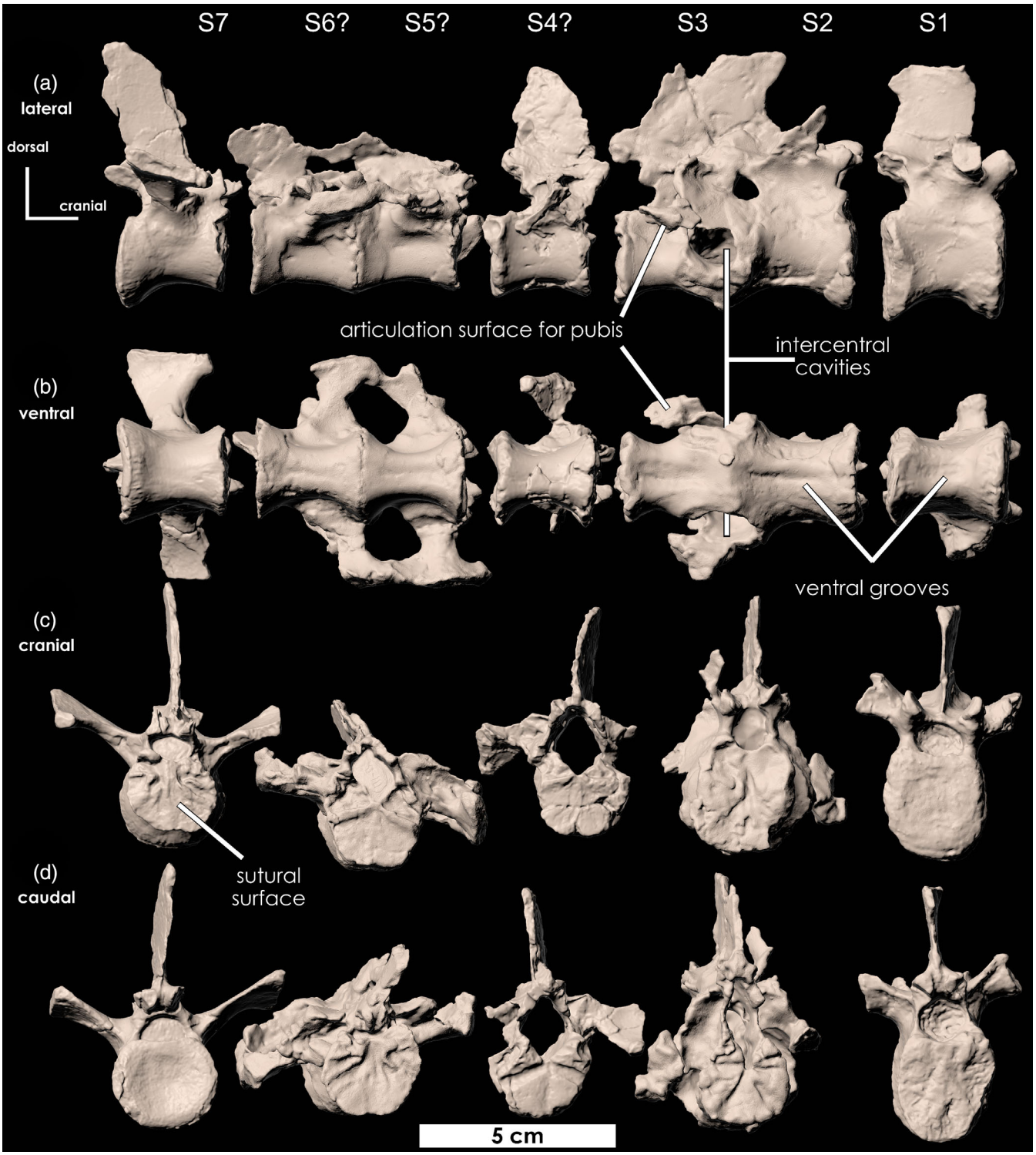

FIGURE 11 Sacral vertebrae of *Fona herzogae*. Reconstructed sacrum of one individual from the Mini Troll locality in (a) lateral, (b) ventral, (c) cranial, and (d) caudal views. From left to right: NCSM 36222, 36219, 36219, 36218, 36218.

Although incompletely preserved, the remaining sacral ribs suture along the cranial margins of the neurocentral sutures on their respective vertebrae. They project laterally, becoming more robust at their flat distal margins, which fuse together to form the iliac attachment. The connection between the second and third fused sacrals is robust and more mediolaterally expanded than the other facet connections in the series, as in TMP 2008.045.0002, *Oryctodromeus*, *Orodromeus*, and *Rhabdodon* (Brown et al., 2013). A robust sacropubal articulation emerges

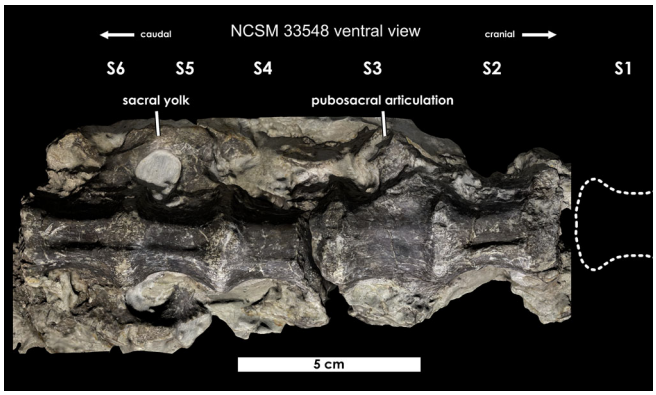

FIGURE 12 Sacrum of *Fona herzogae* NCSM 33548. Reconstruction of the sacrum of *Fona herzogae* in ventral view. Dashed lines represent portions of missing bone.

along the neurocentral suture of the second and third sacrals, and projects ventrolaterally and slightly caudally. On NCSM 36218 massive, laterally symmetrical, intercentral cavities occupy the area directly ventral to the sacropubal articulation, creating a wide cavity that merges internally with the neural canal and another lateral opening that pierces the intervertebral space between the fused zygapophyses (Figure 11a). These ventral openings are absent on NCSM 33548, the other fused pair of sacrals two and three from the Mini Troll locality (NCSM 36217) (Figure 13a,c), and are also absent in the sacrals of all *Th. neglectus*, *Oryctodromeus*, and *Orodromeus* specimens (with the possible exception of MOR 473). Their origin is unclear. The last sacral is craniocaudally asymmetrical, with a caudal articular surface that is both mediolaterally wider and ventrally deeper than the cranial articular surface. The transverse process of the last sacral is relatively more robust than those of preceding sacrals, with thick lateral margins that would have braced the postacetabular process of the ilium.

5.3.6 | Caudal vertebrae

The centra of the first caudal vertebrae are as tall as they are wide, diminishing in height and becoming gradually more elongate caudally. Proximal caudals have skewed profiles in lateral view, with dorsal margins that are slightly more cranially shifted relative to the ventral margins (Figure 14). Their caudoventral chevron facets are more pronounced than the cranial ones, and proximalmost centra possess two deep elliptical lateral pits (Figure 14d), a condition shared by *Zephyrosaurus* (YPM 56695) and some specimens of *Oryctodromeus* (MOR 1642).

The articular surfaces of the centra are smooth and weekly concave, whereas the ventral surface is strongly concave craniocaudally. The ventral surface of some distal caudals bear an elongate groove. This condition is shared by *Orodromeus* (Scheetz, 1999), *Jeholosaurus* (Han et al., 2012), and *Zephyrosaurus* (YPM 56695). In some taxa such as *Parksosaurus* (Sues et al., 2023) and *Oryctodromeus* (Krumenacker, 2017) this groove is present on the proximal caudal vertebrae. In some specimens of *Oryctodromeus* (MOR 1642), this groove is especially prominent, occasionally invading deep into the body of the centra. However, in all proximal caudal vertebrae of *Fona*, these grooves are absent. In ventral view, the centra are spool-shaped with smooth lateral surfaces. Near the distal end of the series, centra become significantly more elongate and their lateral surfaces develop a distinct ridge that runs the length of the centrum. A similar ridge is reported in *Jeholosaurus* (Han et al., 2012), and *Diluvicursor* (Herne et al., 2018).

The transverse processes (=caudal ribs) of the proximal caudals emerge from the neural arch above the suture with the centra. They are slightly dorsally bowed, approximately 1.5 times longer than the length of the centrum and slightly longer than the height of the neural spine, and diminish in length down the series. The ventral surfaces of the proximalmost ribs are marked by either a distinct median groove or ridge that runs the length of the process and attenuates laterally towards the tips; however, they cannot be placed precisely so the positional relationship of these features is unclear. These ridges/grooves appear to be absent in most if not all, specimens of *Oryctodromeus*. Transverse processes diminish in size more rapidly and are lost before the neural spines towards the distal end of the tail.

Neural spines of proximal most caudals are straight and caudally inclined to form an angle of approximately 70° from horizontal. They maintain a consistent craniocaudal width from their base to their tips, gradually becoming more curved and distally expanded down the series. Mid-caudal vertebrae bear lobate neural spines that are wider distally than at their base (FMNH PR 4581).

5.3.7 | Ribs

No axial ribs are preserved in articulation. The capitulum of post-axial cervical ribs is longer than the tuberculum (Figure 15c), a condition shared by *Th. neglectus* (NCSM 15728), *Orodromeus*, *Haya*, *Hypsilophodon*, and *Changchunsaurus* (Barta & Norell, 2021; Butler et al., 2011; Galton, 1974; Scheetz, 1999), but in contrast to the more equally sized capitate processes in *Jeholosaurus* and *Hexinlusaurus* (Barrett et al., 2005; Han et al., 2012). Several caudal cervical ribs bear a lateral ridge that begins at the tubercule junction and attenuates distally (Figure 16). A similar ridge is found in a number of SBEDOs and

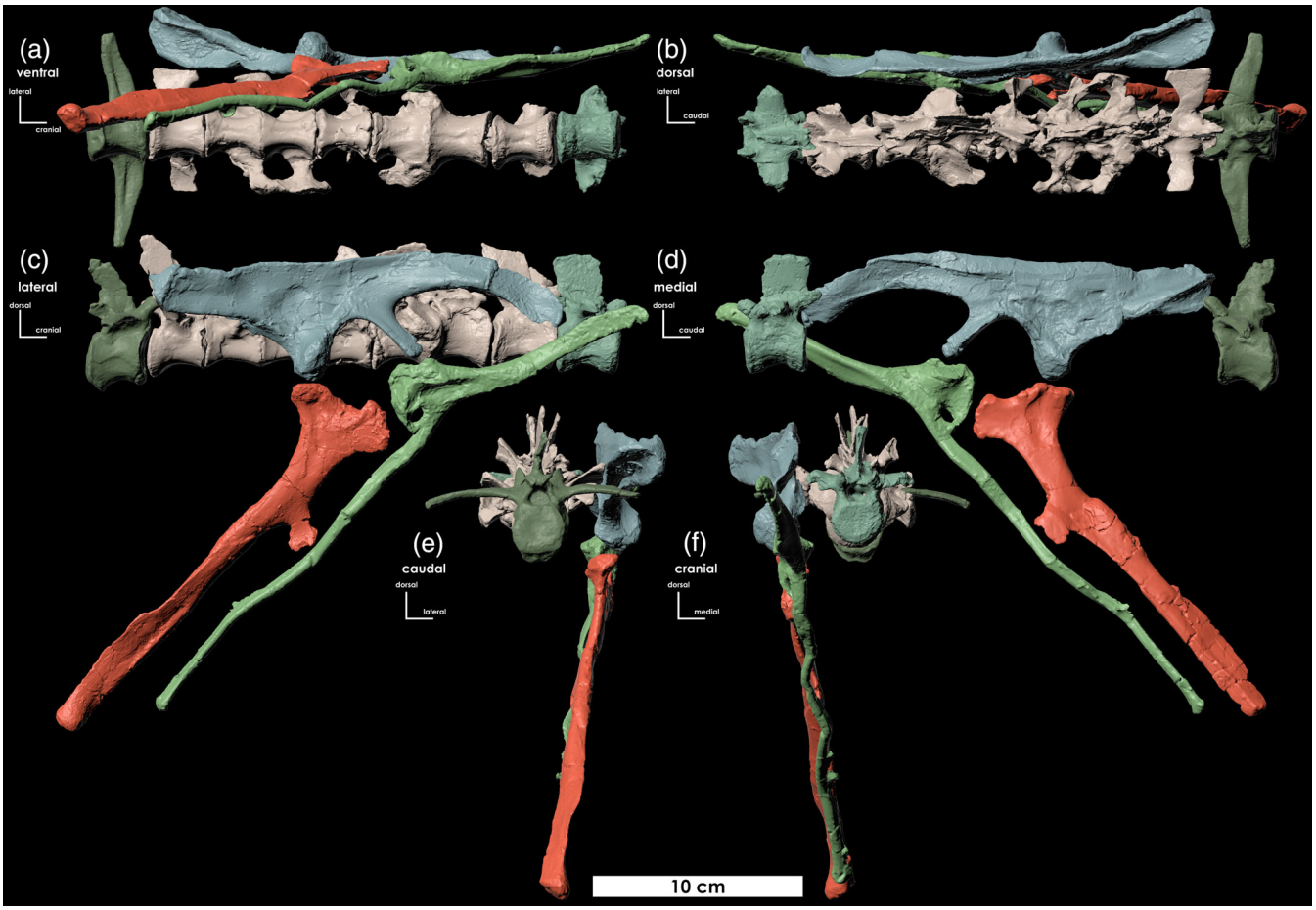

FIGURE 13 Pelvic reconstruction of *Fona herzogae*. Reconstruction of the pelvis of *Fona herzogae* from the Mini Troll locality in (a) ventral, (b) dorsal, (c) lateral, (d) medial, (e) caudal, and (f) cranial views. Ilium (NCSM 36263), ischium in C (NCSM 36259), ischium in D (NCSM 36261), pubis (NCSM 36261). Vertebral column from left to right: NCSM 36212, 36222, 36219, 36219, 36217, 36217, NCSM 36586.

iguanodontians (Barta & Norell, 2021). The caudodorsal margins of these rib shafts form a sharp edge versus the rounder cranioventral margin, and the medial surface is deeply concave to form a "V" shaped cross-section.

The dorsal ribs of NCSM 33548 are preserved in articulation; however, the majority of the proximal and distal ends of cranial dorsal ribs are obscured below partially ossified intercostal plates (Figure 16). Nonetheless, successive ribs appear to increase in length before gradually shortening towards the caudal end of the series. The distance between the capitulum and tuberculum also shortens caudally. Disarticulated cranial dorsal ribs from the Mini Troll locality bear shafts that are extensively laterally bowed, taper distally, and bear an edged caudal margin opposite a rounded cranial margin (Figure 15b). The lateral surface is broadly rounded and the medial surface is slightly flatter and bears a shallow groove that runs parallel to the caudal margin. Caudal dorsal ribs are short, slightly curved, and become splint-like, with a thickened proximal end, a short tapered distal end, and rounded lateral and medial surfaces, forming an oval shape in cross-section (Figure 15a).

5.3.8 | Chevrons

No chevrons are preserved in articulation; however, it can be inferred that longer specimens represent the proximal chevrons, which gradually decrease in length down the series (Figure 15d). Proximally, chevrons maintain parallel cranial and caudal margins down their length. Progressing down the series, the distal ends of chevrons gradually become craniocaudally expanded, a condition shared by a number of SBEDOs such as *Haya* (Barta & Norell, 2021), *Parksosaurus* (Sues et al., 2023), *Gasparinisaura* (Coria & Salgado, 1996), and *Th. neglectus* (Boyd, 2012). In cranial view, the haemal canals form slightly dorsoventrally elongated ellipses that are restricted to the proximal end, in contrast to the more ventrally descending canals of *Haya* (Barta & Norell, 2021). No chevrons are fused or curved in lateral view. This is in contrast

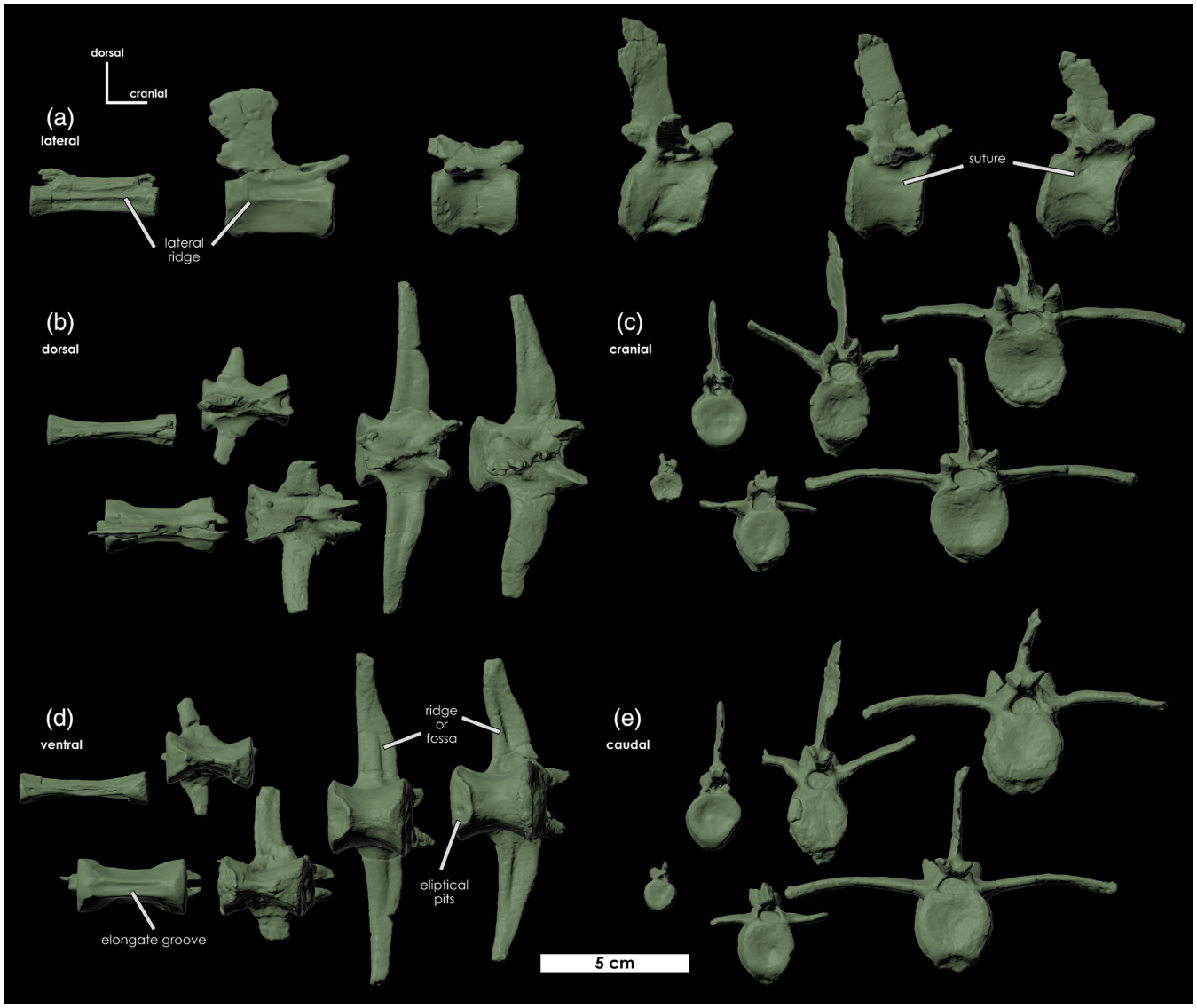

FIGURE 14 Caudal vertebrae of *Fona herzogae*. Caudal vertebrae from the Mini Troll and Manolo localities in (a) lateral, (b) dorsal, (c) cranial, (d) ventral, and (e) caudal views. The exact cervical number is unknown. From left to right: NCSM 36199, FMNH PR 4581, NCSM 36197, NCSM 36216, NCSM 36215, NCSM 36212.

to *Th. neglectus* (NCSM 15728), in which the first two chevrons attached to the cranial and caudal facets of the second proximal caudal become fused immediately distal to their proximal contacts, forming a distally tapering, craniocaudally compressed shaft that bows slightly cranioventrally. This feature may be an as-of-yet unrecognized autapomorphy of *Th. neglectus*.

5.3.9 | Ossified tendons

The presence, density, distribution, arrangement, and preservation of tendons can vary widely across neornithischians such as *Psittacosaurus* and *Ischioceratops* (He et al., 2015; Sereno & Chao, 1988). They are not preserved in the tails of *Orodromeus*, *TMP 2008.045.0002* (Brown et al., 2013), *Agilisaurus* (Peng, 1992), *Jeholosaurus* (Han et al., 2012), *Minimocursor* (Manitkoon, Deesri, Khalloufi, et al., 2023), *Changmiania* (Yang et al., 2020), and *Heterodontosaurus* (Norman et al., 2011). However, they are present along the dorsals and/or sacral vertebrae of TMP 2008.045.0002, *Agilisaurus*, *Camptosaurus* (Carpenter & Galton, 2018), *Valdosaurus* (Barrett, 2016), *Convolosaurus* (Andrzejewski et al., 2019), *Changchunsaurus* (Butler et al., 2011), *Changmiania*, *Haya* (Barta & Norell, 2021), *Heterodontosaurus*, *Jeholosaurus*, *Lesothosaurus* (Baron et al., 2017), *Nanosaurus* (BYU 631), *Orodromeus*, and *Talenkauen* (Rozadilla et al., 2019). In *Tianyulong* (Zheng et al., 2009), *Hexinlusaurus* (He & Cai, 1983), *Minimocursor*, *Hypsilophodon* (Galton, 1974), *Th. neglectus*, *Parksosaurus* (Sues et al., 2023),

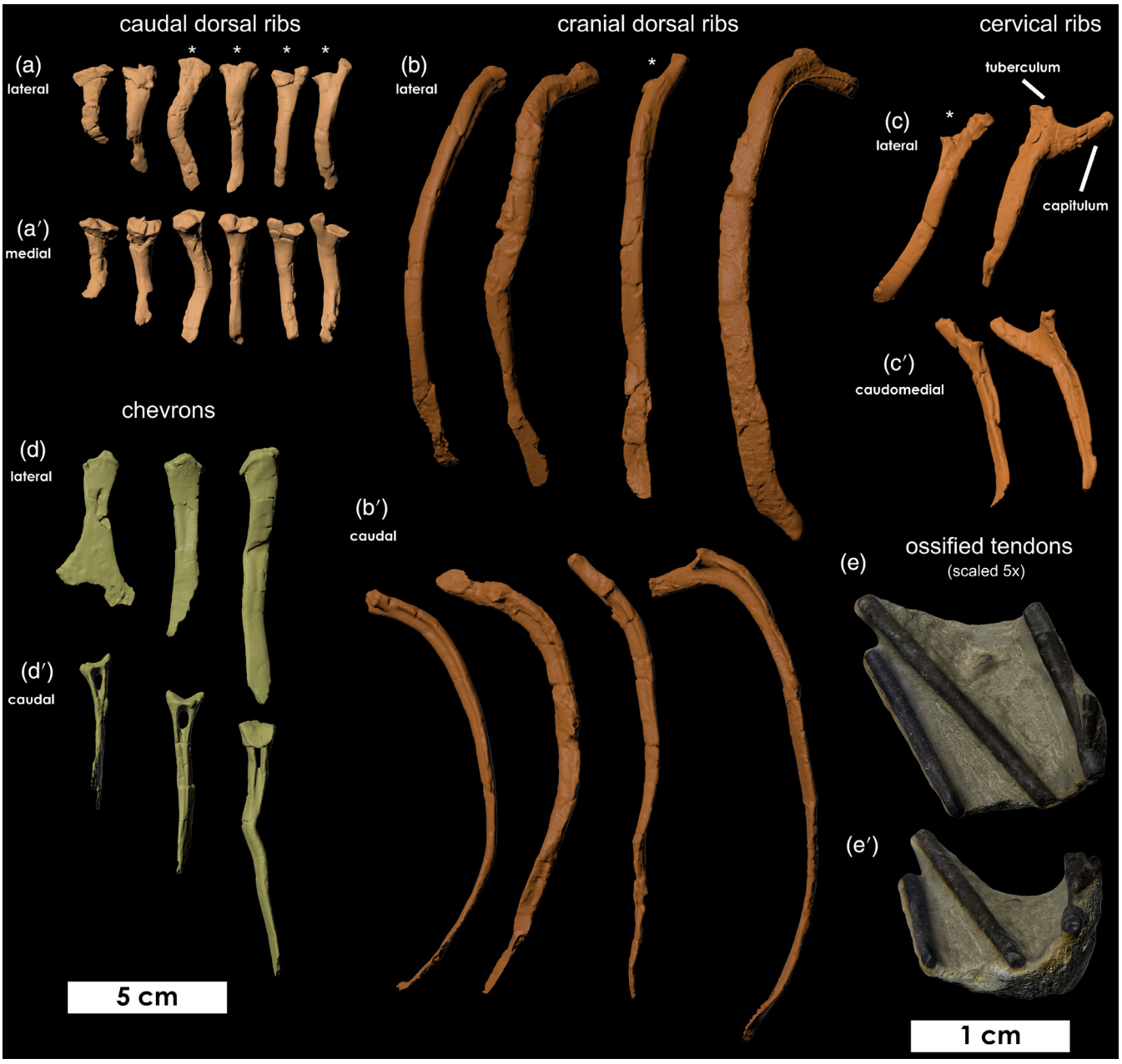

FIGURE 15 Ribs, chevrons, and tendons of *Fona herzogae*. Ribs, chevrons, and ossified tendons from the Mini Troll locality. Caudal dorsal ribs in (a) lateral and (a') medial views. From left to right: NCSM 36235, 36236, 36234, 36233, 36232, 36231. Cranial dorsal ribs in (b) lateral and (b') caudal views. From left to right: NCSM 36230, 36229, 36228, 36227. Cervical ribs in (c) lateral and (c') caudomedial views. NCSM 36226 (left), NCSM 36225 (right). Chevron/haemal arches in (d) lateral and (d′) caudal views. From left to right: NCSM 36239, 36238, 36237. (e) Disarticulated ossified tendons (NCSM 36224) embedded in the original matrix and scaled up five times for visibility. Mirrored elements are denoted noted with an asterisk.

Oryctodromeus (Krumenacker, 2017), and *Te. tilletti* (Forster, 1990) ossified tendons are distributed across dorsal, sacral, and at least some caudal vertebrae. In *Tianyulong* (Sereno, 2012), *Hypsilophodon*, *Parksosaurus*, *Convolosaurus*, possibly *Anabisetia* (Coria & Calvo, 2002), and some specimens of *Oryctodromeus*, the majority of the tail vertebrae are partially encased in a dense sheath of non-hatched, parallel-arranged, epaxial and hypaxial tendons, a condition shared by *Te. tilletti* (Forster, 1990). This is in contrast to the sparse arrangement of caudodorsally oriented epaxial tendons of *Th. neglectus* (NCSM 15728).

On NCSM 33548 epaxial ossified tendons run in parallel near the medial surface of the ilia, with a denser distribution near the preacetabular process. Additionally, numerous tendon pieces were recovered from the surrounding matrix during the preparation of NCSM 33548 and other

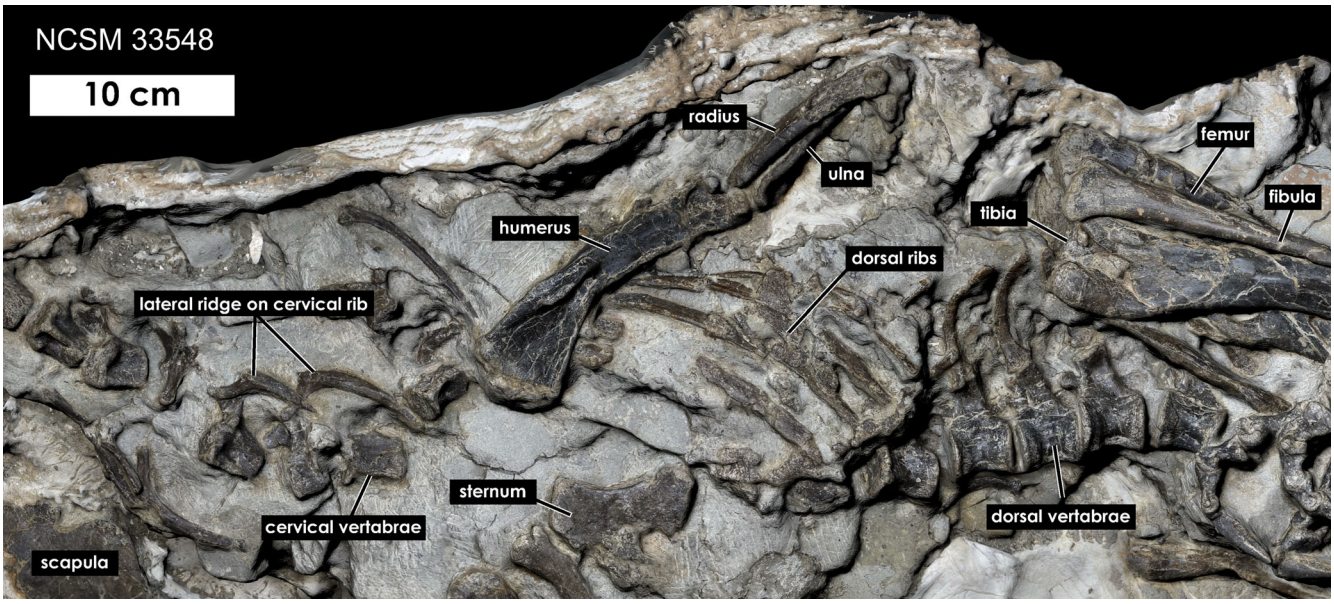

FIGURE 16 Ribcage of *Fona herzogae* NCSM 33548. Articulated neck, chest, forelimb, abdomen, and pelvis of NCSM 33548in oblique left lateral view.

specimens from the Mini Troll and Last Chance Theropod localities (Figure 15e). A portion of articulated distal vertebrae from NCSM 33548 shows several tendons in close proximity and aligned nearly parallel to the centra.

The cross-sections of tendons can range from circular to oval or moderately compressed profiles (Data S6). In *Fona* ossified tendon bundles are preserved in near articulation on FMNH PR 5102. Tendon bundles extend epaxially covering the zygapophyses in lateral view, and hypaxially covering the proximal parts of the chevrons. The tendon bundles are slightly separated at some joints revealing that there are six or more tendons at any section. The tendons run in parallel, not lattice-like as in iguanodontians.

5.3.10 | Sternum

NCSM 33548 preserves an articulated pair of partially preserved sternals. In *Th. neglectus* and *Haya*, the paired sternals form a "V" shape in cross-section, with their broadest margin facing laterally, however on NCSM 33548 the broadest margin faces ventrally, likely due to taphonomy (Figure 17a). In ventral view, they form a "V" shaped profile, contacting each other along their cranial margins. They are about twice as long as wide, in contrast to the more robust and broader sternals of *Oryctodromeus* (MOR 1642). The lateral margin of the left sternal (Figure 17a; shown on the right) is thicker and more rounded than the medial margin and bows strongly medially as in *Haya* (Barta & Norell, 2021), in contrast to the weaker curve of *Orodromeus* (Scheetz, 1999) and *Oryctodromeus* (MOR 1642). However, the lateral margin of the contralateral sternal is less curved, suggesting that this feature may be intraspecifically or taphonomically variable. The boundary of the medial margin for both sternals is difficult to discern due to its thin edge, which is damaged. Nonetheless, under close inspection, it appears the margin is concave. If a correct interpretation, this would be a synapomorphy with *Th. neglectus*, in which the sternals are expanded at their cranial and caudal ends and constricted in the middle (Boyd, 2012), in contrast to *Orodromeus*, *Oryctodromeus*, *Parksosaurus* (Sues et al., 2023), *Haya* (Barta & Norell, 2021), *Changchunsaurus* (Butler et al., 2011), *Hypsilophodon* (Galton, 1974), *Camptosaurus* (Dodson & Madsen, 1981), and *Dryosaurus* (Galton, 1981), which have broadly convex medial margins, or *Macrogryphosaurus*, which has triradiate sternals (Calvo et al., 2007).

Ossified sternal ribs are present, as in *Th. neglectus* (Boyd et al., 2011), *Parksosaurus* (Sues et al., 2023), *Hypsilophodon* (Galton, 1974), and *Othnielosaurus* (Galton & Jensen, 1973). The surface of the bone is highly rugose as in *Th. neglectus* (NCSM 15728), but in contrast to the smoother surface of *Parksosaurus* (Sues et al., 2023, figure 12). Although the ventral aspect of the dorsal ribcage is poorly preserved on NCSM 33548, partially ossified bone material, which may correspond to additional sternal ribs, contacts the distal ends of the first four dorsal ribs (Figure 16).

5.3.11 | Costal plates

Ossified intercostal plates are present in *Fona* (Figure 17), as in *Th. neglectus* (Boyd et al., 2011), *Othnielosaurus*

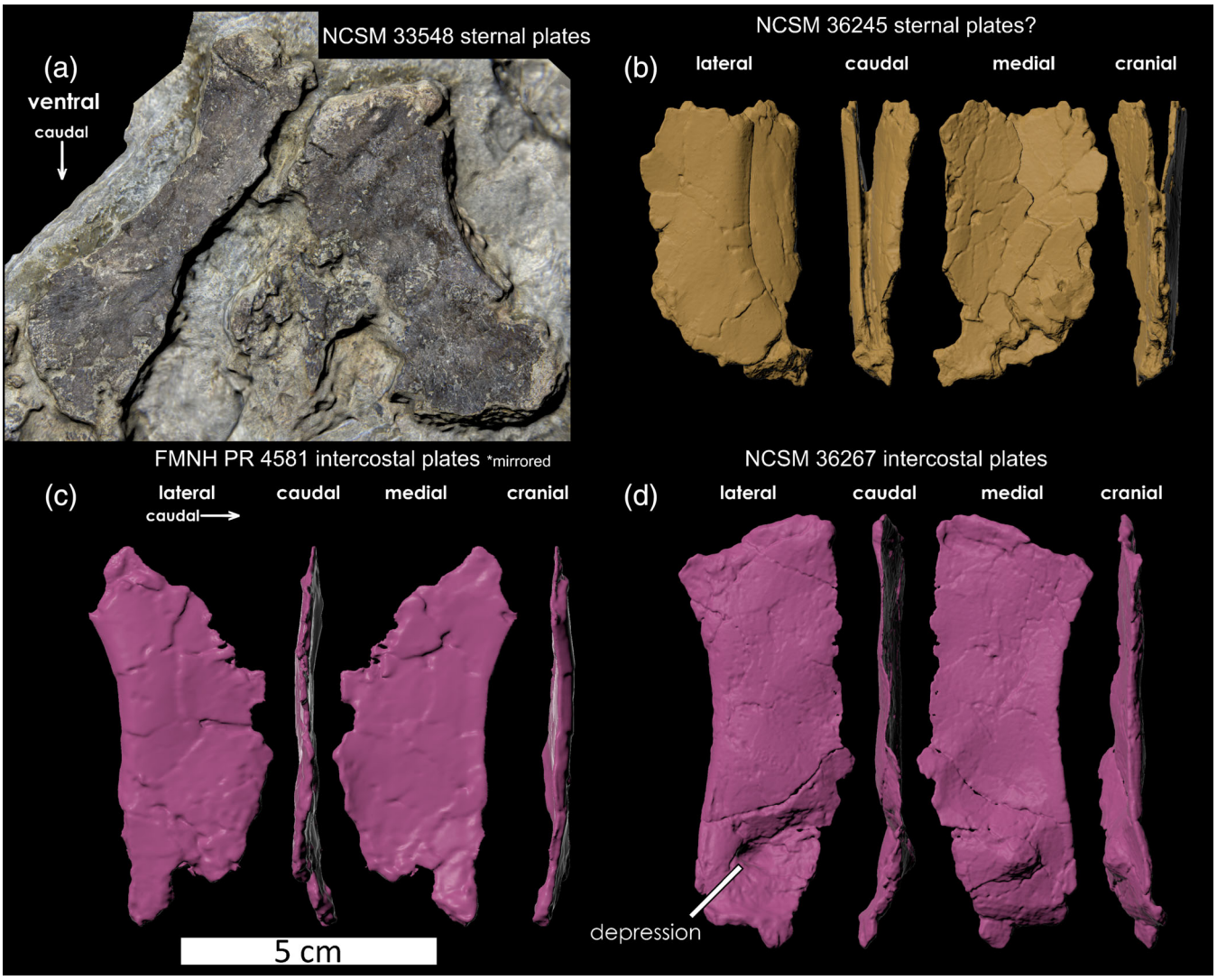

FIGURE 17 Sternal and costal plates of *Fona herzogae*. (a) Articulated sternal plates of NCSM 33548 in ventral (=lateral) view, (b) sternal? plates, (c) costal? plates (d) costal plates. Mirrored elements are noted in the figure.

(Galton, 2012), *Parksosaurus* (Sues et al., 2023), *Hypsilophodon* (Butler & Galton, 2008), *Talenkauen* (Agnolín et al., 2024), *Mahuidacursor* (Cruzado-Caballero et al., 2019), and *Macrogryphosaurus* (Calvo et al., 2007). Disarticulated intercostals may also be present in *Oryctodromeus* (MOR 1642). on NCSM 33548 the intercostal plates are preserved in partial articulation across the dorsal ribcage, but they appear to be only partially ossified and/or poorly preserved, with indiscernible margins (Figure 16). However, disarticulated intercostal plates are preserved from the Mini Troll locality.

NCSM 36267 is a single complete, disarticulated plate. In lateral view, it is a mediolaterally flattened rectangular-shaped bone with a dorsoventral height three times longer than rostrocaudally wide. The medial surface is weakly concave, and the lateral surface is weakly convex. The cranial margin is the thickest part of the element and forms a rounded profile in cross-section. Progressing caudally, the thickness of the element gradually decreases to a thin edge, as in *Th. neglectus* (Boyd et al., 2011: figure 1b). In lateral view, the ventral third is characterized by a prominent depression. This depression is also present on three of the four cranial most intercostal plates of *Th. neglectus* (NCSM 15728). We interpret the element to likely represent the cranial most intercostal plate, as it shares a number of morphological similarities with the first right intercostal plate of NCSM 15728 (Boyd et al., 2011), which is also tall and lacks the larger "D" shaped profile of its preceding neighbors. An additional specimen (NCSM 36245) is either a partially preserved set of two articulated intercostal plates missing their dorsal portions or a partially preserved paired sternum (Figure 17b).

5.4 | Appendicular skeleton

5.4.1 | Scapula

Fona is represented by five scapulae. *Fona* and *Oryctodromeus* share a number of unique morphological conditions (Figure 18). For description, we orient the scapula with its long axis dorsoventrally. The scapula is robust, with a flared distal end that is as wide as the articulation for the coracoid, but separated from it by a narrow neck forming the base of the scapular blade. The angle between the acromion process and the craniodorsal margin of the scapula is approximately 105°, in contrast to other SBEDOs that have broader angles of ~150°. However, it is possible this condition is intraspecifically or taphonomically variable, as a few of the scapulae of *Fona* and *Oryctodromeus* have angles closer to 130°. The distal margin of the scapular blade (the margin between the inferior and superior angles sensu Fearon and Varricchio (2015) forms a rounded profile and is parallel with the curved caudal margin of the scapula, as in *Oryctodromeus*). In contrast, these margins form more of an acute angle in other SBEDOs such as *Th. neglectus*, *Changchunsaurus* (Jin et al., 2010), and *Koreanosaurus* (Huh et al., 2010). There is a low, moundlike tuberosity on the medial surface of scapulae of *Fona* and *Oryctodromeus*, located at the narrowest part of the neck, directly opposite the glenoid ridge. This medial tuberosity is absent in nearly all other SBEDOs except for at least one specimen of *Th. neglectus* (USNM V 7760). Similarly, a subtle bulge is located at the contact with the coracoid in some specimens of *Orodromeus* (MOR 294) as well as *Hypsilophodon*, the latter of which also bears a gentle medial fossa that extends from the coracoid foramen onto the scapula (Galton, 1974, figure 37). Additionally, several early diverging iguanodontians (Zanno, Gates, et al., 2023) and ornithopods of ambiguous taxonomic affinity such as *Convolosaurus* (Andrzejewski et al., 2019) and a specimen from the Early Cretaceous Otway Group of Australia have an elongate ridge or possibly a raised bump (Chanthasit, 2010, figure 4.22 B) in this same location. Lastly, the right scapula of *Othnielosaurus* (SMA 0010) bears a pronounced and sharp protuberance on the medial surface of the neck that borders the caudal margin. However, it is absent on the left.

Along the acromion process, *Oryctodromeus* has a distinct, thinly edged, scapular spine that becomes ventrally folded along its distal half, a condition shared with only *Orodromeus* (Avrahami et al., 2022). However, in six out of seven scapulae of *Fona* from multiple localities, the edge of this spine bears a much more rounded profile, with the seventh scapula (NCSM 36272) showing a somewhat sharper edge forming a triangular cross-section, but still lacking the distinct ventrally folded blade.

As in *Oryctodromeus*, the cranial and caudal margins are extensively striated, likely indicating muscle attachment sites (Fearon & Varricchio, 2016). A prominent supraglenoid boss occupies the lateral sutural surface and spans the suture between the scapula and coracoid in *Haya* (Barta & Norell, 2021), *Oryctodromeus*, and *Orodromeus*. This boss is present with varying degrees of prominence in *Oryctodromeus* and is significantly reduced or absent in all scapulae of *Fona* (Figure 18), except for NCSM 33548 (Figure 19), suggesting it may be intraspecifically variable. The supraglenoid fossa of *Yueosaurus* (Zheng et al., 2012) is only obvious on two *Fona* scapulae, being absent or subtle on all others, suggesting that this feature may also be intraspecifically variable. A distinct foramen is present at the deepest part of the fossa on NCSM 36272. There is no sign of a suprascapula, in contrast to the condition in *Heterodontosaurus* and *Parksosaurus* (Radermacher et al., 2021; Sues et al., 2023).

5.4.2 | Coracoid

Fona is represented by several coracoids from multiple localities (Figure 19). Overall, the coracoid is quadrangular in shape and similar in morphology to *Oryctodromeus*, having a large, hatchet-shaped sternal process that extends farther caudally than the coracoid's contribution to the glenoid process. The narrow and less circular shape of the coracoid glenoid is also similar to the condition in *Oryctodromeus* and *Koreanosaurus* (Huh et al., 2010). Krumenacker (2017) identified a lateral fossa near, and a ventral fossa within, the glenoid fossa as variably present in *Oryctodromeus*. The ventral fossa is present in *Orodromeus* and *Koreanosaurus* (Huh et al., 2010, figure 10a), and the lateral fossa seems to be present in *Fona* and variably present in *Orodromeus*. We consider these fossae to likely represent a single individual complex, which suggests they could represent transient or intraspecifically variable features shared among these taxa.

5.4.3 | Humerus

The humerus is similar in overall morphology to that of other SBEDOs in having modestly expanded proximal and distal ends and a relatively straight shaft distal to the deltopectoral crest. The humeral head is mediolaterally expanded and round across the proximal surface, with weakly defined lateral and medial tuberosities (Figure 20), in contrast to the slightly more well-defined tuberosities of *Koreanosaurus* (Huh

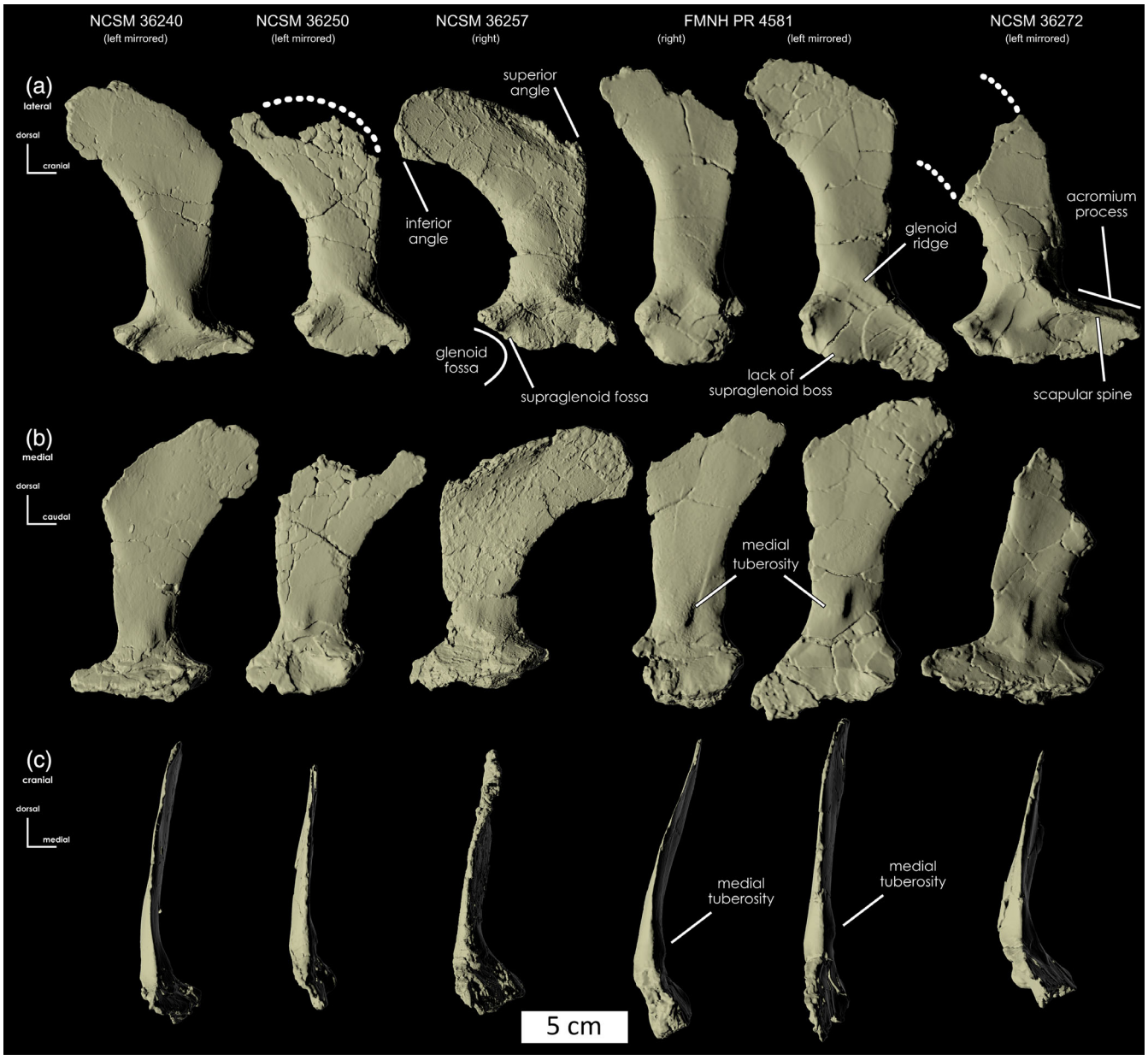

FIGURE 18 Unfused Scapulae of *Fona herzogae*. Unfused scapula of *Fona herzogae* from multiple localities in (a) lateral, (b) medial, and (c) cranial views [with the long axis of scapulae oriented vertically]. Dashed lines represent portions of missing bone. Mirrored elements are noted in the figure.

et al., 2010), or the distinct and well-separated tuberosities of *Zephyrosaurus* (OMNH 32813) (Avrahami, Hauser, & Zanno, 2023). Medial to the deltopectoral crest, the cranial surface is slightly concave to form the bicipital sulcus, a condition shared by many SBEDOs except for *Haya* (Barta & Norell, 2021). In cranial view, the deltopectoral crest extends along the lateral edge, causing the proximal half of the humerus to be mediolaterally expanded, though perhaps not as much as *Koreanosaurus* (Huh et al., 2010). In lateral or medial views, the crest projects cranially and bears a rounded apex that is slightly more pronounced and angular than in *Th. neglectus*, *Haya* (Barta & Norell, 2021), and *Othnielosaurus* (YPM 1235), but less prominent than *Orodromeus* (Scheetz, 1999), *Zephyrosaurus* (OMNH 32813), some specimens of *Oryctodromeus*, and *Convolosaurus* (SMU 72834). The base of the crest merges gradually with the humeral shaft, which has a circular cross-section. The apex of the crest, as well as a foramen located on the opposite caudal surface, occur halfway between the midshaft and the head, in contrast to *Th. neglectus*, in which the crest and foramen occur more distally near the midshaft. In cranial view, the ulnar condyle of one humerus (NCSM 36251) is slightly larger and extends slightly further distally than the radial condyle. A similar condition is present in

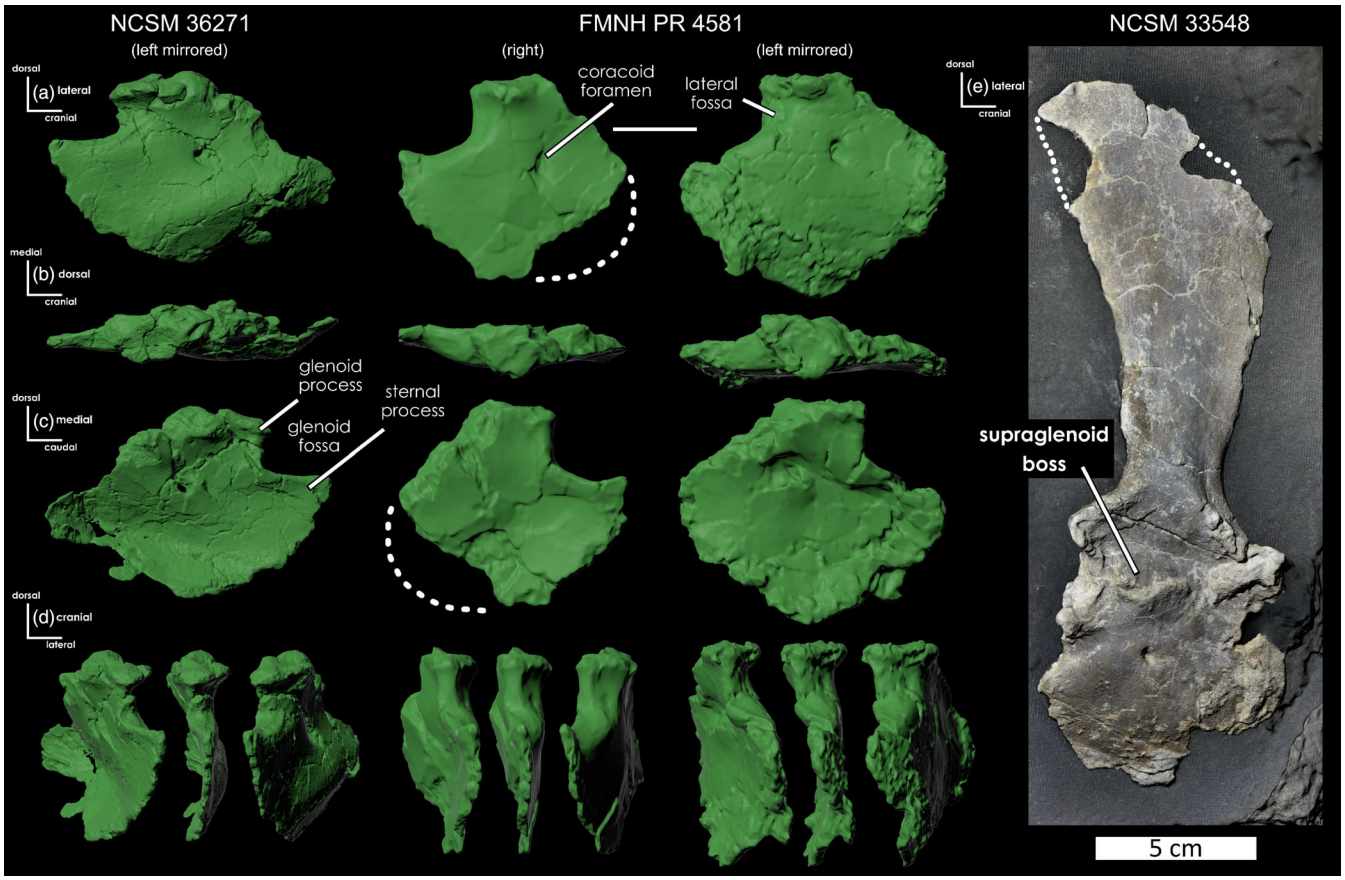

FIGURE 19 Coracoid and Scapulocoracoid of *Fona herzogae*. Coracoids in (a) lateral, (b) dorsal, (c) medial, and (d) craniomedial, cranial, and craniolateral views. (e) Fused scapulocoracoid of NCSM 33548 in lateral view. Dashed lines represent portions of missing bone. Mirrored elements are noted in the figure.

Koreanosaurus (Huh et al., 2010), whereas, in other SBEDOs such as *Oryctodromeus* and *Haya*, the condyles are equally sized. However, the lack of this feature in two other *Fona* humeri (NCSM 36242 and FMNH PR 4581) may suggest it is variable.

5.4.4 | Ulna

In lateral view, the ulna has a straight profile that is robust proximally and tapers distally, flaring at the distalmost end (Figure 21). The ulna is relatively more slender and elongate than in *Orodromeus*, *Haya*, and *Thescelosaurus*, with similar proportions to those of *Oryctodromeus*. Likewise, the olecranon process extends slightly beyond the humeral facet, a condition shared by many other SBEDOs. However, on NCSM 33548 the proximal end bears a rounded profile in lateral view (Figure 22), as in some specimens of *Oryctodromeus* (e.g., MOR 1636), which have the humeral facet located more medially.

The medial surface of the ulnar shaft is flat, giving it a "D" shaped cross-section. This is in contrast to the weakly concave medial surfaces of *Hypsilophodon* and the more prominently concave surface of *Oryctodromeus* (Galton, 1974; Krumenacker, 2017). The ventral margin near the proximal end of the ulna is slightly keeled in some specimens, a condition shared by *Koreanosaurus*, and some specimens of *Haya* (Barta & Norell, 2021) and *Oryctodromeus* (MOR 1642), but in contrast to the rounded margin in *Hypsilophodon* (Galton, 1974) and *Orodromeus* (contra Huh et al., 2010). A wide but subtle longitudinal groove runs across the lateral surface of one ulna (NCSM 36246) but is absent in another (FMNH PR 4581). This condition is variable between two ulnae of *Oryctodromeus* and some specimens of *Haya* (Barta & Norell, 2021). There is no foramen across the dorsolateral surface, in contrast to *Th. neglectus* (NCSM 15728).

5.4.5 | Radius

The radii of *Fona* from the Mini Troll locality are moderately to poorly preserved in some areas (Figures 21 and 22). The midshaft has a circular cross-section, in contrast to the mediolateral compression of *Haya* (Barta & Norell, 2021). In dorsal view, a ridge extends along the length of the shaft,

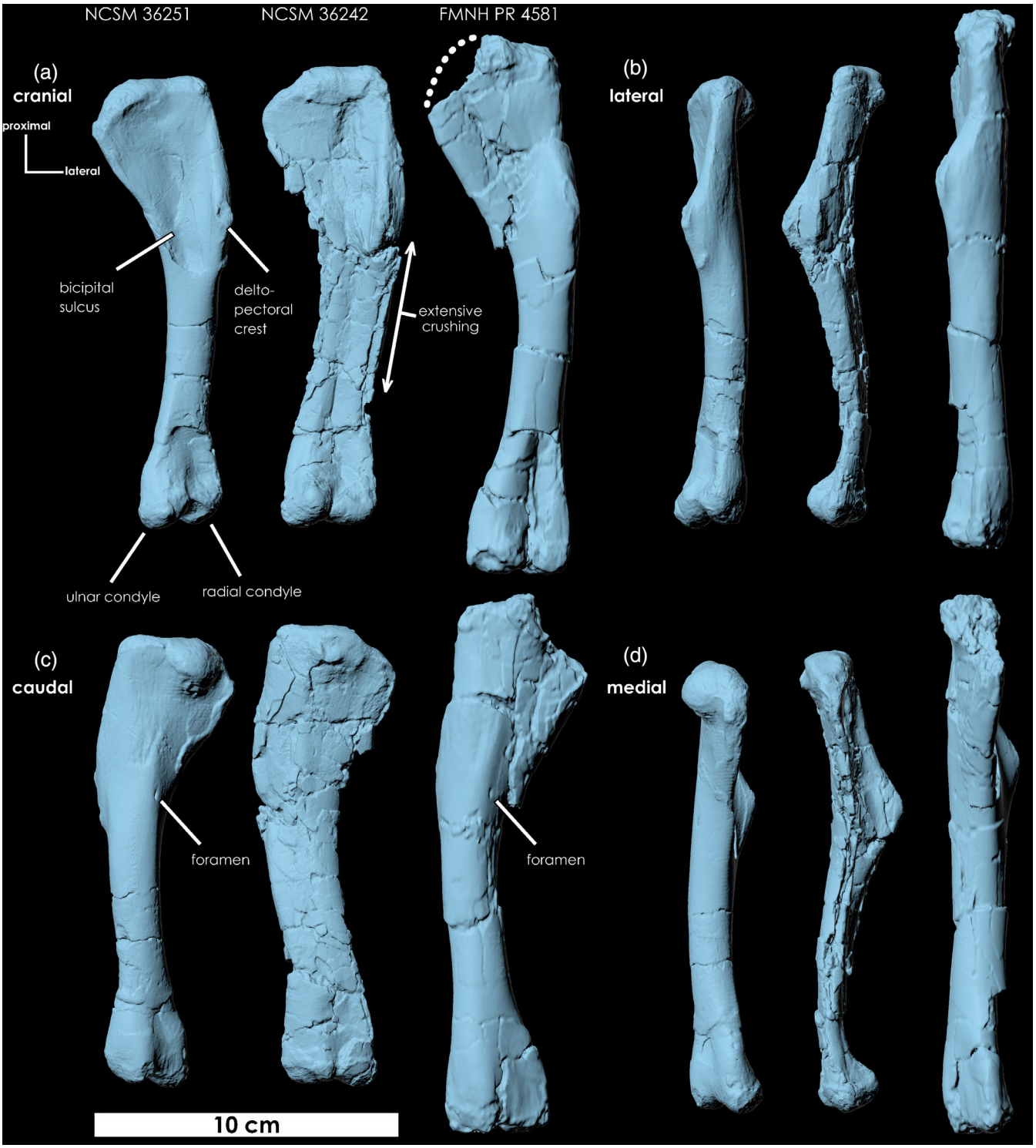

FIGURE 20 Humeri of *Fona herzogae*. Left humeri of *Fona herzogae* from multiple localities in (a) cranial, (b) lateral, (c) caudal, and (d) medial views. Dashed lines represent portions of missing bone.

as in *Haya* (Barta & Norell, 2021) and *Orodromeus* (MOR 473). Although poorly preserved, the proximal articular surfaces of NCSM 36247 and 36248 appear to be flat but could have been slightly concave as in *Haya*, *Orodromeus* (Barta & Norell, 2021; Scheetz, 1999), *Th. neglectus*, and some specimens of *Oryctodromeus* (MOR 1642).

5.4.6 | Manus

The following description of the manus follows the orientation of (Barta & Norell, 2021), in which the palmar and ventral surface are synonymous, the antipalmar and dorsal surface are synonymous, and digit I is medial. Few

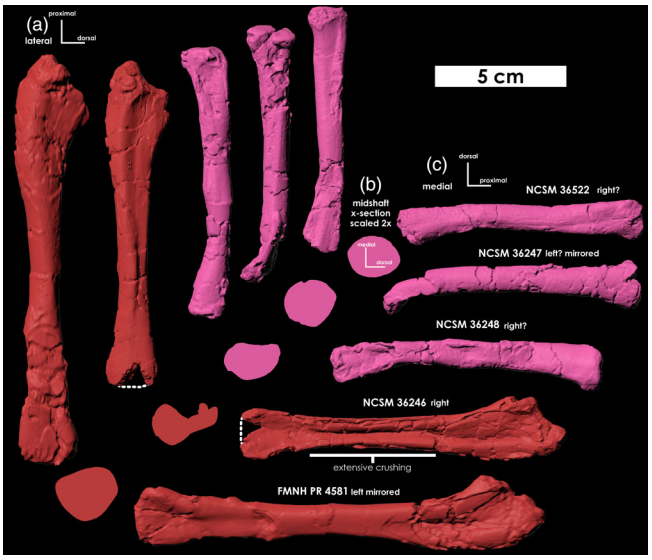

FIGURE 21 Ulna of *Fona herzogae*. Ulnae (bottom left) and radii (top right) of *Fona herzogae* from multiple localities in (a) lateral and (c) medial views. (b) The shape of the cross-section at midshaft. Dashed lines represent portions of missing bone. Mirrored elements are noted in the figure.

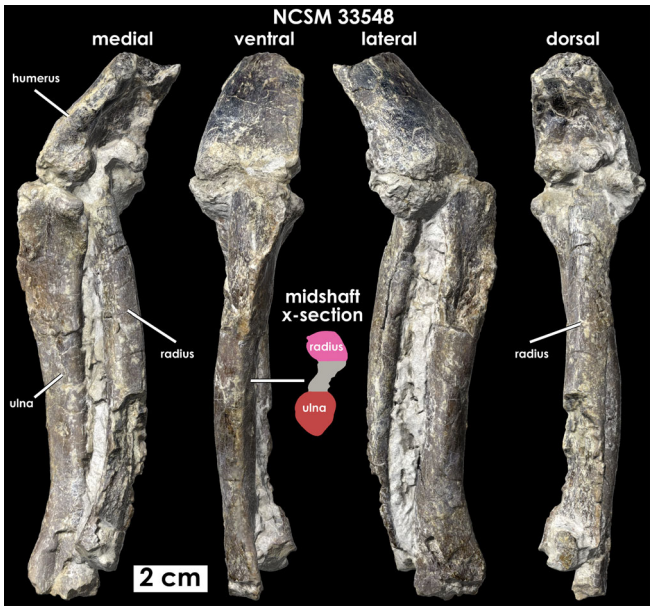

FIGURE 22 Ulna and radius of *Fona herzogae* NCSM 33548. Articulated left ulna, radius, and distal humerus of *Fona herzogae* (NCSM 33548).

manual elements are preserved from the Mini Troll locality. These include two metacarpals, a manual phalanx, and a distal ungual. NCSM 33548 preserves the first three metacarpals in partial articulation, with the fourth and fifth either absent or not preserved (Figure 23).

On NCSM 33548 the second and third metacarpals are ~33% longer than the first. This is in contrast to the equal length of the respective metacarpals of *Th. neglectus* (NCSM 15728), or MCI of the Kaiparowits orodromine, which is only ~15% shorter than MCII–IV (Boyd, 2012; Gates et al., 2013). NCSM 36253 is likely a left MCI, bearing a deeper ligament pit on its lateral side. It is half the length of either MCII, III, or IV (NCSM 36249), a condition more reminiscent of *Heterodontosaurus* (SAM-K1332), *Minimocursor* (Manitkoon, Deesri, Khalloufi, et al., 2023), and *Changmiania* (Yang et al., 2020).

In palmar view, the collateral distal condyles of MCII or III (NCSM 36249) are prominent and bear a groove between them. Manual phalanges are square in palmar view and bear shallow collateral ligament pits.

Most manual claws are triangular in palmar view, and in medial view the dorsal and ventral margins are broadly curved dorsally, converging to a sharp distal point, in contrast to the much flatter profile of the pedal unguals (Figure 23b). Manual ungual I and II from the left manus of *Th. neglectus* (NCSM 15728) are likewise triangular and strongly pointed distally. In contrast, a single disarticulated manual ungual found near the distal ends of the left radius and ulna of NCSM 33548 is more spade-shaped, with rounder lateral and medial margins that converge distally to form a blunt tip (Figure 23c). Additionally, the center of its proximal articular surface bears a prominent circular sulcus, in contrast to the broadly rounded surfaces of the triangular unguals. All unguals are symmetrical in contrast to the medially curved unguals of *Th. neglectus* (NCSM 15728), and likewise lack the prominent medial and lateral hooks near the proximal articular ends of *Th. neglectus* (NCSM 15728).

5.4.7 | Ilium

The dorsal margin of the ilium has a flat to sigmoidal profile in lateral view (Figure 24), a condition shared by *Oryctodromeus* (Krumenacker, 2017), *Thescelosaurus* (Boyd, 2012), *Hexinlusaurus* (He & Cai, 1983), *Dryosaurus* (Galton, 1981), *Dysalotosaurus* (Hübner, 2011), *Eousdryosaurus* (Escaso et al., 2014), *Gasparinisaura* (Coria & Salgado, 1996; Salgado et al., 1997), some specimens of *Convolosaurus* (SMU 77617) (Andrzejewski et al., 2019), and the iguanodontians *Te. tilletti* (Forster, 1990) and *Camptosaurus dispar* (Carpenter & Galton, 2018). This is in contrast to several SBEDOs that have a strongly crescentic dorsal margin such as *Orodromeus* (Scheetz, 1999), *Zephyrosaurus* (Avrahami, Hauser, & Zanno, 2023), TMP 2008.045.0002 (Brown et al., 2013), *Haya* (Barta & Norell, 2021), *Hypsilophodon* (Galton, 1974), and *Jeholosaurus* (Han et al., 2012). The lateral surface of the ilium is craniocaudally concave and the preacetabular process is ventrally hooked ~30° from the long axis of the ilium.

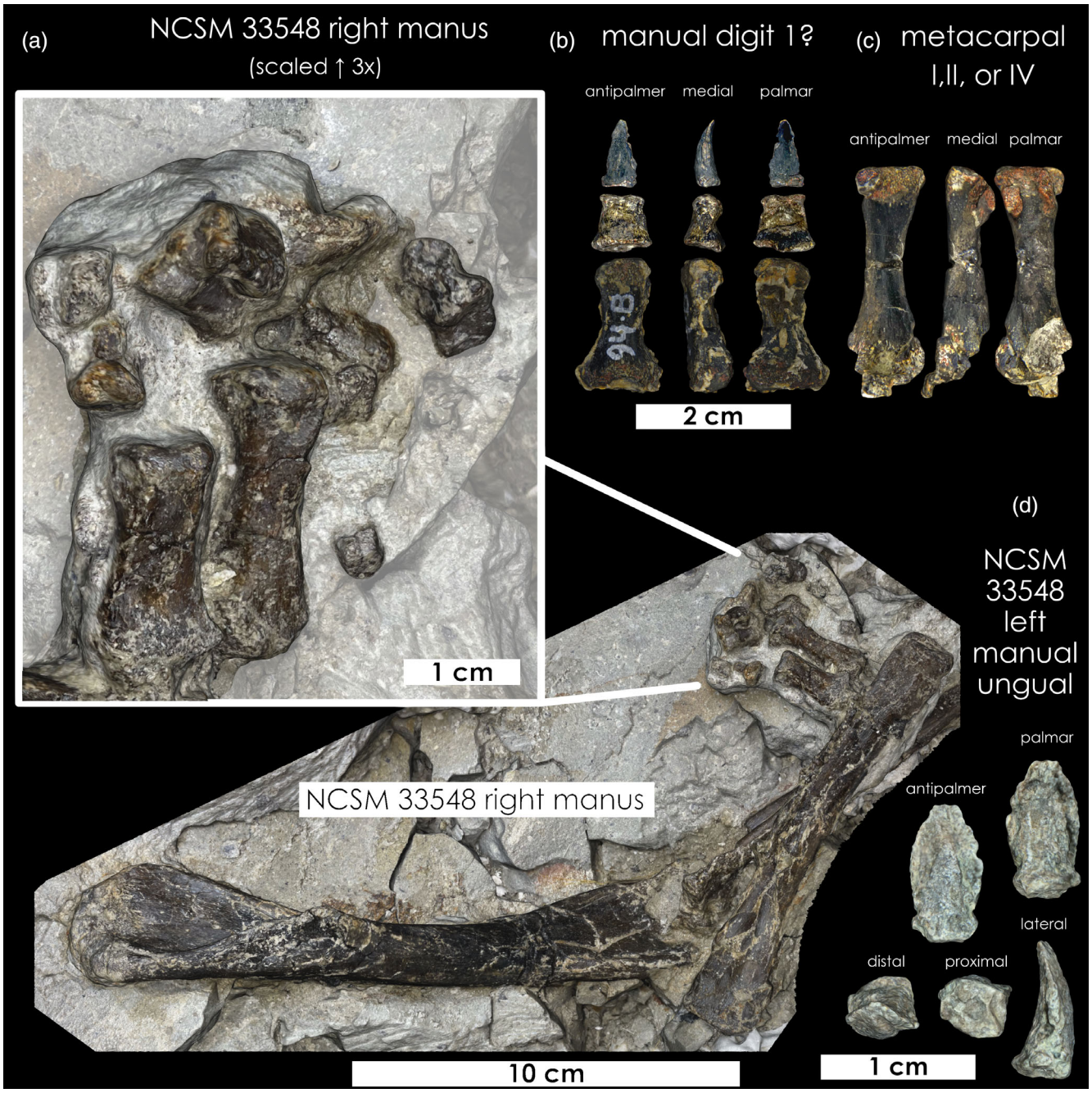

FIGURE 23 Forelimb of *Fona herzogae* NCSM 33548. (a) Right forelimb of NCSM 33548. (b) manual phalanges. From top to bottom: NCSM 36256, 36269, 36253. (c) Metacarpal (NCSM 36249). (d) left manual ungual from NCSM 33548.

Additionally, the preacetabular process twists slightly along its length such that the lateral surface slants ventrolaterally, a condition shared widely across Neornithischia (Norman, Sues, et al., 2004). The preacetabular process constitutes ~41% of the total ilium length in *Fona*, a condition shared by *Hypsilophodon* NHMUK R196 (~44%), *Thescelosaurus* NCSM 15728 (41%–50%), TMP 2008.045.0002 (39%), *Othnielosaurus* (SMA 0010) (39%), *Jeholosaurus* (~40%), and *Haya* (~40%) (Brown et al., 2013; Han et al., 2012). In contrast, in *Orodromeus* this ratio is only 33% and in the single most complete *Oryctodromeus* Ilium (MOR 1642), it is likely somewhere between 35% and 39%, with the latter adding two extra centimeters for the broken tip. The medial surface of the preacetabular process bears a caudoventrally directed ridge present in *Jeholosaurus* (Han et al., 2012), *Othnielosaurus* (SMA 0010), *Orodromeus* (MOR 623), *Oryctodromeus* (MOR 1636), *Thescelosaurus* (AMNH 5889 and 117), *Zephyrosaurus* (OMNH 34812), and *Hypsilophodon* (NHMUK R 196). The distal third of this process's medial

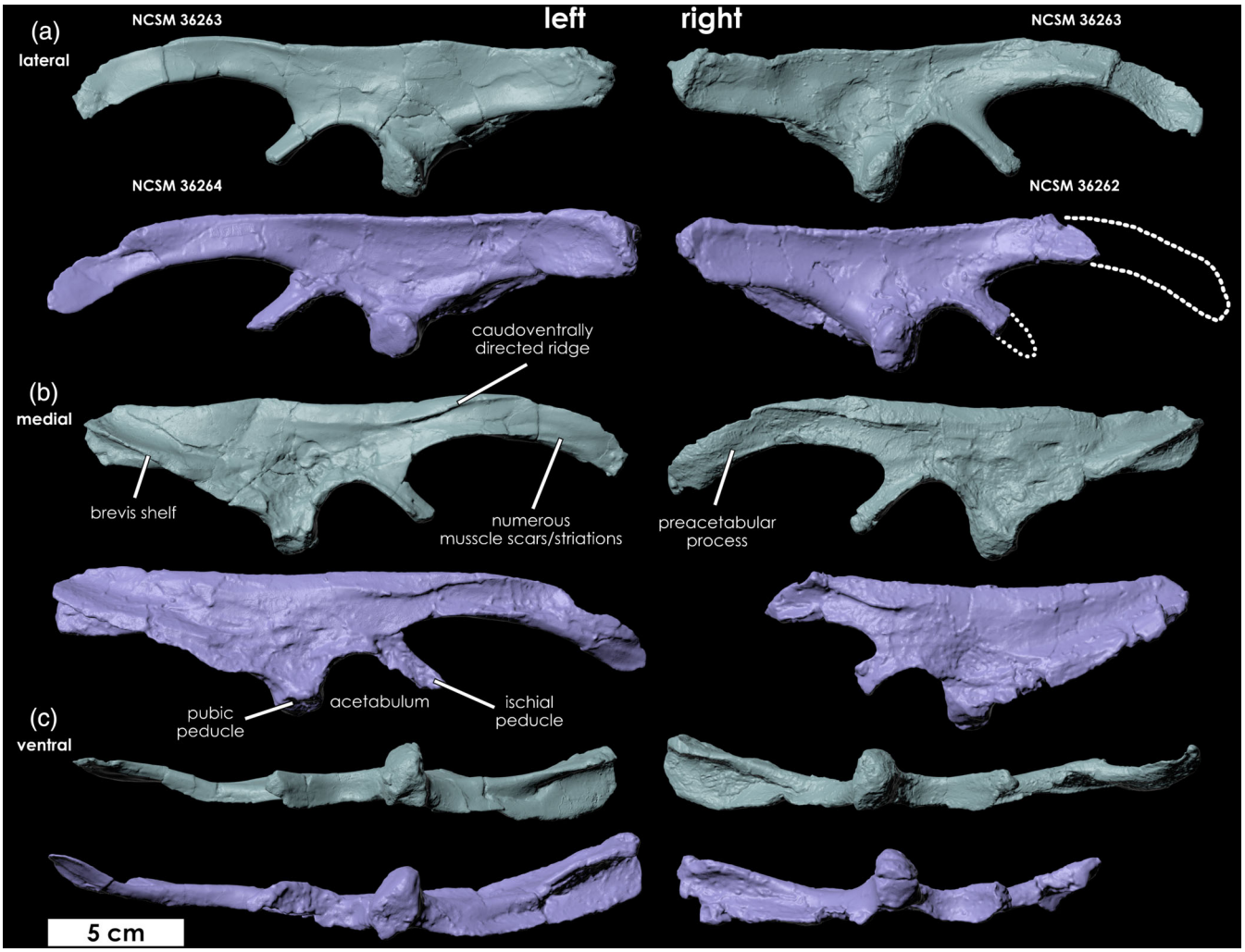

FIGURE 24 Illia of *Fona herzogae*. Illia of *Fona herzogae* from the Mini Troll locality in (a) lateral, (b) medial, and (c) ventral views. Dashed lines represent portions of missing bone.

surface bears numerous muscle scar striations aligned parallel to the long axis of the process.

The dorsal and ventral margins of the postacetabular process are parallel and form a slightly rounded caudal margin in lateral view. This condition is shared with *Th. neglectus* and *Hypsilophodon*, whereas in other SBEDOs these margins display a more tapering profile in lateral view. The brevis shelf becomes medially broad where it emerges near the cranioventral corner of the postacetabular process and in medial view, the shelf is slanted such that it terminates near the dorsal edge of the postacetabular blade. There is no supraacetabular ridge or flange near the lateral rim of the acetabulum, a condition shared by *Changmiania* and *Haya* (Barta & Norell, 2021; Yang et al., 2020).

The angle of the iliac pubic peduncle in *Fona* is intraspecifically variable. NCSM 36263 includes both ilia preserved adjacent to each other (Figure 4). The pubic peduncles are angled approximately 50° cranially from the long axis of the ilia. In contrast, a second, possible pair of ilia (NCSM 36262 and 36264) have public peduncle angles of ~38°, which is more in line with the cranially directed processes in *Oryctodromeus* and other SBEDOs (Brown et al., 2013). A similar range of variation seems to be present in *Orodromeus*. The pubic peduncles of *Fona* and *Oryctodromeus* are more robust than those of *Orodromeus*, having triangular-shaped cross-sections, whereas those of *Orodromeus* are thinner and more strap-like. Additionally, the medial surface of the pubic peduncles lacks the deep excavation noted in *Jeholosaurus* (Han et al., 2012).

5.4.8 | Pubis

The prepubic process emerges from the cuboidal main body and extends craniodorsally. It is relatively long, reaching beyond the last dorsal vertebra in most reconstructions. Due in part to a unique proximolateral swelling (Figure 25), the shaft appears dorsoventrally flattened

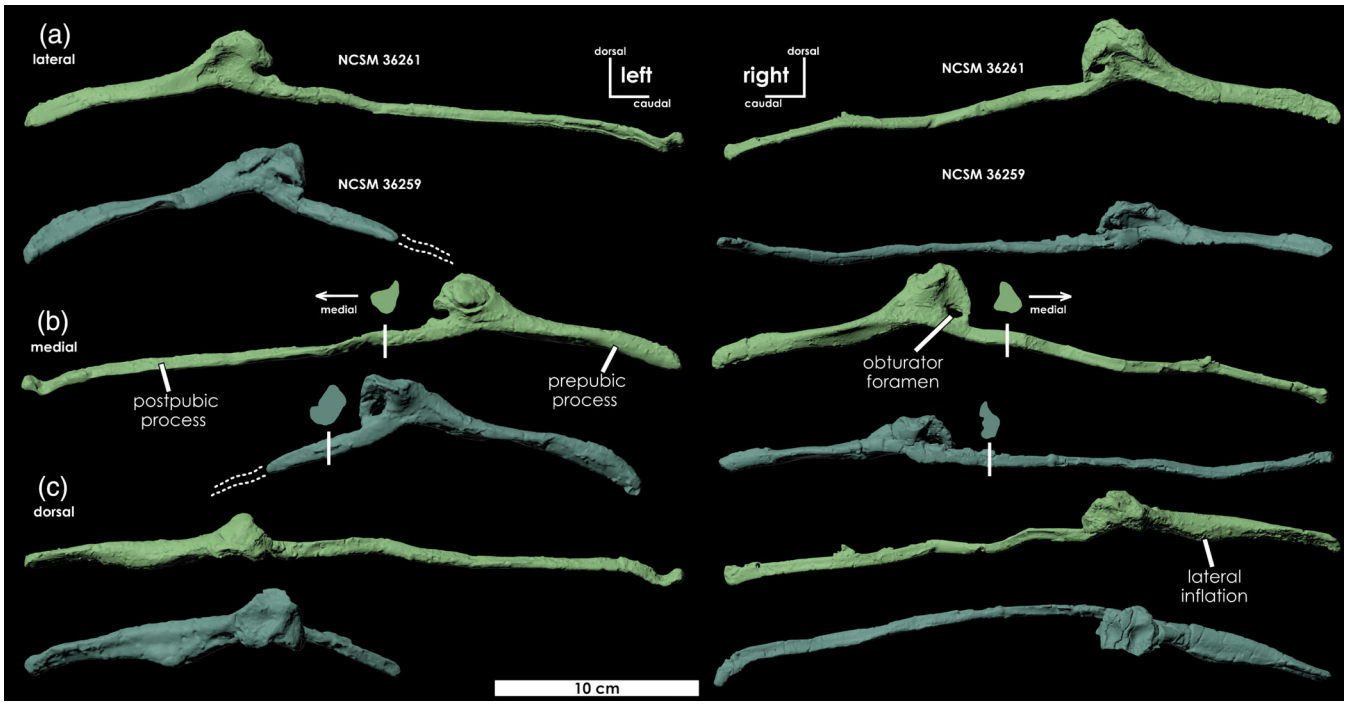

FIGURE 25 Pubes of *Fona herzogae*. Pubes of *Fona herzogae* from the Mini Troll locality in (a) lateral, (b) medial, and (c) dorsal views. Silhouettes above pubes in (b) represent the shape of the postpubic process cross-section directly distal to the cuboidal main body. Silhouettes are 2× scale. Dashed lines represent portions of missing bone.

proximally and mediolaterally flattened distally, in contrast to the thin and mediolaterally compressed processes of *Orodromeus* (MOR 623), dorsoventrally wider but still mediolaterally compressed process of *Th. neglectus* (NCSM 15728), triangular to rod-shaped process of *Oryctodromeus* (MOR 1642), or reverse condition in at least one specimen of *Thescelosaurus* (AMNH 117). The proximolateral swelling occurs approximately a third of the way along the shaft and is present in every specimen, varying slightly in prominence. This lateral swelling is absent in *Th. neglectus*, *Orodromeus*, and *Oryctodromeus* (it may be present, but substantially reduced in *Oryctodromeus* [MOR 1642]). The ventral surface of the process bears a broad shallow groove on three of the four specimens from the Mini Troll locality, as in *Haya* (Barta & Norell, 2021). The distal end is slightly dorsoventrally expanded, a condition shared by *T. neglectus* and at least some specimens of *Orodromeus* (MOR 623).

The cuboidal main body of the pubis becomes mediolaterally expanded dorsally to form a series of connections with the other pelvic elements. The dorsal edge of the cuboidal body of a right pubis (NCSM 36261) bears an elongate facet that appears to form a direct articulation with the distal end of the ventrally folded lateral spine of the fused second and third sacrals (NCSM 36218). If confirmed, such a connection would support a triple junction articulation between the pubic peduncle of the ilia with the sacrum and the pubis, a condition unique to *Th. neglectus*. In contrast, the medial process of the pubis of other SBEDOs contacts the sacral body by inserting into a socket (Scheetz, 1999). Nonetheless, the precise arrangement of the pelvis remains uncertain (Figure 13c). The center of the cuboidal body is characterized by the obturator foramen. On some specimens the foramen opens caudally, a variable condition shared widely among many SBEDOs (Barta & Norell, 2021).

The postpubic process emerges below the obturator foramen and extends caudoventrally. It is about half the thickness of the prepubic process and about double the length. All postpubic processes are moderately deformed on the disarticulated specimens from the Mini Troll locality, but maintain more of their original shapes on NCSM 33548. The postpubic process is triangular in cross-section along its length before terminating at the slightly swollen distal tip. The dorsal margin of the shaft forms an edge that is sharper along the proximal fourth or fifth of the shaft before becoming slightly more rounded distally. This dorsal edge is also present in *Oryctodromeus* (MOR 1642) and appears slightly more prominent.

The angle formed between the pre- and postpubic processes is relatively large compared to other SBEDOs, ranging from 142° to 180° with an average of 160° among the four preserved from the Mini Troll locality. This condition is shared by *Oryctodromeus*, *Orodromeus*, *Haya*, and one specimen of *Th. neglectus* (AMNH 117). In contrast, the pubes of other SBEDOs such as *Dryosaurus* and

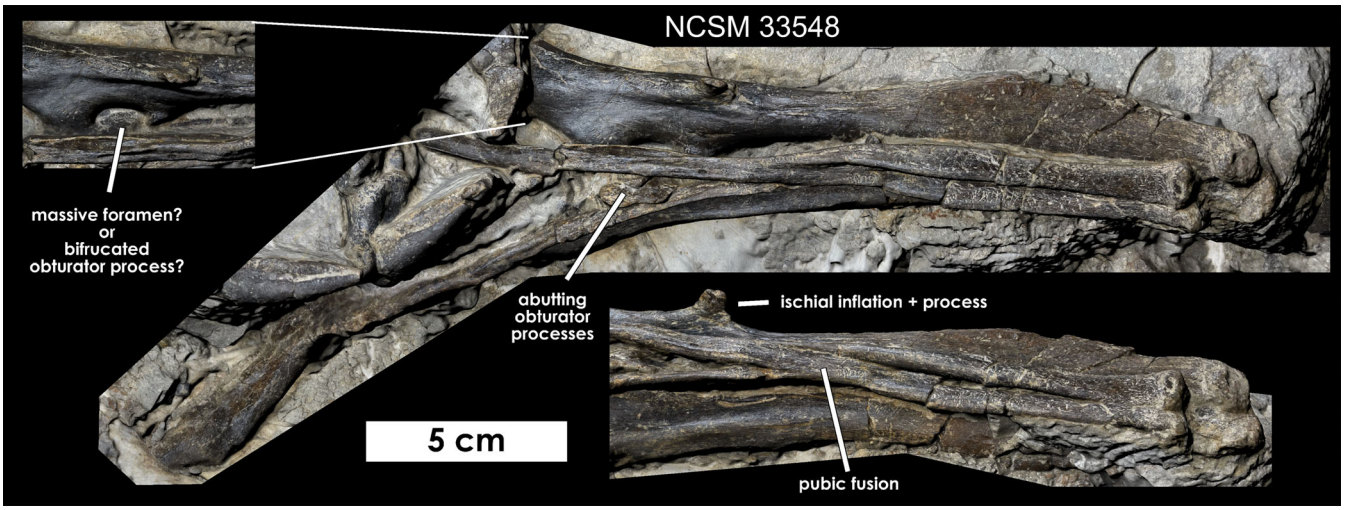

FIGURE 26 Pelvis of *Fona herzogae* NCSM 33548. (A) Exposed articulated ischia and fused pubes of NCSM 33548 in ventral view.

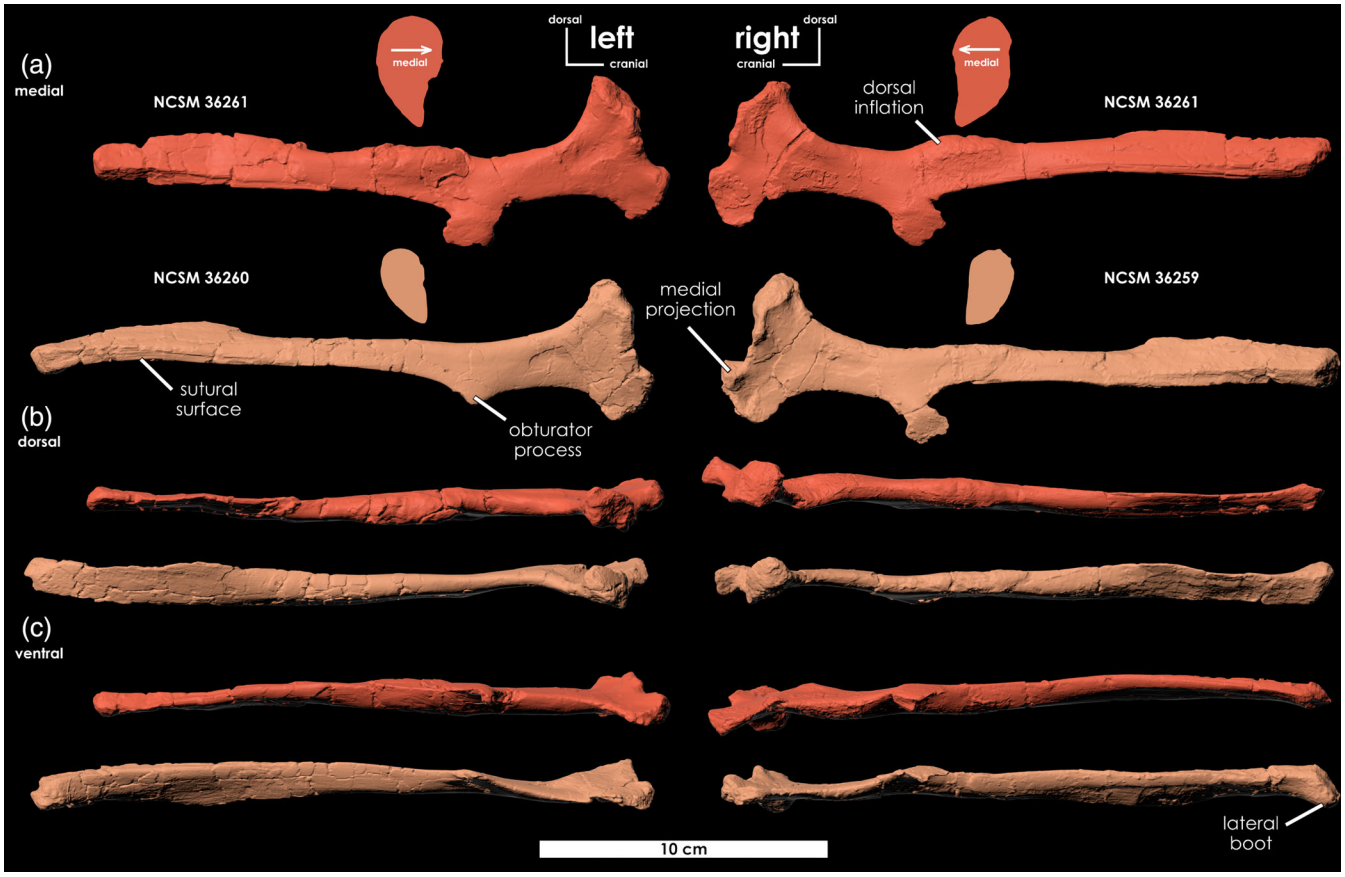

FIGURE 27 Ischia of *Fona herzogae*. Ischia of *Fona herzogae* from the Mini Troll locality in (a) medial, (b) dorsal, and (c) ventral views. Silhouettes above ischia in (a) represent the shape of the ischial shaft's cross-section directly distal to the obturator process. Silhouettes 2x scale.

Hypsilophodon exhibit an angle closer to 130° (at least one disarticulated pubis of *Hypsilophodon* [NHMUK R 193] is approximately 145°, although it is damaged). On NCSM 33548 the postpubic processes of the paired pubes converge midway along the lengths of their shafts, where they fuse into a single structure (Figure 26). However, the orientation of this fusion is not parallel to the sagittal plane, rather it is obliquely tilted, asymmetrical,

and limited to a ~ 5.5 cm section of the two shafts. Distal to this the shafts separate again, yet remain closely appressed. This fusion is present on only a single specimen and it is unclear if it is pathological.

5.4.9 | Ischium

The angle formed between the iliac peduncle, the pubic peduncle, and the long axis of the element is approximately 71°, with a range of 15° between the four ischia from the Mini Troll locality (Figure 27). This is similar to the average of other SBEDOs, which range between ~87° and 65° but contrasts with the angle of ~50° in *Oryctodromeus*, in which the iliac peduncles are tilted more caudodorsally. The pubic peduncles are not longer than the iliac peduncles, in contrast to *Jeholosaurus*, *Haya*, and *Parksosaurus* (Barta & Norell, 2021; Hudgins, 2021). The peduncles are not as broad as those of *Dysalotosaurus* (Hübner, 2011, 2018). The distal shaft is straight along its length in lateral view, a condition shared by *Haya*, *Jeholosaurus*, *Orodromeus*, *Oryctodromeus*, and *Thescelosaurus*. This is in contrast to *Parksosaurus* (Sues et al., 2023), *Sanxiasaurus* (Li et al., 2019), *Kulindadromaeus* (Godefroit et al., 2014), and *Laquintasaura* in which the shaft bows cranioventrally. The shaft is mediolaterally compressed and elliptical in cross-section. At approximately the distal third, the shaft twists such that the dorsal margin faces dorsolaterally, simultaneously the dorsal margin tapers to form a blade-like edge, and the ventral margin shifts from rounded to flat, bearing extensive rugosities for suture with the opposite ischial shaft. This twist is shared by *Th. neglectus* (NCSM 15728), and *Haya* (Barta & Norell, 2021), whereas in *Orodromeus* this twist is absent (Scheetz, 1999). In *Jeholosaurus*, the twist occurs immediately distal to the proximal plate and the ventromedial surface is concave rather than flat (Han et al., 2012).

The distal ends of both peduncles are laterally, and slightly medially thickened, with the transverse thickness of the iliac peduncle approximately twice that of the pubic peduncle. This causes the proximal plate, where the peduncles and shaft converge, to appear slightly medially depressed. A single right ischium (NCSM 36259) bears a small protuberance at the dorsomedial corner of the pubic peduncle, giving it an inverted "L" shaped profile in cranial view, a condition shared by *Jeholosaurus*, *Hypsilophodon* (Galton, 1974; Han et al., 2012), and *Oryctodromeus* (MOR 1642) in which it is especially prominent. The three other ischia lack this protuberance, but their articular surfaces do become mediolaterally thicker towards the dorsal acetabulum.

There is no groove across the dorsal margin or lateral surface of the shaft's proximal end, in contrast to some *Jeholosaurus* specimens (Han et al., 2012), nor is there a lateral groove distal to the obturator process, in contrast to *Orodromeus* (Barta & Norell, 2021). The tab-like obturator process emerges proximally along the shaft from the ventromedial edge, in contrast to its more distal location in *Hypsilophodon* and *Parksosaurus* (Galton, 1974; Parks, 1925). The distal tip of the ischium terminates as a slightly laterally expanded, bulbous boot, a condition shared by *Oryctodromeus* (Krumenacker, 2017), *Th. neglectus* (NCSM 15728) and *Trinisaura* (Coria et al., 2013), but in contrast to *Hypsilophodon* which lacks a distal boot and bears a significantly broader blade-like profile along the overall shaft (Hulke, 1882). On NCSM 33548 the distal ends of the ischia extend slightly further than the distal ends of the partially fused pubes.

The dorsal margin of two paired ischial shafts from the Mini Troll locality bear irregular expansions immediately distal to the obturator process. These swellings are absent on the right element of a second other pair from the same locality (NCSM 36260), and possibly present, but significantly reduced, on the left (NCSM 36259). These swellings are also present on NCSM 33548 (Figure 26) but differ in morphology. On the well-exposed dorsolateral surface of the left ischium of NCSM 33548 a pronounced tab-like process projects from this swelling, and is nearly equivalent in prominence to the obturator process.

On NCSM 33548 the distal ends of the obturator processes come into contact with each other and descend between the pubes, immediately proximal to where the latter fuse. The well-exposed base of the left obturator process bears what appears to be a large, partially enclosed, foramen that pierces through the element. This foramen or embayment causes the obturator process to appear bifurcated, resulting in the ischium possessing three distinct processes. Although the opposite right element is less exposed, it also seems to bear a foramen, albeit smaller, more slit-like, and located slightly further distally.

5.4.10 | Femur

The femoral head is a globular eminence offset from a slightly constricted neck. It emerges from the femoral shaft at an angle ranging between ~100° and 135° (Figure 28), a condition shared by *Haya*, *Oryctodromeus*, *Orodromeus*, *Jeholosaurus*, *Koreanosaurus*, and a number of other SBEDOs (Han et al., 2012 and references therein; Barta & Norell, 2021). The caudal surface of the femoral head is deeply excavated by a wide, "U" shaped groove that extends ventrolaterally, and which serves as the insertion of the *m. iliotrochantericus* (Maidment & Barrett, 2011). This groove is present in many SBEDOs but absent in *Heterodontosaurus*, *Fruitadens*, *Hexinlusaurus*, and *Lesothosaurus*

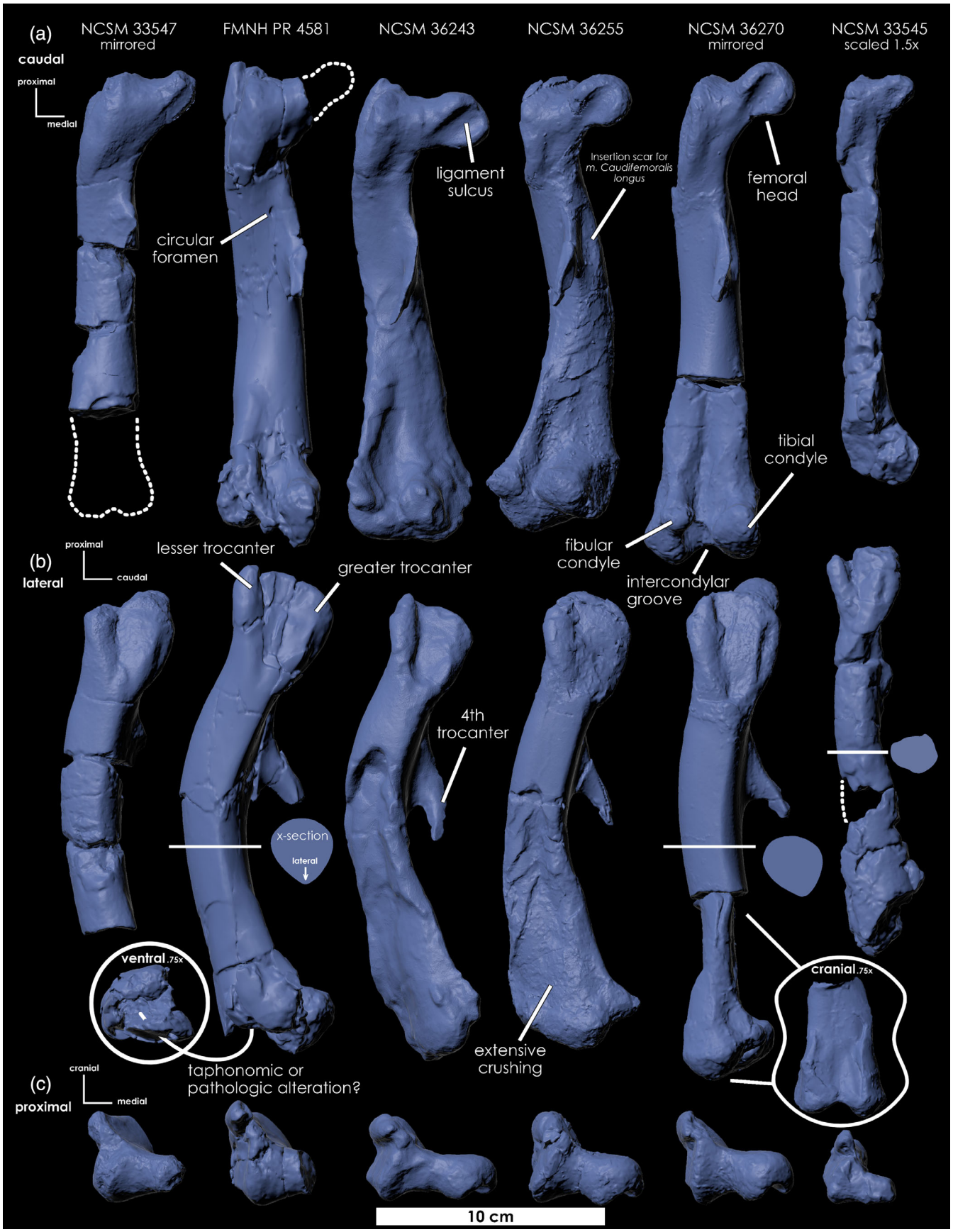

FIGURE 28 Femora of *Fona herzogae*. Left femora of *Fona herzogae* from multiple localities in (a) caudal, (b) medial views, and (c) proximal views. Dashed lines represent portions of missing bone. Mirrored elements are noted in the figure.

(Han et al., 2012 see references therein). In lateral view, the greater trochanter is rostrocaudally expanded and bears a gently curved dorsal margin, as in *Haya* and a number of other SBEDOs (Barta & Norell, 2021). In lateral view, there is a narrow ridge that runs dorsoventrally near the caudal margin of the greater trochanter. This ridge is present in *Jeholosaurus*, *Haya*, *Changchunsaurus*, *Hypsilophodon* (Barta & Norell, 2021; Butler et al., 2011; Galton, 1974; Han et al., 2012), as well as *Oryctodromeus* and *Othnielosaurus* (BYU 163631), but is absent in *Othnielosaurus* (SMA 0010), *Parksosaurus*, and *Dryosaurus* (NMNH V 5826). The lesser and greater trochanters of all largest and most skeletally mature femora are closely appressed to each other along their lengths, in contrast to a deep cleft that separates the trochanters in the smallest femur from the Mini Troll locality (NCSM 33545). A deep cleft is also present in *Minimocursor* (Manitkoon, Deesri, Khalloufi, et al., 2023), the 'Dan Luang neornithischian' (SM2016-1-081) (Manitkoon, Deesri, Warapeang, et al., 2023), YPM 1235, *Gideonmantellia* (Ruiz-Omeñaca et al., 2012), Nevadadromeus (Bonde et al., 2022), and a number of other earlier diverging ornithischians (Barta & Norell, 2021; Han et al., 2012). The proximal (= dorsal) extent of the lesser trochanter varies slightly among specimens, protruding dorsal to the dorsal margin of the greater trochanter in some specimens. In contrast, in others, it is nearly level or terminates substantially ventral to the apex of the greater trochanter. This character may therefore be intraspecifically variable and not a valid phylogenetic character. Different SBEDOs have been described as exhibiting either state (e.g., *Haya*, *Jeholosaurus*, *Changchunsaurus*). The lateral surface of the femur just below the crest of the greater trochanter and caudal to the lesser trochanter is flat as in other thescelosaurines (Boyd, 2015). The columnar body of the lesser trochanter projects laterally relative to this flattened region defining its caudal border. In lateral view, the femoral shaft bows cranially by ~145°–168°. It has a roughly circular cross-section distally and a more rounded triangular cross-section proximally due to the ridge for the *linea intermuscularis caudalis* that runs along the caudolateral edge (Maidment & Barrett, 2011).

The fourth trochanter is located approximately 45% down the total length of the femur, a condition shared by many neornithischians (except *Thescelosaurus*) and iguanodontians (Forster, 1990; Gilmore, 1915). It is pendant-shaped and laterally compressed, with a ridge that runs along its lateral surface, forming a triangular cross-section that points laterally. It is relatively thinner than *Haya* and its medial surface is not as concave (Barta & Norell, 2021). As it emerges from the caudomedial edge of the shaft it begins tapering to a point, while simultaneously drooping ventrally and curving slightly laterally. It is strongly ventrally hooked, as in many other SBEDOs such as *Haya* (Barta & Norell, 2021), *Hypsilophodon* (Hulke, 1882), *Orodromeus* (MOR 473), and *Oryctodromeus* (MOR 1642). At the base of the fourth trochanter's medial surface, a deep dorsoventrally elongate fossa marks the insertion point for the *caudofemoralis longus* (Maidment & Barrett, 2011). On all largest and most skeletally mature femora, there is a small circular nutrient foramen located immediately proximal to the fourth trochanter on the caudolateral surface of the femoral shaft. This foramen is absent in *Haya*, but present in *Jeholosaurus*, *Thescelosaurus* (Barta & Norell, 2021; Gilmore, 1915; Han et al., 2012), *Oryctodromeus* (MOR 1642), and *Orodromeus* (MOR 473). All preserved distal femora are moderately to extensively taphonomically distorted/crushed.

However, NCSM 36270 and FMNH PR 4581 bear the remnant of a subtle intercondylar groove. Among SBEDOs this groove is present only in *Thescelosaurus*, *Dryosaurus* (BYU 12005 and NMNH V 5826), *Morrosaurus* (Rozadilla et al., 2016), a specimen referred to Dryosauridae indet. from the Lourinhã Formation of Portugal (Rotatori et al., 2020), and possibly *Changmiania* (Yang et al., 2020) and *Oryctodromeus* (MOR 1642), whereas in all other SBEDOs, the cranial surface is broadly convex. The medial condyle is larger than the lateral condyle and it does not partially enclose the intercondylar sulcus, in contrast to *Haya*, *Thescelosaurus*, *Orodromeus*, and some elasmarians and iguanodontians (Barta & Norell, 2021; Scheetz, 1999).

5.4.11 | Tibia

In dorsal view, the proximal end of the tibia is rostrocaudally expanded and slightly bowed medially (Figure 29). The proximal end is unusually thin. However, this may be partially due to taphonomic crushing present in all tibiae of *Fona*. The laterally projecting fibular condyle bears an accessory tubercle across its cranial surface that projects craniolaterally and is approximately half the size of the fibular condyle. This tubercle, occasionally referred to as an accessory condyle and possibly homologous with the anterolateral process in some theropods (Samathi et al., 2019), would have been appressed to the concave medial surface of the fibular proximal head, as in *Oryctodromeus*, *Haya*, *Orodromeus*, *Albertadromeus*, and *Koreanosaurus* (Barta & Norell, 2021; Brown et al., 2013; Butler et al., 2011; Galton, 1974; Han et al., 2012; Huh et al., 2010; Krumenacker, 2017). It is absent in *Jeholosaurus*, *Hexinlusaurus*, *Sanxiasaurus*, and some elasmarians (Coria & Calvo, 2002; Coria & Salgado, 1996; Han et al., 2012; He & Cai, 1983; Li et al., 2019).

The deep fossa present on the medial surface of the cnemial crest in *Haya* (MPC-D 1002013) is absent in *Fona* (Barta & Norell, 2021). However, extensive crushing

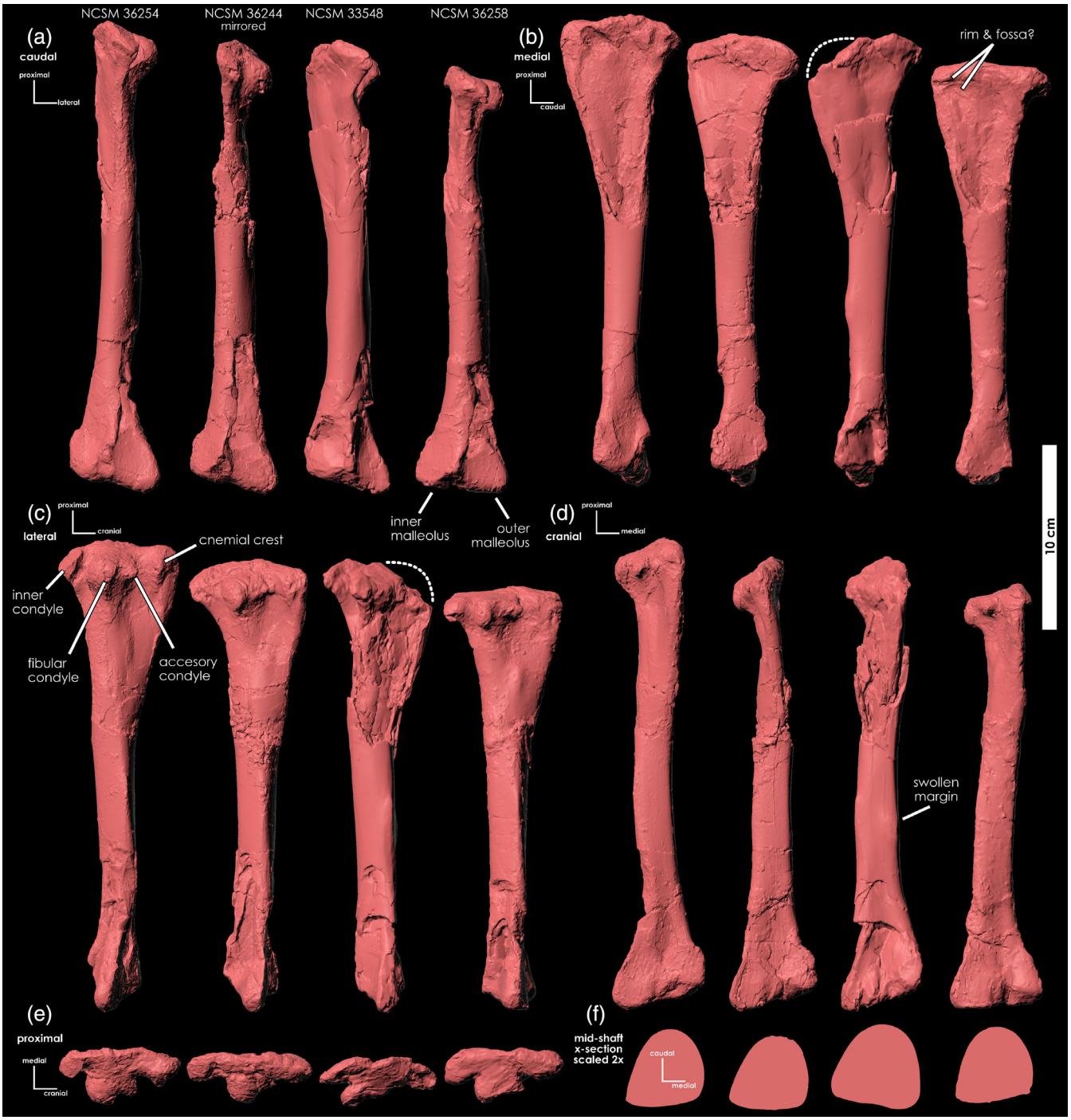

FIGURE 29 Tibiae of *Fona herzogae*. Right tibiae of *Fona herzogae* from multiple localities in (a) caudal, (b) medial, (c) lateral, (d) cranial, (e) proximal, and (f) midshaft cross-sectional views. Dashed lines represent portions of missing bone. Mirrored elements are noted in the figure.

in this region precludes a confident determination. Nonetheless, some tibiae have a rim along the craniodistal margin of this region and NCSM 36254 bears a deep depression that may correspond to this fossa. It is also present on some tibiae of *Oryctodromeus* (MOR 1636a and MOR 1642), *Orodromeus* (MOR 473), and *Othnielosaurus* (BYU 163631 and SMA 0010). It may correspond to the insertion site for the *M. flexor tibialis internus 3*, as in some theropods and extant archosaurs (Carrano & Hutchinson, 2002).

The proximal surfaces of the articular condyles are horizontally aligned, in contrast to the ventrally slanting articular facet in *Albertadromeus* (Brown et al., 2013). The midshaft of the tibia has a sub-triangular cross-section that

points caudally (Figure 29f), in contrast to the more circular cross-section of *Haya* (Barta & Norell, 2021). Immediately distal to the midshaft the craniolateral margin of the shaft slightly swells and forms a sharper, convex edge known as the fibular eminence, as in *Haya*, *Jeholosaurus*, and *Albertadromeus* (Barta & Norell, 2021; Brown et al., 2013; Han et al., 2012). In the right tibia of NCSM 33548, the craniomedial edge also becomes slightly thickened. A similar eminence is noted on the caudomedial surface of *Haya* (Barta & Norell, 2021). Distally, the tibial shaft expands mediolaterally, but not as extensively as in *Parksosaurus* (Parks, 1925). The medial malleolus and the further extending lateral malleolus form a somewhat obtuse triangular cross-section that points caudally, forming a ridge that separates the two malleoli, possibly similar to those noted in *Gasparinisaura* and *Diluvicursor* (Coria & Salgado, 1996; Herne et al., 2018). This ridge, although not as prominent, appears to be present in *Haya* (MPC-D 1002013) (contra Barta & Norell, 2021), as well as *Zephyrosaurus* (YPM 56695), *Orodromeus* (MOR 623), *Othnielosaurus* (SMA 0010), *Hypsilophodon* (BMNH R 5830), *Oryctodromeus*, *Thescelosaurus* (USNM 7757), and *Dryosaurus* (BYU 12005).

5.4.12 | Fibula

The proximal head of the fibula flares craniocaudally, forming a fan shape in lateral view, with a straight dorsal margin that is either horizontally aligned or tilted slightly cranioventrally (Figure 30). The medial surface of the proximal end is slightly craniocaudally concave. Immediately distal, the cranial and caudal margins of the shaft steadily converge towards each other up to the level of the midshaft, at which point they descend in parallel for the remainder of the shaft's length until reaching the bulbous distal articular surface. The concavity continues distally down the fibula's medial surface to form an elongate groove, as in *Haya* and *Jeholosaurus* (Barta & Norell, 2021; Han et al., 2012). None of the fibulae have an obvious patch of rugosity across a lateral bulge, in contrast to *Haya* (Barta & Norell, 2021). However, NCSM 36265 does have a prominent lateral bulge one-third of the distance down the shaft, although this may be pathologic or taphonomic. The distal third of the shaft transitions abruptly from a mostly circular cross-section to a strongly teardrop-shaped outline, with the apex forming a sharp medially projecting flange that attenuates at the distal end of the fibula. The emergence of this flange corresponds to the position where the fibula becomes appressed to the lateral eminence at the craniolateral edge of the tibia, as in *Albertadromeus* (Brown et al., 2013). This flange is also present in *Oryctodromeus* (MOR 1642), *Orodromeus* (Scheetz, 1999), *Haya*, *Changchunsaurus* (Butler et al., 2011), CMN 9483, but is absent in *Jeholosaurus* (Han et al., 2012). The fibula is not fused to the tibia, in contrast to *Albertadromeus* (Brown et al., 2013), although these elements of NCSM 33548 may be partially fused. The distal end of the fibula terminates in a caudoventrally inflected bulb that articulates with the fibular facet on the calcaneum. There is no sign of the distal triangular projection marking the triple juncture contact with the tibia and calcaneum, present in *Haya* (Barta & Norell, 2021).

5.4.13 | Astragalus

The astragalus is unfused to the calcaneum and tibia, in contrast to *Changmiania* (Yang et al., 2020). It wraps around the medial malleolus of the distal tibia. Its proximal surface is deeply concave craniocaudally and slightly convex mediolaterally, forming a crescentic sagittal cross-section (Figure 31e). In cranial view, it narrows laterally towards its contact with the calcaneum. As in *Orodromeus* (Scheetz, 1999) and *Oryctodromeus*, the laterally facing articular surface for the calcaneum consists of a pattern of globular protrusions, in contrast to the concave surface in *Jeholosaurus* (Han et al., 2012). The lateral corner of the cranial margin bears the ascending process, formed by two small projections and a deep, smooth fossa between them. Its condition appears more similar to the forked process in *Orodromeus* and *Jeholosaurus* (Han et al., 2012; Krumenacker, 2017) rather than the single tapered tab-like process in *Haya* and *Hypsilophodon* (Barta & Norell, 2021; Galton, 1974). However, it is more confluent with the main body of the astragalus and lacks the prominent stalk-like protrusion of *Orodromeus* (MOR 623). The distal surface of the astragalus is strongly convex craniocaudally, forming a large triangular strap that cradles the caudal surface of the inner and outer malleolus junction. A single elongate foramen is present ventral to the ascending process and is likely similar to that of *Jeholosaurus* (Han et al., 2012).

5.4.14 | Calcaneum

The calcaneum bears a quarter-moon shaped profile in lateral view that faces dorsally. The caudal concavity forms the facet for the outer malleolus of the distal tibia, whereas the cranial concavity forms the facet for the distal end of the fibula (Figure 31d). In proximal view, these two facets are separated by a sharp ridge that runs diagonally craniomedially to caudolaterally. In medial view, all calcanei are slightly more craniocaudally elongated than dorsoventrally tall, creating an obtuse average angle between the articular facets ($> \sim 120^{\circ}$), a

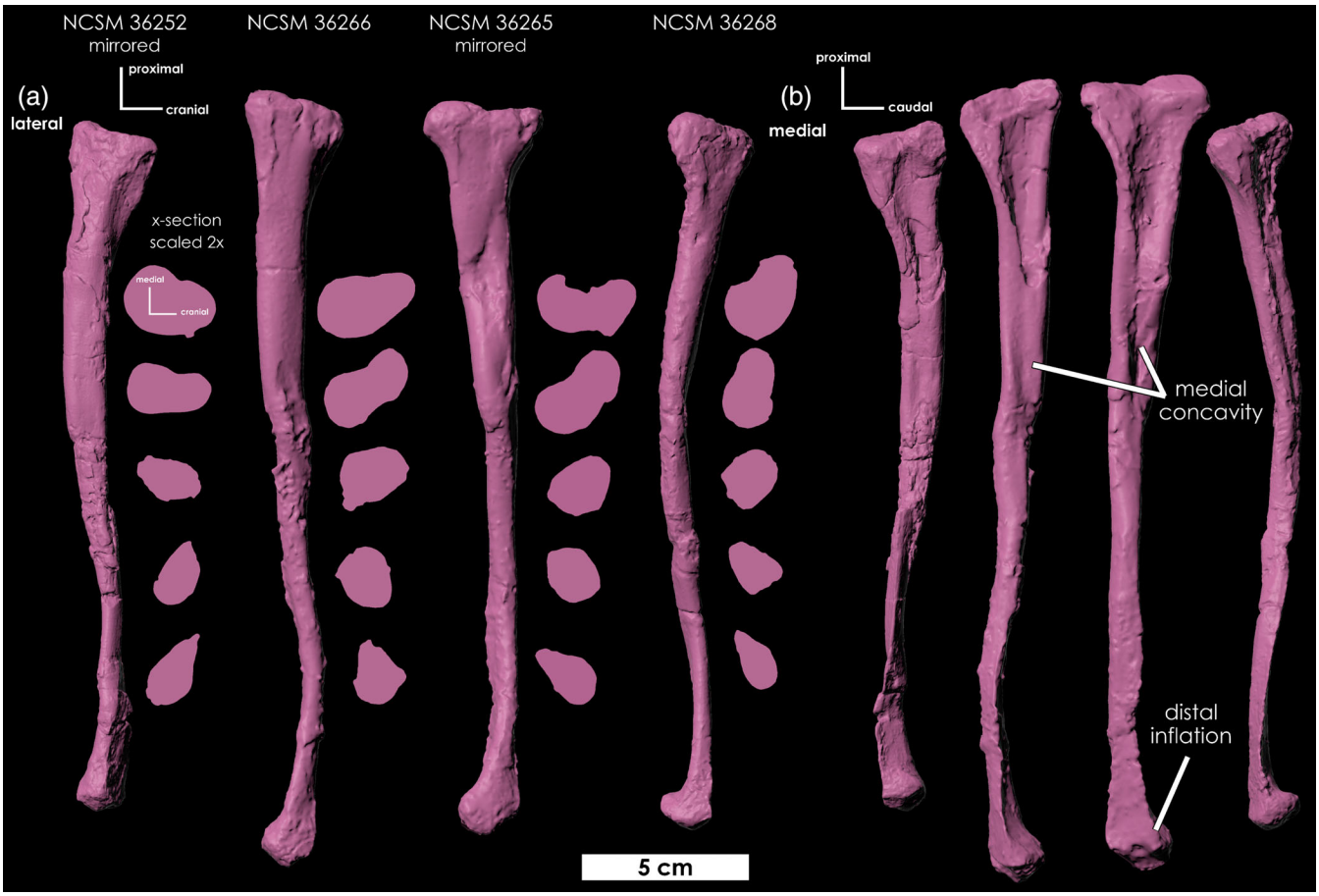

FIGURE 30 Fibulae of *Fona herzogae*. Right fibulae from the Mini Troll locality in (a) lateral view (silhouettes to the right of each fibula represent the cross-sectional shape of the shaft along the horizontally adjacent position) and (b) medial views. Mirrored elements are noted in the figure.

condition shared by *Oryctodromeus*, *Sektensaurus* (Ibiricu et al., 2019), *Dysalotosaurus* (Hübner et al., 2021), *Dryosaurus* (YPM 1884), and possibly *Chakisaurus* (Nogueira et al., 2024). In contrast, all calcanei of *Orodromeus* and *Zephyrosaurus* are slightly less elongated. The lateral surface is broadly concave, as in *Orodromeus*, but not as deep as in *Haya* (Barta & Norell, 2021). The medial surface forms the contact with the astragalus, causing the two tarsal elements to form a dumbbell shape in distal view. In medial view, there is a prominent foramen located in the middle of the contact with the astragalus.

5.4.15 | Distal tarsals

Two distal tarsals occupy the space between the metatarsals and the astragalus and calcaneum. We follow Barta and Norell (2021) in referring to them as the medial (MDT) and lateral distal tarsals (LDT). The MDT is dorsoventrally flattened and bears a rhomboidal outline in proximal view (Figure 31e). In *Fona*, this element is roughly as broad mediolaterally as it is craniocaudally, perhaps with a lateral margin that is only slightly longer, as in *Hypsilophodon* (Galton, 1974). A similar square profile is shared by *Orodromeus* (MOR 623) and at least one specimen of *Haya* (MAE 03–16). In contrast, the MDT is more mediolaterally elongate in *Oryctodromeus*, *Jeholosaurus*, *Haya* (MPC-D 1003178), and the unnamed SBEDO CMN 9483. Additionally, the MDT of *Oryctodromeus* bears a medially projecting tab-like process that emerges from the caudomedial corner with a defined ridge that runs along its caudal (planter) margin. In *Fona* this process is not as prominent and lacks the defined ridge. In *Orodromeus* and *Jeholosaurus* the craniomedial corner appears deeply indented in proximal view, giving the MDT a cubic profile without a craniomedial quadrant. The proximal surface is smooth and broadly convex, becoming gently concave near the caudolateral corner as it increases in depth towards the caudal margin where it forms a distinct sulcus that is slightly cranially inset. This sulcus is far more pronounced on NCSM 36280, where it bears distinct margins and occupies the majority of the

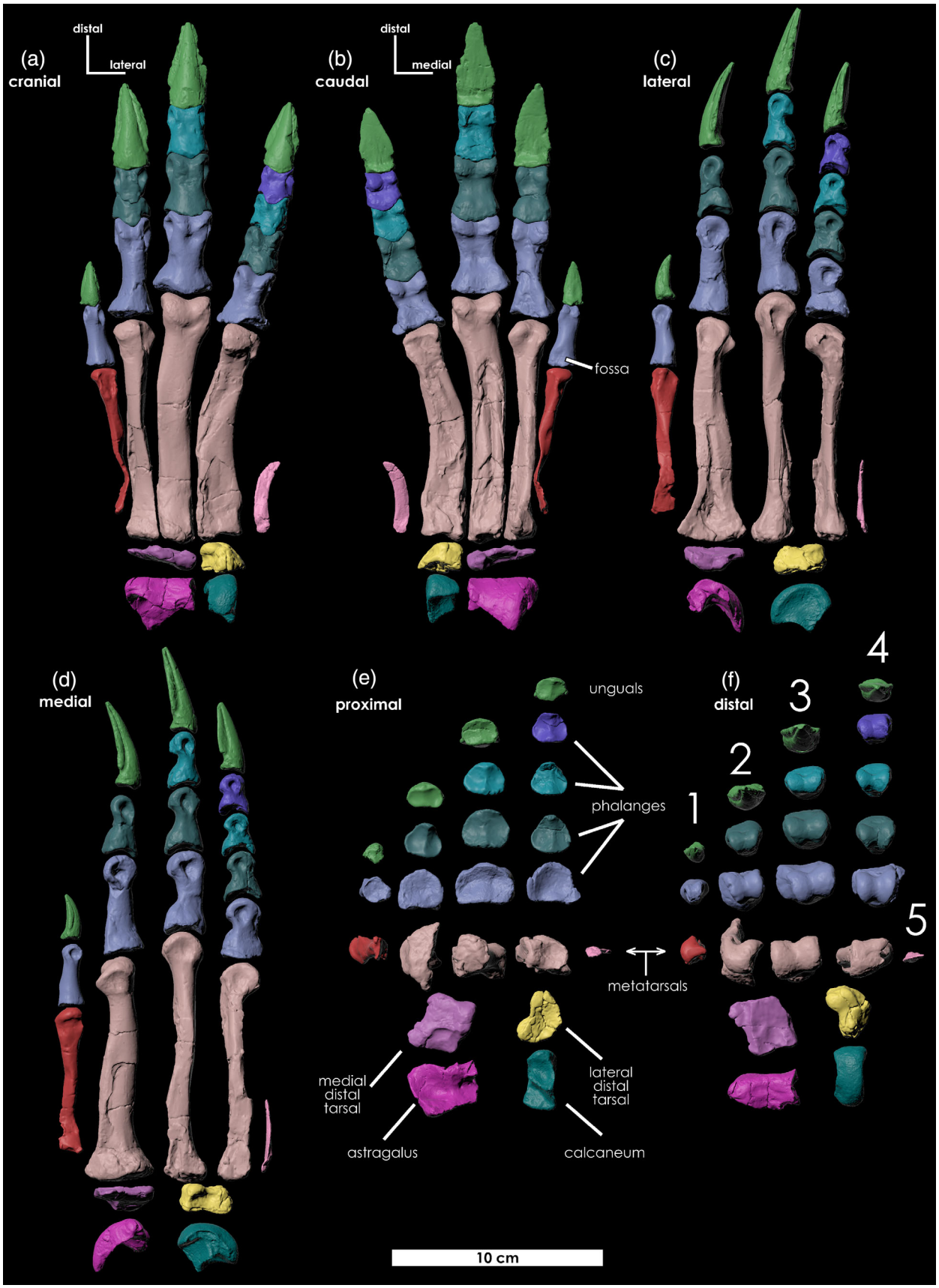

FIGURE 31 Tarsals and Pes of *Fona herzogae*. Reconstruction of the tarsals and pes of *Fona herzogae*, derived from multiple elements from the Mini Troll and LCT localities in (a) cranial, (b) caudal, (c) lateral, (d) medial, (e) proximal, and (f) distal views. Mirrored elements are noted with an asterisk in Data S9. NCSM specimen numbers for each element are provided in Data S7.

caudolateral quadrant. Additionally, the morphology of the caudal margin differs slightly between elements, ranging from a thin sharp edge to a thicker and broadly convex surface. The latter condition is shared by *Orodromeus* (MOR 623).

In distal view, the MDT is characterized by a prominent ridge that runs craniocaudally, which may represent the suture between distal tarsals one and two (sensu Han et al., 2012). In *Orodromeus* this ridge is located closer to the middle of the element, whereas in *Fona* it is greatly offset medially, as in *Hexinlusaurus* (He & Cai, 1983). The surface medial to this ridge forms the thinnest region of the element and appears to form the facet for the proximal head of metatarsal II. Lateral to the ridge is a broad concave trough that runs craniocaudally and forms a facet for metatarsal 3. The lateral margin is the thickest portion of the element, especially at the craniolateral corner, and the distal surface near this corner likely articulated with metatarsal 4, as in *Haya*, and *Oryctodromeus*. The distal surface of this corner also bears a narrow craniocaudally oriented groove, as in *Oryctodromeus* and *Jeholosaurus* (Han et al., 2012; Krumenacker, 2017), which is absent in *Orodromeus* (Scheetz, 1999). In proximal view, the dorsal surface near the cranial margin bears a series of shallow and narrow grooves, as in *Jeholosaurus*, and *Hypsilophodon* (Han et al., 2012). In dorsal view, the lateral margin is somewhat undulatory in order to articulate with the lateral distal tarsal (LDT).

The LDT has a convex lateral surface and a concave medial surface to accept the lateral margin of the MDT (Figure 31e). The proximal surface is broadly concave to articulate with the calcaneum. The distal surface is broadly convex to articulate with the concave facet of metatarsal 4 and is characterized by three subtle bulbous swellings, one at the cranial end, and the other two adjacent to each other along the caudal margin, with the medial swelling being slightly larger than the lateral swelling. The caudal surface is square in cross-section and bears a distinct foramen, as in *Jeholosaurus* and *Heterodontosaurus* (Han et al., 2012; Santa Luca, 1980). The cranial margin is convex, in contrast to the slightly concave condition in *Jeholosaurus* (Han et al., 2012).

5.4.16 | Metatarsals

Metatarsal I has a splint-like shaft that is mediolaterally thin proximally and expands mediolaterally and craniocaudally towards its distal head. At the midshaft, the cross-section bears a "D" shape, with the flat surface appressed to the caudomedial side of Metatarsal II (Figure 31a). The shaft rapidly swells in the distal third to form a rounded articular surface. The lateral surface of

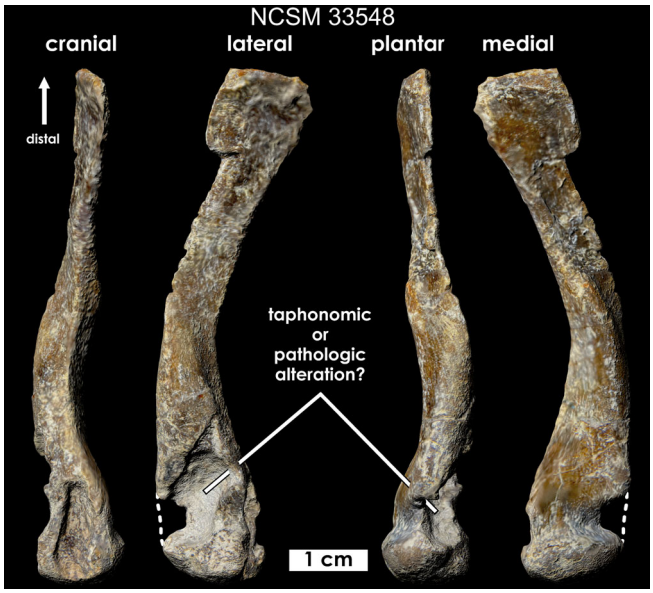

FIGURE 32 Metatarsal I of *Fona herzogae* NCSM 33548. Left MT-I of NCSM 33548. Dashed lines represent portions of missing bone.

the head is deeply concave and the caudal (= plantar) surface forms a mediolaterally concave fossa. Proximally, the shaft becomes mediolaterally flattened, flaring along its proximal fourth, as in *Zephyrosaurus* (YPM 56695). The left Metatarsal I of NCSM 33548 has a prominent irregularly shaped excavated concavity on the lateral surface of the proximal end, which may be pathological or taphonomic (Figure 32).

Metatarsals II, III, and IV are elongate shafts with ginglymoid distal articular surfaces bearing collateral ligament pits, with metatarsal II and IV being slightly shorter than metatarsal III and having asymmetrical distal articulations. Metatarsal II and III are tightly appressed to each other along the majority of their length as in *Oryctodromeus* (Krumenacker, 2017), *Haya* (Barta & Norell, 2021), *Othnielosaurus* (SMA 0010), and most SBEDOs. They diverge slightly at their distal ends as in *Jeholosaurus* (Han et al., 2012). Metatarsal IV is closely appressed to metatarsal III proximally, but becomes strongly lateral deflected at its mid-length, resulting in a prominent distal separation with metatarsal III, which also is slightly deflected laterally. A similar lateral deflection and separation between these two metatarsals also occur in *Parksosaurus* (Sues et al., 2023), *Zephyrosaurus* (YPM 56695), *Oryctodromeus*, *Haya*, and *Jeholosaurus*. However, in *Zephyrosaurus* and *Parksosaurus* the lateral kink is absent in metatarsal III, significantly stronger in metatarsal IV, and occurs proximal to the midshaft in *Zephyrosaurus*. A laterally deflected metatarsal III is absent in *Orodromeus*, which exhibits a reversed condition, with metatarsal III bending slightly medially.

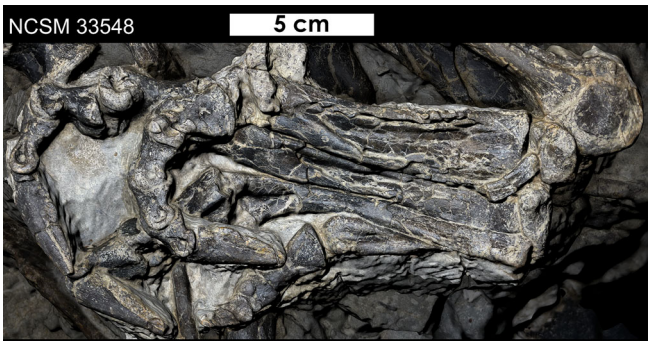

FIGURE 33 Pes of *Fona herzogae* NCSM 33548. (A) Articulated Left pes of NCSM 33548 in plantar view.

However, another *Orodromeus* pes (MOR 530) preserves the gap between metatarsal III and IV despite the medial bend of metatarsal III, suggesting these features may be somewhat intraspecifically or taphonomically variable. Similar variability has been noted in *Changchunsaurus* (Butler et al., 2011). Metatarsals do not diverge in the unnamed SBEDO CMN 9483 and *Hexinlusaurus* (He & Cai, 1983). There is a small fossa located on the cranial surface of the distal end of some metatarsal III specimens, but it is not as deep and broad as in *Jeholosaurus* (Han et al., 2012).

In proximal view, the proximal surface of metatarsal IV is concave and has a cross-section with a "D" shape, with the curved portion facing laterally. The cross-section immediately transitions to a triangular shape with a sharp lateral margin below the articular surface. The caudal surface bears a diagonally oriented longitudinal ridge that runs from the medial margin near the mid-length of the shaft to the lateral margin near the distal condyle, a condition shared with *Jeholosaurus*, *Changchunsaurus*, *Hypsilophodon* (Barta & Norell, 2021), *Othnielosaurus* (SMA 0010), and *Oryctodromeus*.

Metatarsal V is a craniocaudally flattened rectangular bone. In the articulated skeleton (NCSM 33548) it emerges from a gap between the proximal contact of metatarsal IV and the LDT and is tilted distomedially (Figure 33). It is slightly more slender than metatarsal V of *Zephyrosaurus* (YPM 56695) and *Orodromeus* (MOR 623), and significantly more slender than those of *Thescelosaurus* (Morris, 1976) and *Parksosaurus* (Sues et al., 2023). As it flattens rostrocaudally towards the distal tip, the lateral and medial margins remain parallel, whereas in *Parksosaurus*, these margins taper significantly to form a triangular cross-section (Sues et al., 2023), and in *Thescelosaurus* these margins flare near the distal end to form a constricted hourglass profile (Gilmore, 1915). Metatarsal V bears a slight lateral curve across its length, a condition shared by *Oryctodromeus* (Krumenacker, 2017), *Nanosaurus* (Carpenter & Galton, 2018), and *Zephyrosaurus* (YPM 56695), but in contrast to the rodlike condition of *Hypsilophodon* (Galton, 1974), and the strong curvature in *Parksosaurus* (Sues et al., 2023). The dorsal (= cranial) surface of the proximal end bears a swollen bulge, a condition shared by *Oryctodromeus* (MOR 1642), *Orodromeus* (MOR 623), and *Zephyrosaurus* (YPM 56695).

5.4.17 | Pedal phalanges

The pedal phalangeal formula of *Fona* is 2-3-4-5-0, as occurs in most SBEDOs (Figure 31). Overall, the morphology of the phalanges is very similar to other SBEDOs, with proximal surfaces characterized by either one or two articular facets and ginglymoid distal ends characterized by prominent collateral ligament pits.

A proximodorsal lip is absent on all proximal phalanges that articulate with the metatarsals, except for a single PIII-1 that may have a reduced lip. This condition is shared by other SBEDOs but can be variable with PIII-1, as in *Haya* and *Jeholosaurus* (Barta & Norell, 2021; Han et al., 2012).

Phalanx I-1 is 3.2 times as long as it is wide when measured at midshaft. This relatively long condition is shared by most SBEDOs, in which this ratio ranges between ~3 and 4. This is in contrast to the shorter PI-1 of *Jeholosaurus*, which is only twice as long as wide (Han et al., 2012). Both the left and right pedal PI-1 of *Oryctodromeus* possess a deep circular fossa located at the proximolateral corner of the ventral surface, which is also present but less prominent in *Fona*. This fossa may also be present in a specimen of *Orodromeus* (MOR 623) but appears to be absent in *Agilisaurus* (Peng, 1992: figure 6c), *Jeholosaurus* (Han et al., 2012: figure 12), *Hypsilophodon* (Galton, 1974: figure 58), *Parksosaurus* (Sues et al., 2023: figure 17), *Diluvicursor* (Herne et al., 2018: figure 24h), and *Anabisetia* (Coria & Calvo, 2002: figure 8). Interestingly, it may be present in *Nanosaurus agilis* (Carpenter & Galton, 2018: figure 18ee) and a SBEDO from the Early Cretaceous (*Laosaurus minimus*; Gilmore, 1924). Phalanges of digits II and III are generally longer than wide and constricted at midshaft between the articular ends. The nonterminal phalanges of digit IV have stubbier proportions with proximal and distal articulations close together and no waisting at midlength, as in other SBEDOs.

5.4.18 | Pedal unguals

The pedal unguals are distally pointed, elongate bones with pronounced medial and lateral grooves underlain by a broad ventral floor that emerges proximally and converges at the distal tip (Figure 31).

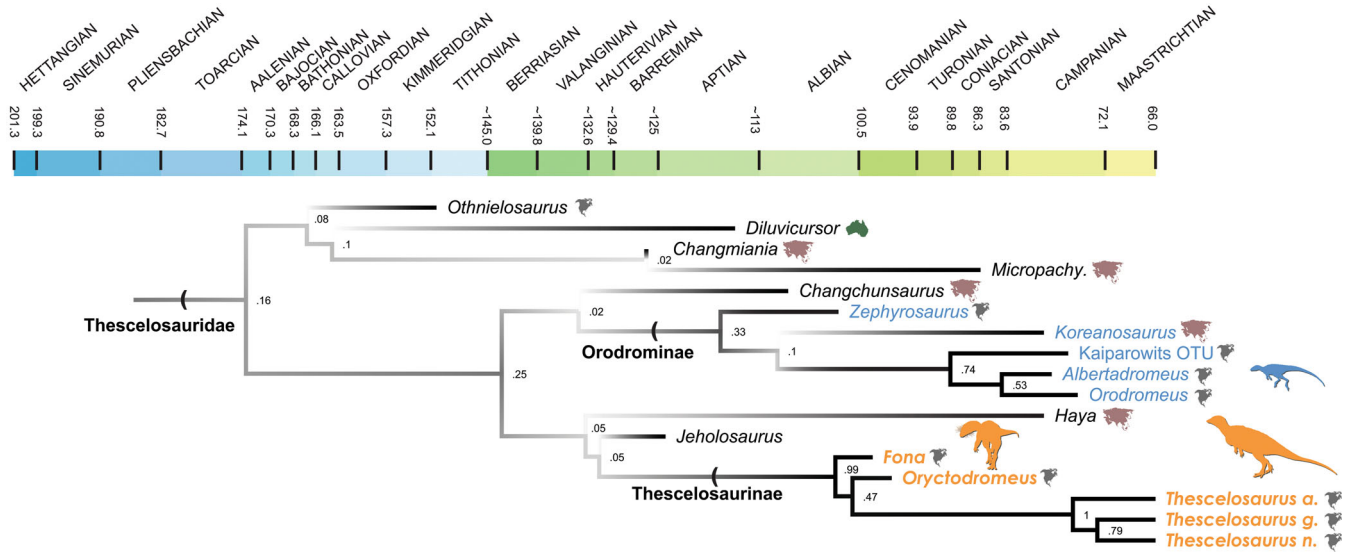

FIGURE 34 Phylogenetic relationships of early diverging ornithischians. Results of a time-calibrated phylogenetic analysis of new neornithischian dataset focusing on Thescelosauridae using Bayesian optimization. The fading color of the branches near nodes indicates the strength of relationship support, with precise posterior probability values nested to the right of each node. Silhouettes representing Dinosauromorpha, Heterodontosauridae, Thyreophora, Ceratopsia, and Ankylopollexia by Scott Hartman; Pachycephalosaurini by Jack Mayer Wood; and Dryosauridae by Tasman Dixon, all downloaded from Phylopic.org.

The ungual of digit I is small, being approximately half the length of the other three claws, in contrast to the more uniformly sized unguals of *Jeholosaurus* (Han et al., 2012). It has a circular cross-section and, in lateral view, it curves slightly ventrally. The plantar surface is marked by a broad, laterally offset, proximodistal running ridge, with an accompanying shallow medial groove. A series of minute pits span the breadth of the groove, while the rest of the plantar surface is marked by small proximodistally oriented crenulations. These crenulations are also present on the plantar surfaces of the unguals of the other digits.

The unguals of digits II, III, and IV are nearly identical in shape, with IV being slightly smaller than the equally sized II and III. However, some variation does exist between specimens. For example, some unguals are symmetrical in dorsal view while others may bow medially or laterally. In lateral view, the dorsal surfaces are arched and the plantar surfaces are flat, with an overall ventral tilt immediately distal to the proximal end, a condition that is shared by *Oryctodromeus* (MOR 1642), but in contrast to the broadly curved unguals of *Parksosaurus* (Sues et al., 2023). Interestingly, an ungual of an articulated third digit from another specimen of *Oryctodromeus* (IMNH 2232 44939) is slightly curved in lateral view with a plantar surface that is broadly concave rather than flat, a condition shared by the strongly curved pedal unguals of *Jeholosaurus* (Han et al., 2012). The left and right unguals of *Oryctodromeus* (MOR 1642) appear relatively longer and sharper than those of *Fona*.

6 | RESULTS

6.1 | Phylogenetic analyses

The composition and topology of Thescelosaurinae are consistent across our analyses in recovering *Fona* and *Oryctodromeus* as a sister clade to the three species of *Thescelosaurus*, except for the time-calibrated analyses, which places *Oryctodromeus* as diverging after *Fona* (Figure 34). The composition of Orodrominae is consistent in nearly all analyses. Intraclade relationships of orodromines are unresolved under parsimony optimization, whereas the Bayesian analyses consistently recover *Zephyrosaurus* as the earliest-diverging member and *Orodromeus* as the latest, but vary in the position of the Kaiparowits OTU, *Albertadromeus*, and the poorly supported inclusion of *Koreanosaurus*. Outside of these two stable clades, the composition and topology of Thescelosauridae, as redefined by Madzia et al. (2021), is unstable across all analyses. *Changchunsaurus*, *Haya*, *Jeholosaurus*, *Koreanosaurus*, and *Diluvicursor* remain thescelosaurids in all analyses. However, their positions fluctuate with poor node support. Additionally, several SBEDOs fall within or outside the clade between different analyses. These include *Changmiania*, *Othnielosaurus*, *Micropachycephalosaurus*, *Kulindadromeus*, and *Leaellynasaura*, all of which show weak node support in the Bayesian analyses. Interestingly, neither *Hypsilophodon* nor *Parksosaurus* are ever recovered within Thescelosauridae, consistently falling out as slightly later diverging.

6.2 | Synapomorphies

Here we elaborate on and reevaluate the synapomorphic traits of Thescelosauridae, Thescelosaurinae, and Orodrominae based on our best-supported topologies within the taxonomic nomenclatorial framework established by Madzia et al. (2021).

6.2.1 | Thescelosauridae

Our phylogenetic analyses recover 13 synapomorphies of Thescelosauridae (although none are unambiguous): (1) a concavity within the caudal end of the premaxilla near the lateral margin for receipt of the rostrolateral boss of the maxilla (char. 27:1) unites all thescelosaurids preserving a premaxilla and is shared by *Changmiania* and *Hypsilophodon*; (2) the presence of an accessory supraorbital (char. 46:2) unites *Th. neglectus*, *Haya*, and *Jeholosaurus*, whereas orodromines retain the primitive condition of a single supraorbital; (3) contribution of the jugal to the caudal margin of the infratemporal fenestra (char. 56:0) unites *Th. neglectus*, *Haya*, *Chanchunsaurus*, and *Jeholosaurus*, and is convergently present in *Kulindadromeus*, *Leaellynasaura*, and several other SBEDOs, but reversed in *Fona* and *Orodromeus*; (4) dorsolaterally inclined quadrate ventral condyles (char. 81:1) unite all thescelosaurids except *Haya*, which shares the horizontal condition of *Lesothosaurus*; (5) a surangular foramen (char. 145:1) and a surangular lateral ridge (char. 146:1) unite all thescelosaurids that preserve a surangular. These features are also common in multiple outgroups; (6) a basisphenoid that is rostrocaudally shorter than the basioccipital (char. 171:1) unites seven members of Thescelosauridae. However, *Haya* and *Orodromeus* possess the alternate condition in which both elements are subequal in length; (7) absence of denticles on premaxillary teeth (char. 183:1) unites *Th. neglectus*, *Zephyrosaurus*, *Haya*, *Changchunsaurus*, and *Jeholosaurus*, but is reversed in *Fona*, and convergently present in *Kulindadromeus* and *Talenkauen*; (8) presence of a sharp ventral keel on the cervical vertebrae (char. 217:2) unites several members of Thescelosauridae except for *Jeholosaurus*, *Changchunsaurus*, and *Th. neglectus*, but remains ambiguously distributed across several earlier and later diverging SBEDOs; (9) location of the proximalmost chevron on the distal end of the second caudal vertebra rather than the first (char. 252:1) unites *Th. neglectus*, *Haya*, and *Jeholosaurus* (although this is known to vary intraspecifically in extant taxa; Erickson et al., 2005). It is reversed in *Orodromeus* and *Diluvicursor*, and convergently present in *Parksosaurus*, *Hypsilophodon*, and, *Gasparinisaura*; (10) presence of a sharp scapular spine that runs across the lateral surface of the acromion process (char. 255:1 or 2) unites all thescelosaurids that preserve a scapula and is also present in *Changmiania*, *Othnielosaurus*, and *Trinisaura*; (11) a scapula length-to-width ratio of 5.7 or less (char. 257:0) unites several thescelosaurids, except *Haya* and all orodromines that preserve a scapula; lastly, (12) a prominent cranial expansion of the greater trochanter beyond the femoral head (char. 348:2) unites all thescelosaurids that preserve a femur yet is convergently present in A*nabisetia*, *Gasparinisaura*, *Morosaurus*, and *Eousdryosaurus*.

6.2.2 | Thescelosaurinae

In our phylogenetic analyses, 14 ambiguous synapomorphies unite the members of Thescelosaurinae: (1) a caudoventral prong of the jugal that underlaps the ventral surface of the quadratojugal (char. 58:1) unites *Fona* and *Th. neglectus*, but is also present in *Jeholosaurus* and *Changmiania*; (2) a lateral fossa on the postorbital that opens caudally towards the infratemporal fenestra (char. 100:1) unites *Fona*, *Oryctodromeus*, and *Th. neglectus*, but is also present in *Hexinlusaurus* and at least one specimen referred to *Jeholosaurus* (BMNHC Ph800); (3) a double-pronged predentary ventral process (char. 118:1) unites all thescelosaurines that preserve a predentary (absent in the thescelosaurid *Jeholosaurus*); (4) presence of a dorsally directed, finger-like process on the surangular (char. 146:2) (Figure 3d) unites *Fona* and *Th. neglectus*, and is also present in *Talenkauen* and *Te. tilletti*; (5) a dorsally open posttemporal foramen located along the dorsal margin of the paroccipital process that contacts the squamosal (char. 164:1) unites *Fona*, *Th. neglectus*, and *Th. assiniboiensis*, and convergently evolved in *Dryosaurus* and *Dysalotosaurus*; (6) caudally positioned dorsal neural spines (char. 223:1) unites *Fona*, *Oryctodromeus*, and all three species of *Thescelosaurus*. This trait is also present in *Parksosaurus*, *Yueosaurus*, and several other earlier and later diverging SBEDOs; (7) the presence of ossified intercostal plates (char. 231:1) unites *Fona*, *Oryctodromeus*, and *Th. neglectus*, but is also present in *Othnielosaurus*, *Parksosaurus*, *Hypsilophodon*, *Macrogryphosaurus*, *Talenkauen*, and *Mahuidacursor*; (8) likewise, partially ossified sternal segments of the cranial dorsal ribs (char. 232:1) unite *Fona* and *Th. neglectus*, but are also more widely distributed; (9) pubes supported by a sacral rib (char. 242:1) unite *Fona* and *Th. neglectus*, yet are also present in *Hypsilophodon* and *Gasparinisaura*, with an alternative articulation condition expressed by *Haya*, *Othnielosaurus*, at least some orodromines; 10) proximal caudal neural spines that are over 1.5 times taller than their centra (char. 243:1) unite *Fona*,

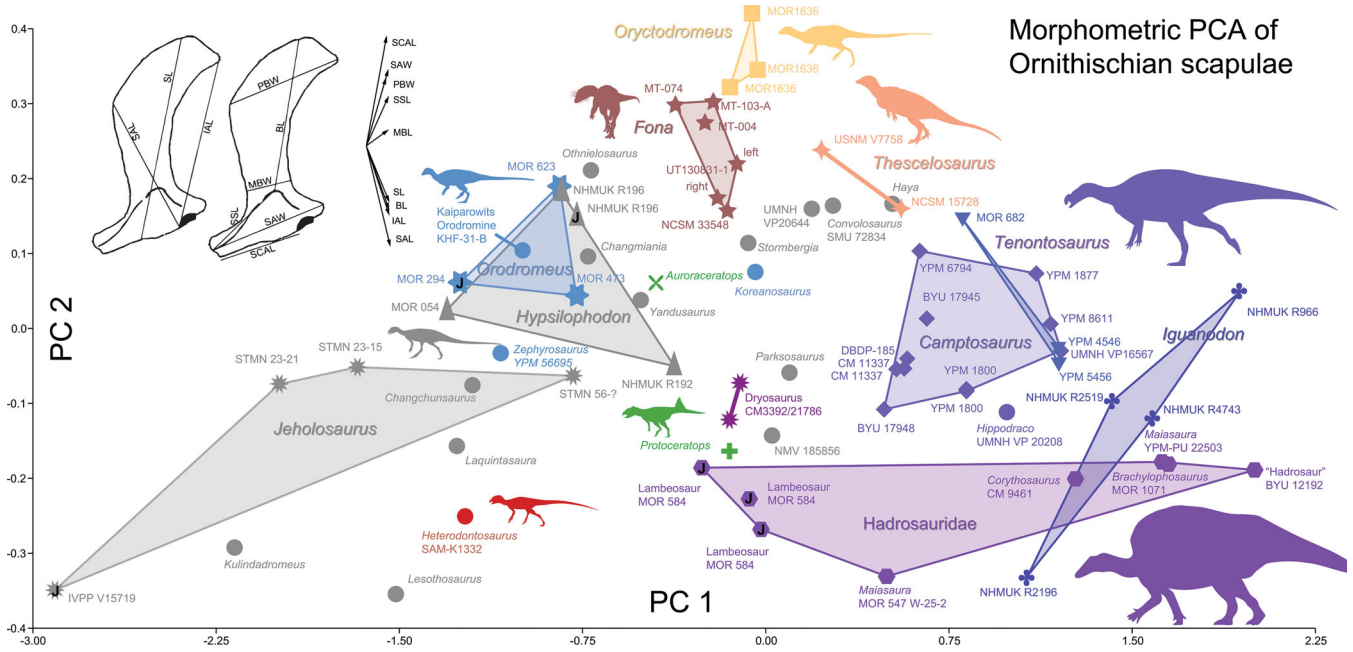

FIGURE 35 Principal component analysis of Ornithischian scapulae. PCA of an updated Fearon and Varricchio (2015) dataset measuring 70 scapulae. All linear measurements were collected in millimeters and log-transformed before analysis in PAST. Eigenvectors correspond to nine measurement variables. Datapoints containing a "J" represent juvenile specimens. Measurements of several taxa were estimated from publication figures, photographs, or 3D scans using either Image J or Blender. Datapoints denoted by gray symbols and text represent phylogenetically unstable SBEDOs.

Oryctodromeus, and *Th. neglectus*, but are also present in *Zephyrosaurus*, *Othnielosaurus*, *Changmiania*, *Hypsilophodon*, and several other SBEDOs; 11) a shallow intercondylar groove on the distal femur (char. 357:1) unites all thescelosaurines, but is also present in *Changmiania*, *Anabisetia*, possibly *Leaellynasaura*, and several other SBEDOs; 12) the presence of a distal femoral medial condyle that protrudes cranially beyond the lateral condyle and forms a diaphyseal ridge that runs proximodistally across the cranial surface (char. 364:1) unites *Th. neglectus*, *Th. assiniboiensis*, and possibly *Oryctodromeus* and *Fona*; 13) the presence of ossified hypaxial tendons on the tail (char. 406:1) unites *Fona*, *Oryctodromeus*, *Th. neglectus*, and *Th. assiniboiensis*, and is also present in *Parksosaurus*, *Hypsilophodon*, possibly *Lesothosaurus*, and several other later diverging SBEDOs; lastly, 14) the presence of longitudinally arranged ossified epaxial tendons (char. 408:0) unites *Oryctodromeus* and *Th. neglectus* but is also present in *Parksosaurus*, *Hypsilophodon*, *Gasparinisaura*, *Lesothosaurus*, and *Eousdryosaurus*.

6.2.3 | Orodrominae

Orodrominae is supported by six synapomorphies: (1) *Zephyrosaurus*, *Orodromeus*, and the Kaiparowits OTU are united by the presence of a tall, non-ornamented, caudally projecting boss on the lateral surface of the jugal (char. 60:3), convergent in some heterodontosaurids; (2) a jugal with subrectangular parallel dorsal and ventral margins (char. 67:1); (3) ventral orientation of the basipterygoid processes (char. 172:1); (4) cranial dorsal ribs with non-laterally compressed, circular to oval cross-sections along their distal shafts (char. 228:0) unite *Orodromeus* and *Zephyrosaurus* (unknown in other taxa); (5) *Orodromeus* and *Zephyrosaurus* are united in the lack of an ischial shaft rotation/twist about their axis (char. 340:0); lastly; (6) an angle >120° formed between the tibial and fibular facets on the calcaneum (char. 383:0) unites orodromines.

6.3 | Morphometric PCA

Our PCA analysis indicates that the scapulae of *Fona* form a cluster that is close to, but distinct from *Oryctodromeus*, with the variation in PC axis 2 associated with the breadth and robusticity of the element, especially at the scapular head (Figure 35). The two clusters are closer to each other than to other taxa but are separated along this important shape axis. Crucially, neither taxon overlaps in morphospace with other SBEDO taxa.

7 | DISCUSSION

7.1 | Evolutionary and Paleoecological implications

The interrelationships of early diverging ornithischians persist as one of the most problematic areas of dinosaur phylogenetics (Brown et al., 2021), with recent studies resolving dramatically different interrelationships, often with multiple poorly supported (e.g., Boyd, 2015; Dieudonné et al., 2021). Since the establishment of Orodrominae by Brown et al. (2013), phylogenetic analyses tend to recover this clade with higher consistency and stability, particularly in studies utilizing updated derivations of the Boyd (2015) matrix, which includes *Zephyrosaurus*, *Albertadromeus*, *Koreanosaurus*, *Oryctodromeus*, and *Orodromeus* and consistently recovers them as orodromines (Barta & Norell, 2021; Madzia et al., 2018; Sues et al., 2023). Likewise, a number of other recent studies (Han et al., 2018; Poole, 2023), recover Thescelosaurinae as a relatively stable clade containing *Th. neglectus*, *Th. assiniboiensis* (when included in the taxon list), and *Parksosaurus*, although the latter taxon is sometimes recovered outside the clade (Dieudonné et al., 2021; Yang et al., 2020).

However, the vast majority of SBEDOs (e.g., *Kulindadromeus*, *Othnielosaurus*, *Yueosaurus*, *Yandusaurus*, *Hexinlusaurus*) fluctuate wildly across the different phylogenetic topologies, despite many being well represented both in terms of skeletal completeness (e.g., *Changchunsaurus*, *Changmiania*) and quantity of individuals (e.g., *Haya*, *Jeholosaurus*, *Hypsilophodon*). Here we recover *Oryctodromeus* and *Fona* within Thescelosaurinae rather than Orodrominae. The Bayesian analysis recovers this relationship as strongly supported with a 95% posterior probability.

Recent chronostratigraphic work (Tucker et al., 2023) confidently dates *Fona herzogae* between 99.466 + 0.046/−0.053 and 99.231 + 0.090/−0.052 Myr, thus representing the oldest definitive thescelosaurine. Given its early divergence, *Fona* clarifies the timing of Thescelosaurinae morphological evolution. At some point between the earliest to latest Late Cretaceous, thescelosaurines evolved elongated skulls with preorbital portions that take up over 50% the total skull length. The external naris and antorbital fossa descend ventrally below the level of the orbit and the accessory maxillary fenestra and rostral maxillary boss disappear, reverting to the ancestral state. The lateral surface of the jugal becomes smooth, lacking rugosity or protuberances. The frontals become rostrocaudally shorter and mediolaterally broader, and their contribution to the orbital margin decreases to <25%. The lateral processes of the predentary become elongated, the premaxillary teeth increase from five to six, along with this rostral elongation, and the rostral tip of the dentary becomes ventrally deflected. The angular forms a lateral depression with an upper margin defined by a ridge and the otoccipitals migrate medially to partially exclude the supraoccipital from the foramen magnum. A comprehensive assessment of the quality, validity, and usefulness of these characters will be pursued in a subsequent study focusing on a broad reassessment of neornithischian phylogeny.

Finally, our results demonstrate that thescelosaurines did not emerge in North America inexplicably near the end of the Cretaceous, but were an already well-established clade on the continent by the Cenomanian. Additionally, our results suggest that at least two distinct groups of small-bodied bipedal ornithischians (thescelosaurines and orodromines) inhabited the continent simultaneously throughout the Late Cretaceous, although, as of yet, orodromines and thescelosaurines have not been found in the same assemblage, suggesting potential distinct paleoenvironmental ecosystem preferences for each clade.

7.2 | Intraspecific variation in *Fona*

Specimens of *Fona* exhibit morphological variability, between opposite elements of a single individual, associated specimens preserved in close proximity, and elements from different localities. These include the presence or absence of the premaxillary semilunate fossa (Figure 3a); frontal midline depression (Figure 7e); premaxillary tooth denticles, the prominence of the jugal's lateral protuberance (Figures 3a, 5g and 7a,b); prominence of the parietal midline ridge (= sagittal crest) (Figure 8e); basioccipital ventral "box" below the occipital condyle (Figures 7c and 8c); prominence of the basioccipital ventral keel (Figures 7a and 8a); width and prominence of the basisphenoid/parasphenoid ventral groove (Figures 7c and 8c); sacral vertebrae ventral grooves, keels, fusion, and intercentral cavities (Figures 11b, 12, and 13a, and Data S8); presence of fully ossified intercostal plates (Figures 16 and 17); presence of a scapular glenoid boss and supraglenoid fossae (Figures 18a and 19e); scapulocoracoid fusion (Figures 18a and 19e), size of humeral distal condyles (Figure 20), ulnar lateral grooves (Figure 21a); fusion of pubes (Figures 13, 25, and 26); medial projection of ischial pubic peduncle (Figure 27); ischial shaft dorsal swelling (Figures 13, 26, and 27); dorsal height of the lesser trochanter versus the greater trochanter of the femur (Figure 28b), proximal tibiae medial rim or fossae near the cnemial crest (Figure 29b), and prominence of the caudolateral fossa on the proximal surface MDT (Figure 31). *Fona* also displays intraspecific variation in the number of foramina on the prefrontal and surangular (Figures 3 and 7); mediolateral thickness of dorsal

neural spines (Figure 10b); sacral neural canal shape; scapular spine edge shape (Figure 18a); and the angle formed between the iliac and pubic peduncles of the ilia (Figure 24).

The variability present across specimens of *Fona* could be attributable to the following (nonexclusive) factors including taphonomic distortion, sexual dimorphism, ontogeny, phenotypic variation, the presence of multiple species, and pathology. Among these possible causes, only a few are currently testable, with several outside the current scope of this study. Sexual dimorphism is an exciting possibility, particularly under the assumption that the two (or more) individuals from the Mini Troll locality represent conspecific burrow mates that were found intertwined with each other. Taphonomy is likely to account for some of the variation in elements susceptible to sheering, twisting, bending, flattening, crushing, and/or abrasion forces (Arbour & Currie, 2012; Hedrick & Dodson, 2013; Kammerer et al., 2020). For example, taphonomic subsurface rotting or arthropod burrowing (Roberts et al., 2007) are possible causes of deep excavations present on the distal end of femur FMNH PR 4581, the proximal end of left metatarsal 1 NCSM 33548, and the distal end of right radius NCSM 36522, all of which share a similar rough texture across the internal surface of the aberration. However, taphonomy is unlikely to account for the significant disparities such as asymmetrical scaling or the presence/absence of particular features such as tubercles, foramina, and ridges. Taphonomy is more likely to cause heterogenous effects and therefore unlikely to be responsible for differences observed in contralateral elements between individuals.

We hypothesize that much of the variation is attributable to ontogeny. Notably, the larger and ostensibly more ontogenetically mature individuals from the Manolo, Magic Man, and Karmic localities evince a striking convergence in several morphological traits with *Oryctodromeus*. This convergence is particularly evident in the presence of fused scapulocoracoids, more pronounced scapular spines, a basioccipital fused to the basisphenoid with a wide ventral groove, and the conspicuous presence of a "ventral box" situated on the ventral aspect of the basioccipital. A ventral box was originally ascribed as an autapomorphy of *Oryctodromeus* (Varricchio et al., 2007). However, this box is absent on the other *Oryctodromeus* basioccipital (MOR 1636) and is variably present in specimens of *Fona* (absent on FMNH PR 4581 and present on NCSM 33548). Additional research will be needed to parse among these potential causes of intraspecific variation in *Fona*.

7.3 | Paleobiological implications

Despite being a small-bodied dinosaur with hollow bones, *Fona* is one of the most common taxa in the Mussentuchit Member, close in abundance to the large-bodied, heavily built hadrosauromorph *Eolambia*. This relatively high abundance is in contrast to what would be expected taphonomically (Brown et al., 2013). Additionally, *Fona* represents one of the only vertebrates from the Mussentuchit Member that is commonly preserved in partial or full articulation, a condition shared by *Oryctodromeus* (Krumenacker et al., 2019). Furthermore, the preservation of Mussentuchit thescelosaurids from the Karmic, Mini Troll, Monolo, and Magic Man localities preserves a peculiar pattern in which the largest density of bone is usually constrained to a ~1–2-m square block and elements are tightly packed and border each other (Figures 4 and 6). In contrast, other non-thescelosaurid localities throughout the Mussentuchit commonly lack this preservational pattern. Skeletal elements are often preserved in bonebeds, highly disarticulated and/or spread over larger areas, or are less complete. Altogether, these taphonomic and preservational conditions point to semi-fossoriality, a behavior that has been documented or inferred in other thescelosaurines (Button & Zanno, 2023; Hannebaum & Varricchio, 2022; Varricchio et al., 2007), SBEDOs (Yang et al., 2020), as well as a number of other extinct taxa.

Fossorial, semi-fossorial, and/or digging behavior is hypothesized to correlate with a variety of ecomorphological features in extant taxa. These include the flattened phalanges and unguals in aetosaurs (Dróżdż, 2018), specializations including pelvic girdle and forelimb morphology, large claws, strong neck regions, and worn rostral teeth in crocodyliform taxa (Georgi & Krause, 2010; Marinho & Carvalho, 2009; Sertich & Groenke, 2010), shortened manus in early diverging ceratopsians (Longrich, 2010; Senter, 2007), modifications to the pes for nest building in sauropods (Fowler & Hall, 2011), and various skeletal modifications providing improved stability, forelimb function, and sensory modifications in stem turtles (Lyson et al., 2016). Behavioral inferences based on convergent features adapted for fossoriality have been made in Early Cretaceous cynodonts (Mao et al., 2021), whereas taphonomic evidence along with morphometric analyses have been used to infer burrowing morphology in Mesozoic-aged multituberculate mammals (Weaver et al., 2020). Morphological specializations for scratch-digging have also been hypothesized for some theropod dinosaurs such as alvarezsaurids (Senter, 2023), which are suggested to display a number of limb morphologies similar to burrowing mammals (Lautenschlager, 2014).

In other cases, structures found in Permian and Mesozoic aged sediments have been interpreted as burrows, with varying degrees of confidence. Likewise, the construction of these trace fossils has been ascribed to a variety of extinct

taxa such as therapsids (Groenewald et al., 2001; Hasiotis et al., 2004; Miller et al., 2001; Smith, 1987), cynodonts (McLoughlin et al., 2020), dicynodonts (Smith et al., 2021; Yang et al., 2018), theropod dinosaurs (Simpson et al., 2010), neornithischian dinosaurs (Csiki-Sava et al., 2016; Krumenacker et al., 2019; Martin, 2009), ankylosaurids (Park et al., 2021), and notosuchians (Martinelli et al., 2019). These inferences are further supported when taxa are found in what appears to be a burrow or when the conditions of preservation are suggested to represent burial within a burrow (Damiani et al., 2003; Gomani, 1997; Krumenacker, 2017; Varricchio et al., 2007; Yang et al., 2020). However, even in these situations, fossoriality cannot be directly inferred, especially when the presence of a burrow structure is not certain (Voorhies, 1975b).

Proposed osteological correlates of burrowing behavior in *Oryctodromeus* include a robust humerus, expanded posteroventral margin for the scapula, an elongated acromion process, a fused scapulocoracoid, fused premaxillae, expanded sacral region, and reinforced attachment between the pelvis and sacral vertebrae (Fearon & Varricchio, 2015; Varricchio et al., 2007). The expanded scapula is thought to be associated with providing more attachment space to support the *M. deltoideus scapularis* muscle and the *teres major* (Fearon, 2013). The enlarged *M. deltoideus scapularis* and *M. teres major* are suggested to provide strong retraction potential to the humerus (Fearon & Varricchio, 2016). A possible *coracobrachialis brevis* muscle was suggested to provide humeral protraction, and the presence of the *M. triceps brachii* was suggested to allow extension of the elbow (Fearon & Varricchio, 2016). Fearon and Varricchio (2016) provide additional evidence for burrowing from the abundance of muscle scars across the scapula, which would have potentially provided stability to the girdle. Nearly all these traits are present in *Fona*.

Several osteological features unique to *Fona* may add further support for biomechanical adaptations for a semi-fossorial lifestyle. These include the extensive fusion of several pelvic elements, and an expanded fused sacral series, both of which may provide biomechanical rigidity to the hips during the high torsional forces induced during burrowing, as fusion of certain skeletal elements have been proposed to provide biomechanical adaptations for burrowing in a number of mammalian taxa (eg. Rose & Emry, 1983; VanBuren & Evans, 2017).

The presence of expanded tuberosities and processes on the pubes and ischia of *Fona* are reminiscent of similar anatomical structures in *Ischioceratops* (He et al., 2015) and may indicate an extensive origin site for the *M. flexor tibialis internus 3*. This is further supported by the roughened medial surface on the proximal tibia, which serves as the insertion site. The presence of these structures has biomechanical implications and may relate to adaptations for a semi-fossorial lifestyle in this clade. Finally, the feet appear to show enlarged proportions relative to the rest of the body (Figure 2); in contrast to the diminutive manus, and the forelimbs of some thescelosaurids, which have been suggested to have a limited range of motion (Senter & Mackey, 2023). Taken together, these features may indicate a combination of forelimb-hindlimb burrowing, or simply a hindlimb-dominated burrowing style, a condition known to provide particular biomechanical advantages (e.g., Emerson, 1976), among a number of modern terrestrial bipeds such as megapode brush turkeys (Platt et al., 2016), Springhares (Butynski & Mattingly, 1979; Peinke & Brown, 2005), Jerboa (Naderi et al., 2011; Ponomarenko, 2023), and Kangaroo rats (Edelman, 2011; Voorhies, 1975a), the latter of which are known to burrow in dense, clay-rich substrates (Siciliano-Martina et al., 2023) similar to the ground conditions *Fona* would have faced in the mud-dominated floodplains of the Mussentuchit environment. However, biomechanical and ecomorphological studies are needed to verify these speculations in *Fona*.

Although an obvious burrow structure has not yet been observed during excavation at any of the Mussentuchit localities, this absence may be an artifact of paleoenvironmental differences between the Mussentuchit Member and the Wayan-Vaughn Assemblage (Krumenacker, 2019) and does not rule out semi-fossoriality behavior in *Fona*. Additionally, physical experiments have shown that skeletal remains in a burrow can become disarticulated during burial (Woodruff & Varricchio, 2011).

Evidence against burrowing in *Oryctodromeus* includes the complex network of ossified tendons that run along the axial skeleton from the sacral region to the tail, which would have increased the rigidity of the tail along a substantial portion of its length. In addition to being relatively inflexible, it was long making up more than half the total length of the animal. It is unclear if this condition was present in *Fona*. These ossified tendon networks have been suggested to create rigidity in the tail, preventing mobility within a burrow (Fearon, 2013). However, the functional nature of these tendon networks is not well understood among smaller-bodied ornithischian taxa (Adams & Organ, 2005; Organ, 2006; Organ & Adams, 2005), and their phylogenetic context and ontogenetic development remain poorly understood. Furthermore, the location of the *triceps longus* in relation to the ulna and the glenoid, combined with the modest development of the olecranon process, may not support the ability for strong musculature action as this arrangement is suggested to produce reduced biomechanical leverage (Fearon & Varricchio, 2016). Although this does not preclude fossoriality altogether, it may suggest a reduced role for the forelimbs.

It is also possible that the burial locations of *Fona* are indeed burrow structures, but that they were constructed by a different creature such as a crocodile. In such a case, *Fona* may have just occupied burrows constructed by an ecosystem cohabitant, a phenomenon known to occur in modern taxa (Dupuis-Désormeaux et al., 2023) and extinct taxa (Fernandez et al., 2013). Alternatively, the resultant remains of *Fona* may be the result of scavenged material within such a burrow. Extant crocodiles are known to be extensive burrowers and can produce burrows up to 10 m in length and three meters deep (Campbell & Mazzotti, 2004; Kley & Kearney, 2007), with the Chinese alligator producing dens exceeding 50 meters long (Huang, 1982; Whitaker, 1982). However, none of the recovered *Fona* materials preserve any indication of damage by predatory mastication.

8 | CONCLUSION

Fona herzogae adds to the cryptic diversity of the Mussentuchit Member dinosaur fauna, serving as an important component of this exceptional mid-Cretaceous ecosystem. It would have lived alongside the hadrosauromorph *Eolambia caroljonesa* (McDonald et al., 2017), the Rhabdadontomorph *Iani smithi* (Zanno, Gates, et al., 2023), the small-bodied tyrannosaur *Moros intrepidus* (Zanno, Tucker, et al., 2019), the large-bodied allosaurian *Siats meekerorum* (Zanno & Makovicky, 2013), an unnamed oviraptorosaur (Zanno, Avrahami, et al., 2019) and neoceratopsian (Zanno, Tucker, et al., 2023), and a collection of other terrestrial vertebrates (Avrahami et al., 2018).

The presence of a distinct thescelosaurine taxon in the Mussentuchit member supports the hypothesis that the ancestors of *Thescelosaurus* were present in North America as early as the Cenomanian, co-inhabiting the continent with their sister-taxon Orodrominae. To date, members of these clades have not been found together, suggesting different habitat preferences. Shared ecomorphology with, and a close phylogenetic affinity with *Oryctodromeus* demonstrated here, supports a shared semi-fossorial lifestyle. Some of the extensive intraspecific variation among specimens of *Fona* is likely attributable to ontogenetic transformations, whereas others may suggest a broad phenotypic range for the taxon or may point to sexual dimorphism.

AUTHOR CONTRIBUTIONS

Haviv M. Avrahami: Conceptualization; investigation; funding acquisition; writing – original draft; methodology; validation; visualization; writing – review and editing; formal analysis; project administration; data curation; resources; software. **Peter J. Makovicky:** Conceptualization; writing – review and editing; data curation; resources; funding acquisition. **Ryan T. Tucker:** Visualization; writing – review and editing; data curation. **Lindsay E. Zanno:** Conceptualization; investigation; funding acquisition; methodology; validation; writing – review and editing; project administration; data curation; supervision; resources; formal analysis; writing – original draft.

ACKNOWLEDGMENTS

We thank A. Giterman for preparation of *Fona* specimens from the Mini Troll, Last Chance Theropod, Magic Man, and Karmic localities. A. Knowles prepared the entire articulated postcranial skeleton of NCSM 33548. We thank E. Lund for preparation of specimens from the Mini Troll locality, A. Shinya for the preparation of FMNH PR 4581, and L. Herzog for the initial discovery of the Mini Troll locality as well as ongoing assistance, specimen management, and CT-scanning assistance. We thank S. Moran and W. Simpson for cataloging and providing institution numbers for all NCSM and FMNH specimens. Additionally, we thank all NCSM, NCSU, and FMNH volunteers who have contributed to the collection, preparation, and digitization of these specimens including E. Bender, H. Miller, C. Hauser, K. Lindsay, B. Dale, E. Schubarg, A. Moore, H. Orlowski, and V. Harpe. Special thanks to F. Gallastegui for the discovery of FMNH PR 4581. We thank Z. Hannebaum, D. Varricchio, E. Metz, J. Scannella, and E. Lamm for facilitating multiple collection visits to the Museum of the Rockies to view comparative material of *Orodromeus* and *Oryctodromeus*. Additionally, we thank B. Peecook (IMNH), C. Kammerer (NCMNS), T. Scheyer & D. Hansen (NMZ), Y. Schicker-Siber (SMA), J. Sertich (DMNS), R. Cifelli & J. Larsen (OMNH), D. Evans & B. Iwama (ROM), S. Johnston & C. Byrd (MCZ), J. Kirkland & M. Hayden (UGS), R. Irmis (NHMU), V. Rhue and D. Brinkman (YPM), M. Jin and C. Mehling (AMNH), L. Jacobs and D. Winkler (SMU), R. Scheetz (BYU), A. Millhouse (NMNH), P. Barrett, S. Maidment, M. Jones, M. Day (NHMUK) and X. Zheng (STMN) who facilitated collection visits. We thank D. Barta, L.J. Krumenacker, C. Boyd, K. Poole, and J. Napoli, T. Gates, A. Canoville, for training and conversations that improved this research. We thank A. Hartstone-Rose, B. Stuart, B. Langerhans, and K. Wegmann for serving as the dissertation committee members of the first author. We thank the staff of BLM Utah and the Price Field Office for permitting support. This research is supported by the Jurassic Foundation, the Paleontological Society, the Canyonlands Natural History Association, the North Carolina Fossil Club, and the National Science Foundation under Grant Nos. FRES 1925973 & 1925884. This study was performed in part at the Analytical Instrumentation Facility (AIF) at North Carolina State University,

which is supported by the State of North Carolina and the National Science Foundation (award number ECCS-2025064). The AIF is a member of the North Carolina Research Triangle Nanotechnology Network (RTNN), a site in the National Nanotechnology Coordinated Infrastructure (NNCI).

ORCID

Haviv M. Avrahami https://orcid.org/0009-0006-5197-2119

REFERENCES

Adams, J. S., & Organ, C. L. (2005). Histologic determination of ontogenetic patterns and processes in hadrosaurian ossified tendons. *Journal of Vertebrate Paleontology*, *25*, 614–622.

Agnolín, F. L., Herrera, G. Á., Rolando, M. A., Motta, M., Rozadilla, S., Verdiquio, L., D'Angelo, J. S., Moyano-Paz, D., Varela, A. N., & Sterli, J. (2024). Fossil vertebrates from the Cerro Fortaleza Formation (Upper Cretaceous), Santa Cruz Province, Argentina. *Cretaceous Research*, *154*, 105735.

Allison, B., Lamaster, T., Avrahami, H. M., & Zanno, L. E. (2019). Buccal tooth development, replacement rate, and microstructure in Parksosauridae (Dinosauria: Neornithischia). *Journal of Vertebrate Paleontology* Program Abstract:79:53.

Andrzejewski, K. A., Winkler, D. A., & Jacobs, L. L. (2019). A new basal ornithopod (Dinosauria: Ornithischia) from the Early Cretaceous of Texas. *PLoS One*, *14*, 1–44.

Arbour, V. M., & Currie, P. J. (2012). Analyzing taphonomic deformation of ankylosaur skulls using retrodeformation and finite element analysis. *PLoS One*, *7*, e39323.

Avrahami, H. M., Gates, T. A., Heckert, A. B., Makovicky, P., & Zanno, L. E. (2018). A new microvertebrate assemblage from the Mussentuchit Member, Cedar Mountain Formation: Insights into the paleobiodiversity and paleobiogeography of Early Late Cretaceous ecosystems in western North America. *PeerJ*, *6*, e5883.

Avrahami, H. M., Hauser, C. M., & Zanno, L. E. (2023). New additions to the early diverging ornithischian *Zephyrosaurs shaffi* from the Cretaceous Cloverly Formation of North America. *Journal of Vertebrate Paleontology* Program Abstract:83:77.

Avrahami, H. M., Lindsey, K. P., & Herzog, L. (2023). Advances in 3D surface scanning: Mobile device applications set a new standard for the digitization of fossils and museum artifacts. *Journal of Vertebrate Paleontology* Program Abstract 83:77.

Avrahami, H. M., Mackovicky, P. J., & Zanno, L. E. (2022). A New Orodromine from the Mussentuchit Member of the Cedar Mountain Formation, Utah. *Journal of Vertebrate Paleontology* Program Abstract:82:71.

Avrahami, H. M., Mackovicky, P. J., & Zanno, L. E. (in prep). The cranial anatomy of the semi-fossorial neornithischian *Fona herzogae* from the Cenomanian-age Mussentuchit Member of the Cedar Mountain Formation. *Utah*.

Barbosa, F. F., Mermudes, J. R. M., & Russo, C. A. (2024). Performance of tree-building methods using a morphological dataset and a well-supported Hexapoda phylogeny. *PeerJ*, *12*, e16706.

Barker, C. T., Naish, D., Newham, E., Katsamenis, O. L., & Dyke, G. (2017). Complex neuroanatomy in the rostrum of the Isle of Wight theropod *Neovenator salerii*. *Scientific Reports*, *7*, 1–8.

Baron, M. G. (2019). *Pisanosaurus mertii* and the Triassic ornithischian crisis: Could phylogeny offer a solution? *Historical Biology*, *31*, 967–981.

Baron, M. G., Norman, D. B., & Barrett, P. M. (2017). Postcranial anatomy of *Lesothosaurus diagnosticus* (Dinosauria: Ornithischia) from the Lower Jurassic of southern Africa: Implications for basal ornithischian taxonomy and systematics. *Zoological Journal of the Linnean Society*, *179*, 125–168.

Barrett, P. M. (2016). A new specimen of *Valdosaurus canaliculatus* (Ornithopoda: Dryosauridae) from the Lower Cretaceous of the Isle of Wight, England.

Barrett, P. M., Butler, R. J., & Knoll, F. (2005). Small-bodied ornithischian dinosaurs from the Middle Jurassic of Sichuan, China. *Journal of Vertebrate Paleontology*, *25*, 823–834.

Barrett, P. M., Butler, R. J., Mundil, R., Scheyer, T. M., Irmis, R. B., & Sánchez-Villagra, M. R. (2014). A palaeoequatorial ornithischian and new constraints on early dinosaur diversification. *Proceedings of the Royal Society B: Biological Sciences*, *281*, 1–6.

Barrett, P. M., Butler, R. J., & Nesbitt, S. J. (2011). The roles of herbivory and omnivory in early dinosaur evolution. *Earth and Environmental Science Transactions of the Royal Society of Edinburgh*, *101*, 383–396.

Barrett, P. M., & Han, F.-L. (2009). Cranial anatomy of *Jeholosaurus shangyuanensis* (Dinosauria: Ornithischia) from the Early Cretaceous of China. *Zootaxa*, *2072*, 31–55.

Barta, D. E., & Norell, M. A. (2021). The osteology of *Haya griva* (Dinosauria: Ornithischia) from the Late Cretaceous of Mongolia. *Bulletin of the American Museum of Natural History*, *445*, 1–112.

Becerra, M. G., Pol, D., Porro, L. B., Paulina-Carabajal, A., & Rauhut, O. W. (2022). Craniomandibular osteology of *Manidens condorensis* (Ornithischia: Heterodontosauridae) from the Upper Lower Jurassic of Argentina. *Journal of Vertebrate Paleontology*, *42*, e2181087.

Bolotsky, Y. L., & Godefroit, P. (2004). A new hadrosaurine dinosaur from the Late Cretaceous of far eastern Russia. *Journal of Vertebrate Paleontology*, *24*, 351–365.

Bonde, J. W., Hall, R. L., Krumenacker, L., & Varricchio, D. J. (2022). *Nevadadromeus schmitti* (gen. et sp. nov.), a New basal Neornithischian with affinities to the Thescelosaurinae, from the Upper Cretaceous (Cenomanian) Willow Tank Formation of southern Nevada. *Journal of the Arizona-Nevada Academy of Science*, *50*, 1–8.

Borja-Quichocho-Calvo, K. (2021). *Returning to Fo'Na, returning home: Rematriating education for CHamorus in Guåhan*. University of Hawai'i at Manoa.

Bouckaert, R., Vaughan, T. G., Barido-Sottani, J., Duchêne, S., Fourment, M., Gavryushkina, A., Heled, J., Jones, G., Kühnert, D., & de Maio, N. (2019). BEAST 2.5: An advanced software platform for Bayesian evolutionary analysis. *PLoS Computational Biology*, *15*, e1006650.

Bourke, J. M., Ruger Porter, W. M., Ridgely, R. C., Lyson, T. R., Schachner, E. R., Bell, P. R., & Witmer, L. M. (2014). Breathing life into dinosaurs: Tackling challenges of soft-tissue restoration and nasal airflow in extinct species. *The Anatomical Record*, *297*, 2148–2186.

Boyd CA. 2012. *Taxonomic revision of latest Cretaceous North American basal neornithischian taxa and a phylogenetic analysis of basal ornithischian relationships*.

Boyd, C. A. (2014). The cranial anatomy of the neornithischian dinosaur *Thescelosaurus neglectus*. *PeerJ*, *2*, e669.

Boyd, C. A. (2015). The systematic relationships and biogeographic history of ornithischian dinosaurs. *PeerJ*, *3*, e1523.

Boyd, C. A., Brown, C. M., Scheetz, R. D., & Clarke, J. A. (2009). Taxonomic revison of the basal Neornithischian taxa *Thescelosaurus* and *Bugenasaura*. *Journal of Vertebrate Paleontology*, *29*, 758–770.

Boyd, C. A., Cleland, T. P., & Novas, F. (2011). Osteogenesis, homology, and function of the intercostal plates in ornithischian dinosaurs (Tetrapoda, Sauropsida). *Zoomorphology*, *130*, 305–313.

Brown, C. M., Boyd, C. A., & Russell, A. P. (2011). A new basal ornithopod dinosaur (Frenchman Formation, Saskatchewan, Canada), and implications for Late Maastrichtian ornithischian diversity in North America. *Zoological Journal of the Linnean Society*, *163*, 1157–1198.

Brown, C. M., Evans, D. C., Ryan, M. J., & Russell, A. P. (2013). New data on the diversity and abundance of small-bodied ornithopods (Dinosauria, Ornithischia) from the Belly River Group (Campanian) of Alberta. *Journal of Vertebrate Paleontology*, *33*, 495–520.

Brown, E. E., Butler, R. J., Barrett, P. M., & Maidment, S. C. (2021). Assessing conflict between early neornithischian tree topologies. *Journal of Systematic Palaeontology*, *19*, 1183–1206.

Butler, R. J., & Galton, P. M. (2008). The "dermal armour" of the ornithopod dinosaur *Hypsilophodon* from the Wealden (Early Cretaceous: Barremian) of the Isle of Wight: A reappraisal. *Cretaceous Research*, *29*, 636–642.

Butler, R. J., Jin, L., Jun, C., & Godefroit, P. (2011). The postcranial osteology and phylogenetic position of the small ornithischian dinosaur *Changchunsaurus parvus* from the Quantou Formation (Cretaceous: Aptian-Cenomanian) of Jilin Province, northeastern China. *Palaeontology*, *54*, 667–683.

Butler, R. J., Porro, L. B., Galton, P. M., & Chiappe, L. M. (2012). Anatomy and cranial functional morphology of the small-bodied dinosaur *Fruitadens haagarorum* from the Upper Jurassic of the USA. *PLoS One*, *7*, e31556.

Butler, R. J., Upchurch, P., & Norman, D. B. (2008). The phylogeny of the ornithischian dinosaurs. *Journal of Systematic Palaeontology*, *6*, 1–40.

Button, D. J., Porro, L. B., Lautenschlager, S., Jones, M. E., & Barrett, P. M. (2023). Multiple pathways to herbivory underpinned deep divergences in ornithischian evolution. *Current Biology*, *33*, 557–565.e7.

Button, D. J., & Zanno, L. E. (2023). Neuroanatomy of the Late Cretaceous *Thescelosaurus neglectus* (Neornithischia: Thescelosauridae) reveals novel ecological specialisations within Dinosauria. *Scientific Reports*, *13*, 19224.

Butynski, T. M., & Mattingly, R. (1979). Burrow structure and fossorial ecology of the springhare *Pedetes capensis* in Botswana. *African Journal of Ecology*, *17*, 205–215.

Calvo, J. O., Porfiri, J. D., & Novas, F. E. (2007). Discovery of a new ornithopod dinosaur from the Portezuelo Formation (Upper Cretaceous), Neuquen, Patagonia, Argentina. *Arquivos Do Museu Nacional*, *65*, 471–483.

Campbell, M. R., & Mazzotti, F. J. (2004). Characterization of natural and artificial alligator holes. *Southeastern Naturalist*, *3*, 583–594.

Carpenter, K., & Galton, P. (2018). A photo documentation of bipedal ornithischian dinosaurs from the Upper Jurassic Morrison Formation, USA. *Geology of the Intermountain West*, *5*, 167–207.

Carrano, M. T., & Hutchinson, J. H. (2002). Pelvic and hindlimb musculature of *Tyrannosaurus rex* (Dinosauria: Theropoda). *Journal of Morphology*, *253*, 207–228.

Cepeda, J. (2021). Jeremy Cepeda talks about the Chamorro language with Pauly Suba. In P. Charfauros (Ed.), *K57 interviews*.

Chanthasit, P. (2010). *The ornithopod dinosaur Rhabdodon from the Late Cretaceous of France: Anatomy, systematics and paleobiology*. Université Claude Bernard-Lyon I.

Chinnery, B. J., & Horner, J. R. (2007). A new neoceratopsian dinosaur linking North American and Asian taxa. *Journal of Vertebrate Paleontology*, *27*, 625–641.

Coria, R. A., & Calvo, J. O. (2002). A new iguanodontian ornithopod from Neuquen Basin, Patagonia, Argentina. *Journal of Vertebrate Paleontology*, *22*, 503–509.

Coria, R. A., Moly, J. J., Reguero, M., Santillana, S., & Marenssi, S. (2013). A new ornithopod (Dinosauria; Ornithischia) from Antarctica. *Cretaceous Research*, *41*, 186–193.

Coria, R. A., & Salgado, L. (1996). A basal iguanodontian (Ornithischia: Ornithopoda) from the Late Cretaceous of South America. *Journal of Vertebrate Paleontology*, *16*, 445–457.

Cruz, B. L. (2022). *Rediscovering Fo'na and Pontan*. Guampedia.

Cruzado-Caballero, P., Gasca, J. M., Filippi, L. S., Cerda, I. A., & Garrido, A. C. (2019). A new ornithopod dinosaur from the Santonian of northern Patagonia (Rincón de los sauces, Argentina). *Cretaceous Research*, *98*, 211–229.

Csiki-Sava, Z., Vremir, M., Vasile, Ş., Brusatte, S. L., Dyke, G., Naish, D., Norell, M. A., & Totoianu, R. (2016). The East Side story: The Transylvanian latest Cretaceous continental vertebrate record and its implications for understanding Cretaceous–Paleogene boundary events. *Cretaceous Research*, *57*, 662–698.

Cunningham, L. J. (1992). *Ancient Chamorro society*. Bess Press.

Currie, B. S. (2002). Structural configuration of the Early Cretaceous cordilleran foreland-basin system and Sevier thrust belt, Utah and Colorado. *The Journal of Geology*, *110*, 697–718.

Dalmasso, A., Peláez-Campomanes, P., & López-Antoñanzas, R. (2022). Relative performance of Bayesian morphological clock and parsimony methods for phylogenetic reconstructions: Insights from the case of Myomiminae and Dryomyinae glirid rodents. *Cladistics*, *38*, 702–710.

Damiani, R., Modesto, S., Yates, A., & Neveling, J. (2003). Earliest evidence of cynodont burrowing. *Proceedings of the Royal Society of London Series B: Biological Sciences*, *270*, 1747–1751.

DeCelles, P. G., & Coogan, J. C. (2006). Regional structure and kinematic history of the Sevier fold-and-thrust belt, central Utah. *Geological Society of America Bulletin*, *118*, 841–864.

Dieudonné, P.-E., Cruzado-Caballero, P., Godefroit, P., & Tortosa, T. (2021). A new phylogeny of cerapodan dinosaurs. *Historical Biology*, *33*, 1–21.

Dodson, P., & Madsen, J. H. (1981). On the sternum of *Camptosaurus*. *Journal of Paleontology Memoir*, *55*, 109–112.

Dróżdż, D. (2018). Osteology of a forelimb of an aetosaur *Stagonolepis olenkae* (Archosauria: Pseudosuchia: Aetosauria) from the Krasiejów locality in Poland and its probable adaptations for a scratch-digging behavior. *PeerJ*, *6*, e5595.

Duhaylonsod, D. J. U., & Cepeda, J. (2022). Personal communication: Meeting to discuss dinosaur naming with Chamoru cultural significance.

Dupuis-Désormeaux, M., Dheer, A., Gilisho, S., Kaaria, T. N., Davidson, Z., & MacDonald, S. E. (2023). Teeth, tusks, and spikes: Repeated den sharing between predator and prey in an African Savannah. *African Journal of Ecology.*, *61*, 1006–1009.

Edelman, A. J. (2011). Kangaroo rats remodel burrows in response to seasonal changes in environmental conditions. *Ethology*, *117*, 430–439.

Edmund, A. G. (1957). On the special foramina in the jaws of many ornithischian dinosaurs. *Contributions of the Royal Ontario Museum Division of Zoology and Palaeontology*, *48*, 1–14.

Emerson, S. B. (1976). Burrowing in frogs. *Journal of Morphology*, *149*, 437–458.

Erickson, G. M., Lappin, A. K., & Larson, P. (2005). Androgynous rex: The utility of chevrons for determining the sex of crocodilians and non-avian dinosaurs. *Zoology*, *108*, 277–286.

Escaso, F., Ortega, F., Dantas, P., Malafaia, E., Silva, B., Gasulla, J. M., Mocho, P., In, N., & JâL, S. (2014). A new dryosaurid ornithopod (Dinosauria, Ornithischia) from the Late Jurassic of Portugal. *Journal of Vertebrate Paleontology*, *34*, 1102–1112.

Fearon, J. L. (2013). *Scratch-digging in the Cretaceous basal ornithopod dinosaur Oryctodromeus cubicularis: Evidence from morphometric analyses and reconstruction of the forelimb musculature*. Montana State University-Bozeman, College of Letters & Science.

Fearon, J. L., & Varricchio, D. J. (2015). Morphometric analysis of the forelimb and pectoral girdle of the Cretaceous ornithopod dinosaur *Oryctodromeus cubicularis* and implications for digging. *Journal of Vertebrate Paleontology*, *35*, e936555.

Fearon, J. L., & Varricchio, D. J. (2016). Reconstruction of the forelimb musculature of the Cretaceous ornithopod dinosaur *Oryctodromeus cubicularis*: Implications for digging. *Journal of Vertebrate Paleontology*, *36*, e1078341.

Fernandez, V., Abdala, F., Carlson, K. J., Cook, D. C., Rubidge, B. S., Yates, A., & Tafforeau, P. (2013). Synchrotron reveals Early Triassic odd couple: Injured amphibian and aestivating Therapsid share burrow. *PLoS One*, *8*, e64978.

Forster, C. A. (1990). The postcranial skeleton of the ornithopod dinosaurs *Tenontosaurus tilletti*. *Journal of Vertebrate Paleontology*, *10*, 273–294.

Fowler, D. W., & Hall, L. E. (2011). Scratch-digging sauropods, revisited. *Historical Biology*, *23*, 27–40.

Galton, P., & Jensen, J. (1973). Skeleton of a hypsilophodontid dinosaur (*Nanosaurus* (?) *rex*) from the Upper Jurassic of Utah. *Brigham Young University Geology Studies*, *20*, 137–157.

Galton, P. M. (1973). Redescription of the skull and mandible of *Parksosaurus* from the Late Cretaceous.

Galton, P. M. (1974). The ornithischian dinosaur *Hypsilophodon* from the Wealden of the Isle of Wight. *Bulletin of the British Museum (Natural History)*, *25*, 1–152.

Galton, P. M. (1981). *Dryosaurus*, a hypsilophodontid dinosaur from the Upper Jurassic of North America and Africa postcranial skeleton. *Paläontologische Zeitschrift*, *55*, 271–312.

Galton, P. M. (1989). Crania and endocranial casts from ornithopod dinosaurs of the families Dryosauridae and Hypsilophodentidae (Reptilia: Ornithischia). *Geologica et Palaeontologica*, *23*, 217–239.

Galton, P. M. (1997). Cranial anatomy of the basal hypsilophodontid dinosaur *Thescelosaurus neglectus* Gilmore (Ornithischia: Ornithopoda) from the Upper Cretaceous of North America. *Revue Paléobiologie Genéve*, *16*, 231–258.

Galton, P. M. (2012). *Hypsilophodon foxii and other smaller bipedal ornithischian dinosaurs from the Lower Cretaceous of southern England* (pp. 225–281). Bernissart dinosaurs and Early Cretaceous terrestrial ecosystems Indiana University Press.

Gates, T. A., Lund, E. K., Boyd, C., DeBlieux, D. D., Titus, A. L., Evans, D. C., Getty, M. A., Kirkland, J. I., & Eaton, J. G. (2013). Ornithopod dinosaurs from the Grand Staircase-Escalante National Monument Region, Utah, and their role in paleobiogeographic and macroevolutionary studies. At the Top of the Grand Staircase: The Late Cretaceous in Utah: 463–481.

Georgi, J. A., & Krause, D. W. (2010). Postcranial axial skeleton of *Simosuchus clarki* (Crocodyliformes: Notosuchia) from the Late Cretaceous of Madagascar. *Journal of Vertebrate Paleontology*, *30*, 99–121.

Gilmore, C. W. (1915). Osteology of *Thescelosaurus*, an orthopodous dinosaur from the Lance Formation of Wyoming. *Proceedings of the United States National Museum*, *49*, 591–616.

Gilmore, C. W. (1924). *A new species of Laosaurus, an ornithischian dinosaur from the Cretaceous of Alberta*. Royal Society of Canada.

Godefroit, P., Bolotsky, Y. L., & Lauters, P. (2012). A New Saurolophine dinosaur from the latest Cretaceous of far eastern Russia. *PLoS One*, *7*, e36849.

Godefroit, P., Sinitsa, S. M., Dhouailly, D., Bolotsky, Y. L., Sizov, A. V., McNamara, M. E., Benton, M. J., & Spagna, P. (2014). A Jurassic ornithischian dinosaur from Siberia with both feathers and scales. *Science*, *345*, 451–455.

Goloboff, P. A., & Morales, M. E. (2023). TNT version 1.6, with a graphical interface for MacOS and Linux, including new routines in parallel. *Cladistics*, *39*, 144–153.

Goloboff, P. A., Pittman, M., Pol, D., & Xu, X. (2019). Morphological data sets fit a common mechanism much more poorly than DNA sequences and call into question the Mkv model. *Systematic Biology*, *68*, 494–504.

Gomani, E. M. (1997). A crocodyliform from the Early Cretaceous dinosaur beds, northern Malawi. *Journal of Vertebrate Paleontology*, *17*, 280–294.

Groenewald, G. H., Welman, J., & MacEachern, J. A. (2001). Vertebrate burrow complexes from the Early Triassic *Cynognathus* zone (Driekoppen Formation, Beaufort Group) of the Karoo Basin, South Africa. *PALAIOS*, *16*, 148–160.

Hammer, Ø., Harper, D., & Ryan, P. (2001). Paleontological statistics software: Package for education and data analysis. *Palaeontologia Electronica*, *4*, 1–92.

Han, F., Barrett, P. M., Butler, R. J., & Xu, X. (2012). Postcranial anatomy of *Jeholosaurus shangyuanensis* (Dinosauria, Ornithischia) from the Lower Cretaceous Yixian Formation of China. *Journal of Vertebrate Paleontology*, *32*, 1370–1395.

Han, F., Forster, C. A., Clark, J. M., & Xu, X. (2016). Cranial anatomy of *Yinlong downsi* (Ornithischia: Ceratopsia) from the Upper Jurassic Shishugou Formation of Xinjiang, China. *Journal of Vertebrate Paleontology*, *36*, e1029579.

Han, F., Forster, C. A., Xu, X., & Clark, J. M. (2018). Postcranial anatomy of *Yinlong downsi* (Dinosauria: Ceratopsia) from the Upper Jurassic Shishugou Formation of China and the phylogeny of basal ornithischians. *Journal of Systematic Palaeontology*, *16*, 1159–1187.

Hannebaum, Z. J., & Varricchio, D. J. (2022). A study of *Orodromeus* taphonomy at egg mountain, part of the Upper Cretaceous Two Medicine Formation near Choteau, Montana. *Journal of Vertebrate Paleontology Program Abstract*, *164*, 77.

Hasiotis, S. T., Wellner, R. W., Martin, A. J., & Demko, T. M. (2004). Vertebrate burrows from Triassic and Jurassic continental deposits of North America and Antarctica: Their paleoenvironmental and paleoecological significance. *Ichnos*, *11*, 103–124.

He, X., & Cai, K. (1983). A new species of *Yandusaurus* (Hypsilophodont dinosaur) from the Middle Jurassic of Dashanpu, Zigong, Sichuan. *Journal of the Chengdu College of Geology Supplement*, *1*, 14–25.

He, X., & Cai, K. (1984). The Middle Jurassic dinosaurian Fauna from Dashanpu, Zigong, Sichuan. Vol 1, the Ornithopod dinosaurs. *Chengdu: Sichuan Scientific and Technological Publishing House*, *71*, 1–66.

He, Y., Makovicky, P. J., Wang, K., Chen, S., Sullivan, C., Han, F., & Xu, X. (2015). A new leptoceratopsid (Ornithischia, Ceratopsia) with a unique ischium from the Upper Cretaceous of Shandong Province, China. *PLoS One*, *10*, e0144148.

Hedrick, B. P., & Dodson, P. (2013). Lujiatun psittacosaurids: Understanding individual and taphonomic variation using 3D geometric morphometrics. *PLoS One*, *8*, e69265.

Herne, M. C., Nair, J. P., Evans, A. R., & Tait, A. M. (2019). New small-bodied ornithopods (Dinosauria, Neornithischia) from the Early Cretaceous Wonthaggi Formation (Strzelecki Group) of the Australian-Antarctic rift system, with revision of *Qantassaurus intrepidus* Rich and Vickers-Rich, 1999. *Journal of Paleontology Memoir*, *93*, 543–584.

Herne, M. C., Tait, A. M., Weisbecker, V., Hall, M., Nair, J. P., Cleeland, M., & Salisbury, S. W. (2018). A new small-bodied ornithopod (Dinosauria, Ornithischia) from a deep, high-energy Early Cretaceous river of the Australian–Antarctic rift system. *PeerJ*, *5*, e4113.

Huang, C.-c. (1982). The ecology of the Chinese alligator and changes in its geographical distribution. In *Crocodiles. Proceedings of the 5th working meeting of the IUCN/SSC crocodile specialist group, gland*. International Union for Conservation of Nature and Natural Resources.

Hübner, T. (2011). *Ontogeny in Dysalotosaurus lettowvorbecki*. lmu.

Hübner, T. (2018). The postcranial ontogeny of *Dysalotosaurus lettowvorbecki* (Ornithischia: Iguanodontia) and implications for the evolution of ornithopod dinosaurs. *Palaeontographica Abteilung A*, *310*, 43–120.

Hübner, T. R., Foth, C., Heinrich, W.-D., Schwarz, D., & Bussert, R. (2021). Research history, taphonomy, and age structure of a mass accumulation of the ornithopod dinosaur *Dysalotosaurus lettowvorbecki* from the Upper Jurassic of Tanzania. *Acta Palaeontologica Polonica*, *66*, 275–300.

Hübner, T. R., & Rauhut, O. W. (2010). A juvenile skull of *Dysalotosaurus lettowvorbecki* (Ornithischia: Iguanodontia), and implications for cranial ontogeny, phylogeny, and taxonomy in ornithopod dinosaurs. *Zoological Journal of the Linnean Society*, *160*, 366–396.

Hudgins, M. N. (2021). The Paleobiology, Paleoecology, and Evolution of Thescelosauridae (Ornithischia) from Alberta, Canada.

Huh, M., Lee, D.-G., Kim, J.-K., Lim, J.-D., & Godefroit, P. (2010). A new basal ornithopod dinosaur from the Upper Cretaceous of South Korea. *Neues Jahrbuch für Geologie Und Paläontologie Abhandlungen*, *259*, 1–24.

Hulke, J. W. (1882). XXIV. An attempt at a complete osteology of *hypsilophodon foxii*; a British Wealden dinosaur. *Philosophical Transactions of the Royal Society of London*, *173*, 1035–1062.

Huxley, T. H. (1870). On *Hypsilophodon foxii*, a new dinosaurian from the Wealden of the Isle of Wight. *Quarterly Journal of the Geological Society of London*, *32*, 3–12.

Ibiricu, L. M., Casal, G. A., Martínez, R. D., Luna, M., Canale, J. I., Álvarez, B. N., & Riga, B. G. (2019). A new ornithopod dinosaur (Dinosauria: Ornithischia) from the Late Cretaceous of central Patagonia. *Cretaceous Research*, *98*, 276–291.

Ibiricu, L. M., Martinez, R. D., Luna, M., & Casal, G. A. (2014). A reappraisal of *Notohypshilophodon comodorensis* (Ornithischia: Ornithopoda) from the Late Cretaceous of Patagonia, Argentina.

Jin, L., Jun, C., Zan, S., Butler, R. J., & Godefroit, P. (2010). Cranial anatomy of the small ornithischian dinosaur *Changchunsaurus parvus* from the Quantou Formation (Cretaceous: Aptian-Cenomanian) of Jilin Province, northeastern China. *Journal of Vertebrate Paleontology*, *30*, 196–214.

Kammerer, C. F., Deutsch, M., Lungmus, J. K., & Angielczyk, K. D. (2020). Effects of taphonomic deformation on geometric morphometric analysis of fossils: A study using the dicynodont *Diictodon feliceps* (Therapsida, Anomodontia). *PeerJ*, *8*, e9925.

Kirkland, J. I., Suarez, M., Suarez, C., & Hunt-Foster, R. (2016). The Lower Cretaceous in east-Central Utah: The Cedar Mountain Formation and its bounding strata (field trip guide). *Geology of the Intermountain West*, *3*, 101–228.

Kley, N., & Kearney, M. (2007). Adaptations for digging and burrowing. *Fins into Limbs: Evolution, Development, and Transformation*, 284–309.

Krumenacker, L. (2017). *Osteology, phylogeny, taphonomy, and ontogenetic histology of Oryctodromeus cubicularis, from the Middle Cretaceous (Albian-Cenomanian) of Montana and Idaho*. Montana State University.

Krumenacker, L. (2019). Paleontological and chronostratigraphic correlations of the mid-Cretaceous Wayan-Vaughn depositional system of southwestern Montana and southeastern Idaho. *Historical Biology*, *32*, 1–11.

Krumenacker, L., Varricchio, D. J., Wilson, J. P., Martin, A., & Ferguson, A. (2019). Taphonomy of and new burrows from *Oryctodromeus cubicularis*, a burrowing neornithischian dinosaur, from the mid-Cretaceous (Albian-Cenomanian) of Idaho and Montana, USA. *Palaeogeography, Palaeoclimatology, Palaeoecology*, *530*, 300–311.

Laskowski, A. K., DeCelles, P. G., & Gehrels, G. E. (2013). Detrital zircon geochronology of Cordilleran retroarc foreland basin strata, western North America. *Tectonics*, *32*, 1027–1048.

Lautenschlager, S. (2014). Morphological and functional diversity in therizinosaur claws and the implications for theropod claw evolution. *Proceedings of the Royal Society of London B: Biological Sciences*, *281*, 20140497.

Li, N., Dai, H., Tan, C., Hu, X., Wei, Z., Lin, Y., Wei, G., Li, D., Meng, L., & Hao, B. (2019). A neornithischian dinosaur from the Middle Jurassic Xintiangou Formation of Yunyang, Chongqing, China: The earliest record in Asia. *Historical Biology*, *33*, 1089–1102.

Longrich, N. (2010). *Mojoceratops perifania*, a new chasmosaurine ceratopsid from the Late Campanian of western Canada. *Journal of Paleontology Memoir*, *84*, 681–694.

Lyson, T. R., Rubidge, B. S., Scheyer, T. M., de Queiroz, K., Schachner, E. R., Smith, R. M., Botha-Brink, J., & Bever, G. (2016). Fossorial origin of the turtle shell. *Current Biology*, *26*, 1887–1894.

Madzia, D., Arbour, V. M., Boyd, C. A., Farke, A. A., Cruzado-Caballero, P., & Evans, D. C. (2021). The phylogenetic nomenclature of ornithischian dinosaurs. *PeerJ*, *9*, e12362.

Madzia, D., Boyd, C. A., & Mazuch, M. (2018). A basal ornithopod dinosaur from the Cenomanian of The Czech Republic. *Journal of Systematic Palaeontology*, *16*, 967–979.

Maidment, S. C. R., & Barrett, P. M. (2011). The locomotor musculature of basal ornithischian dinosaurs. *Journal of Vertebrate Paleontology*, *31*, 1265–1291.

Makovicky, P. J., Kilbourne, B. M., Sadleir, R. W., & Norell, M. A. (2011). A new basal ornithopod (Dinosauria, Ornithischia) from the Late Cretaceous of Mongolia. *Journal of Vertebrate Paleontology*, *31*, 626–640.

Manitkoon, S., Deesri, U., Khalloufi, B., Nonsrirach, T., Suteethorn, V., Chanthasit, P., Boonla, W., & Buffetaut, E. (2023). A new basal neornithischian dinosaur from the Phu Kradung Formation (Upper Jurassic) of northeastern Thailand. *Diversity*, *15*, 851.

Manitkoon, S., Deesri, U., Warapeang, P., Nonsrirach, T., & Chanthasit, P. (2023). Ornithischian dinosaurs in Southeast Asia: A review with palaeobiogeographic implications. *Fossil Record*, *26*, 1–25.

Mao, F., Zhang, C., Liu, C., & Meng, J. (2021). Fossoriality and evolutionary development in two Cretaceous mammaliamorphs. *Nature*, *592*, 577–582.

Marinho, T. S., & Carvalho, I. S. (2009). An armadillo-like sphagesaurid crocodyliform from the Late Cretaceous of Brazil. *Journal of South American Earth Sciences*, *27*, 36–41.

Martin, A. J. (2009). Dinosaur burrows in the Otway Group (Albian) of Victoria, Australia, and their relation to Cretaceous polar environments. *Cretaceous Research*, *30*, 1223–1237.

Martinelli, A. G., Basilici, G., Fiorelli, L. E., Klock, C., Karfunkel, J., Diniz, A. C., Soares, M. V., Marconato, A., da Silva, J. I., & Ribeiro, L. C. B. (2019). Palaeoecological implications of an Upper Cretaceous tetrapod burrow (Bauru Basin; Peirópolis, Minas Gerais, Brazil). *Palaeogeography, Palaeoclimatology, Palaeoecology*, *528*, 147–159.

McDonald, A. T., Gates, T. A., Zanno, L. E., & Makovicky, P. J. (2017). Anatomy, taphonomy, and phylogenetic implications of a new specimen of *Eolambia caroljonesa* (Dinosauria: Ornithopoda) from the Cedar Mountain Formation, Utah, USA. *PLoS One*, *12*, e0176896.

McLoughlin, S., Mays, C., Vajda, V., Bocking, M., Frank, T. D., & Fielding, C. R. (2020). Dwelling in the dead zone: Vertebrate burrows immediately succeeding the end-Permian extinction event in Australia. *PALAIOS*, *35*, 342–357.

Miller, M. F., Hasiotis, S. T., Babcock, L. E., Isbell, J. L., & Collinson, J. W. (2001). Tetrapod and large burrows of uncertain origin in Triassic high paleolatitude floodplain deposits, Antarctica. *PALAIOS*, *16*, 218–232.

Monarrez, P. M., Zimmt, J. B., Clement, A. M., Gearty, W., Jacisin, J. J., Jenkins, K. M., Kusnerik, K. M., Poust, A. W., Robson, S. V., & Sclafani, J. A. (2021). Our past creates our present: A brief overview of racism and colonialism in Western paleontology. *Paleobiology*, *48*, 1–13.

Morris, W. J. (1976). Hypsilophodont dinosaurs: A new species and comments on their systematics. In C. S. Churcher (Ed.), *Essays on palaeontology in honour of Loris Shano Russell* (pp. 93–113). Royal Ontario Museum Life Sciences Miscellaneous Publication.

Naderi, G., Hemami, M. R., Mohammadi, S., Riazi, B., Karami, M., Kaboli, M., & Alesheikh, A. A. (2011). Effect of vegetation and soil conditions on burrow structure and site selection of rare desert rodent: Iranian jerboa (*Allactaga firouzi*). *Polish Journal of Ecology*, *59*, 403–411.

Naholowa'a, L. S. A. (2018). Reconnecting to precolonial Chamorro women in Guam. *Pacific Asia Inquiry*, *9*, 75–85.

Nogueira, R. A., Rozadilla, S., Agnolín, F. L., Marsà, J. A. G., Motta, M. J., & Novas, F. E. (2024). *A new Ornithopod from the Upper Cretaceous (Huincul Formation) of northwestern Patagonia* (105874). Implications On Elasmarian Postcranial Anatomy. Cretaceous Research.

Norman, D. B. (2004). Basal Iguanodontia. In D. B. Weishampel, P. Dodson, & H. Osmólska (Eds.), *The Dinosauria* (2nd ed., pp. 413–437). University of California Press.

Norman, D. B., Crompton, A. W., Butler, R. J., Porro, L. B., & Charig, A. J. (2011). The Lower Jurassic ornithischian dinosaur *Heterodontosaurus tucki* Crompton & Charig, 1962: Cranial anatomy, functional morphology, taxonomy, and relationships. *Zoological Journal of the Linnean Society*, *163*, 182–276.

Norman, D. B., Sues, H.-D., Witmer, L. M., & Coria, R. A. (2004). Basal Ornithopoda. In D. B. Weishampel, P. Dodson, & H. Osmólska (Eds.), *The Dinosauria* (2nd ed., pp. 393–412). University of California Press.

Norman, D. B., Witmer, L. M., & Weishampel, D. B. (2004). Basal Ornithischia. In D. B. Weishampel, P. Dodson, & H. Osmólska (Eds.), *The Dinosauria* (Second ed., pp. 325–334). University of California Press.

Novas, F., Agnolin, F., Rozadilla, S., Aranciaga-Rolando, A. M., Brisson-Egli, F., Motta, M. J., Cerroni, M., Ezcurra, M. D., Martinelli, A. G., & Álvarez-Herrera, G. (2019). Paleontological discoveries in the Chorrillo Formation (Upper Campanian-Lower Maastrichtian, Upper Cretaceous), Santa Cruz Province, Patagonia, Argentina. *Revista del Museo Argentino de Ciencias Naturales*, *21*, 217–293.

Novas, F. E., Cambiaso, A. V., & Ambrosio, A. (2004). A new basal iguanodontian (Dinosauria, Ornithischia) from the Upper Cretaceous of Patagonia. *Ameghiniana*, *41*, 75–82.

O'Gorman, E. J., & Hone, D. W. E. (2012). Body size distribution of the dinosaurs. *PLoS One*, *7*, e51925.

Organ, C. L. (2006). Biomechanics of ossified tendons in ornithopod dinosaurs. *Paleobiology*, *32*, 652–665.

Organ, C. L., & Adams, J. (2005). The histology of ossified tendon in dinosaurs. *Journal of Vertebrate Paleontology*, *25*, 602–613.

Owen, R. (1842). Report on British fossil reptiles. *Report of the British Association of Advanced Sciences*, *9*, 60–204.

Park, J.-Y., Lee, Y.-N., Currie, P. J., Ryan, M. J., Bell, P., Sissons, R., Koppelhus, E. B., Barsbold, R., Lee, S., & Kim, S.-H. (2021). A new ankylosaurid skeleton from the Upper Cretaceous Baruungoyot Formation of Mongolia: Its implications for ankylosaurid postcranial evolution. *Scientific Reports*, *11*, 4101.

Parks, W. A. (1925). *Thescelosaurus warreni*, a new species of orthopodous dinosaur from the Edmonton Formation of Alberta. *University of Toronto Studies, Geological Series*, *21*, 3–42.

Peinke, D., & Brown, C. (2005). Burrow utilization by springhares (*Pedetes capensis*) in the eastern cape, South Africa. *African Zoology*, *40*, 37–44.

Peng, G. (1992). Jurassic ornithopod *Agilisaurus louderbacki* (Ornithopoda: Fabrosauridae) from Zigong, Sichuan, China. *Vertebrata PalAsiatica*, *30*, 39–51.

Perez, C. (2021). *Fo'na mother of the Chamorro people*. Guampedia.

Perez, T. L. (2019). *CHAMORU LEGENDS: A gathering of stories*. University of Guam Press.

Platt, B. F., Kolb, D. J., Kunhardt, C. G., Milo, S. P., & New, L. G. (2016). Burrowing through the literature: The impact of soil-disturbing vertebrates on physical and chemical properties of soil. *Soil Science*, *181*, 175–191.

Ponomarenko, D. (2023). Fossil burrows from the Eopleistocene Paleoichnological Locality of Sopaty Kurgan. *Paleontological Journal*, *57*, 343–352.

Poole, K. (2023). Placing juvenile specimens in phylogenies: An ontogenetically sensitive phylogenetic assessment of a new genus of iguanodontian dinosaur from the Early Cretaceous Kirkwood Formation, South Africa. *The Anatomical Record*, *306*(7), 1939–1950.

Poole, K. E. (2015). *Phylogeny and biogeography of Iguanodontian dinosaurs, with implications from ontogeny and an examination of the function of the fused carpal-digit I complex*. The George Washington University.

Porro, L. B., Witmer, L. M., & Barrett, P. M. (2015). Digital preparation and osteology of the skull of *Lesothosaurus diagnosticus* (Ornithischia: Dinosauria). *PeerJ*, *3*, e1494.

Puttick, M. N., O'Reilly, J. E., Pisani, D., & Donoghue, P. C. (2019). Probabilistic methods outperform parsimony in the phylogenetic analysis of data simulated without a probabilistic model. *Palaeontology*, *62*, 1–17.

Radermacher, V. J., Fernandez, V., Schachner, E. R., Butler, R. J., Bordy, E. M., Naylor Hudgins, M., de Klerk, W. J., Chapelle, K. E., & Choiniere, J. N. (2021). A new *Heterodontosaurus* specimen elucidates the unique ventilatory macroevolution of ornithischian dinosaurs. *eLife*, *10*, e66036.

Rambaut, A., Drummond, A. J., Xie, D., Baele, G., & Suchard, M. A. (2018). Posterior summarization in Bayesian phylogenetics using tracer 1.7. *Systematic Biology*, *67*, 901–904.

Rich, T. H., Galton, P. M., & Vickers-Rich, P. (2010). The holotype individual of the ornithopod dinosaur *Leaellynasaura amicagraphica* Rich & Rich, 1989 (Late Early Cretaceous, Victoria, Australia). *Alcheringa*, *34*, 385–396.

Roberts, E. M., Rogers, R. R., & Foreman, B. Z. (2007). Continental insect borings in dinosaur bone: Examples from the Late Cretaceous of Madagascar and Utah. *Journal of Paleontology Memoir*, *81*, 201–208.

Rose, K. D., & Emry, R. J. (1983). Extraordinary fossorial adaptations in the Oligocene palaeanodonts *Epoicotherium* and *Xenocranium* (Mammalia). *Journal of Morphology*, *175*, 33–56.

Rotatori, F. M., Moreno-Azanza, M., & Mateus, O. (2020). New information on ornithopod dinosaurs from the Late Jurassic of Portugal. *Acta Palaeontologica Polonica*, *65*, 35–57.

Rozadilla, S., Agnolín, F. L., & Novas, F. E. (2019). Osteology of the Patagonian ornithopod *Talenkauen santacrucensis* (Dinosauria, Ornithischia). *Journal of Systematic Palaeontology*, *17*, 2043–2089.

Rozadilla, S., Agnolin, F. L., Novas, F. E., Rolando, A. M. A., Motta, M. J., Lirio, J. M., & Isasi, M. P. (2016). A new ornithopod (Dinosauria, Ornithischia) from the Upper Cretaceous of Antarctica and its palaeobiogeographical implications. *Cretaceous Research*, *57*, 311–324.

Ruiz-Omeñaca, J. I., Canudo, J. I., Cuenca-Bescós, G., Cruzado-Caballero, P., Gasca, J. M., & Moreno-Azanza, M. (2012). A new basal ornithopod dinosaur from the Barremian of Galve, Spain. *Comptes Rendus Palevol*, *11*, 435–444.

Salgado, L., Canudo, J. I., Garrido, A. C., Moreno-Azanza, M., Martínez, L. C., Coria, R. A., & Gasca, J. M. (2017). A new primitive Neornithischian dinosaur from the Jurassic of Patagonia with gut contents. *Scientific Reports*, *7*, 1–10.

Salgado, L., Coria, R. A., & Heredia, S. E. (1997). New materials of *Gasparinisaura cincosaltensis* (Ornithischia, Ornithopoda) from the Upper Cretaceous of Argentina. *Journal of Paleontology Memoir*, *71*, 933–940.

Samathi, A., Chanthasit, P., & Sander, P. M. (2019). Two new basal coelurosaurian theropod dinosaurs from the Lower Cretaceous Sao Khua Formation of Thailand. *Acta Palaeontologica Polonica*, *64*, 239–260.

Santa Luca, A. P. (1980). The postcranial skeleton of *Heterodontosaurus tucki* from the Stormberg of South Africa. *Annals of the South African Museum*, *79*, 159–211.

Scheetz, R. D. (1999). *Osteology of Orodromeus makelai and the phylogeny of basal ornithopod dinosaurs*. Citeseer.

Schrago, C. G., Aguiar, B. O., & Mello, B. (2018). Comparative evaluation of maximum parsimony and Bayesian phylogenetic reconstruction using empirical morphological data. *Journal of Evolutionary Biology*, *31*, 1477–1484.

Seeley, H. G. (1887). On the classification of the fossil animals commonly named Dinosauria. *Proceedings of the Royal Society of London*, *43*, 165–171.

Senter, P. (2007). Analysis of forelimb function in basal ceratopsians. *Journal of Zoology*, *273*, 305–314.

Senter, P. J. (2023). Restudy of shoulder motion in the theropod dinosaur *Mononykus olecranus* (Alvarezsauridae). *PeerJ*, *11*, e16605.

Senter, P. J., & Mackey, J. J. (2023). Forelimb motion and orientation in the ornithischian dinosaurs *Styracosaurus* and *Thescelosaurus*, and its implications for locomotion and other behavior. *Palaeontologia Electronica*, *26*, 1–19.

Sereno, P. C. (1991). *Lesothosaurus*, "fabrosaurids," and the early evolution of Ornithischia. *Journal of Vertebrate Paleontology*, *11*, 168–197.

Sereno, P. C. (1997). The origin and evolution of dinosaurs. *Annual Reviews of Earth and Planetary Sciences*, *25*, 435–489.

Sereno, P. C. (2012). Taxonomy, morphology, masticatory function and phylogeny of heterodontosaurid dinosaurs. *ZooKeys*, *226*, 1–225.

Sereno, P. C., & Chao, S. (1988). *Psittacosaurus xinjiangensis* (Ornithischia: Ceratopsia), a new psittacosaur from the Lower Cretaceous of northwestern China. *Journal of Vertebrate Paleontology*, *8*, 353–365.

Sereno, P. C., & Zhimin, D. (1992). The skull of the basal stegosaur *Huayangosaurus taibaii* and a cladistic diagnosis of Stegosauria. *Journal of Vertebrate Paleontology*, *12*, 318–343.

Sertich, J. J. W., & Groenke, J. R. (2010). Appendicular skeleton of *Simosuchus clarki* (Crocodyliformes: Notosuchia) from the Late Cretaceous of Madagascar. *Journal of Vertebrate Paleontology*, *30*, 122–153.

Sharp, A. C., Siu, K., & Rich, T. (2017). Revealing the skeleton of the polar dinosaur *Leaellynasaura amicagraphica* using synchrotron computed tomography. In: Society of Vertebrate Paleontology 77th Annual Meeting, Meeting Program and Abstracts.

Siciliano-Martina, L., Guerra, D. A., & Veech, J. A. (2023). Forelimb morphology as an adaptation for burrowing in kangaroo rat species (genus *Dipodomys*) that inhabit different soil substrates. *Journal of Mammalogy*, *104*, 1377–1389.

Simões, T. R., Caldwell, M. W., Palci, A., & Nydam, R. L. (2017). Giant taxon-character matrices: Quality of character constructions remains critical regardless of size. *Cladistics*, *33*, 198–219.

Simpson, E. L., Hilbert-Wolf, H. L., Wizevich, M. C., Tindall, S. E., Fasinski, B. R., Storm, L. P., & Needle, M. D. (2010). Predatory digging behavior by dinosaurs. *Geology*, *38*, 699–702.

Smith, R. M. (1987). Helical burrow casts of therapsid origin from the Beaufort group (Permian) of South Africa. *Palaeogeography, Palaeoclimatology, Palaeoecology*, *60*, 155–169.

Smith, R. M., Angielczyk, K. D., Benoit, J., & Fernandez, V. (2021). Neonate aggregation in the Permian dicynodont *Diictodon* (Therapsida, Anomodontia): Evidence for a reproductive function for burrows? *Palaeogeography, Palaeoclimatology, Palaeoecology*, *569*, 110311.

Sobral, G., Hipsley, C. A., & Müller, J. (2012). Braincase redescription of *Dysalotosaurus lettowvorbecki* (Dinosauria, Ornithopoda) based on computed tomography. *Journal of Vertebrate Paleontology*, *32*, 1090–1102.

Sternberg, C. (1937). A classification of *Thescelosaurus*, with a description of a new species. *Proceedings of the Geological Society of America*, *1936*, 375.

Sternberg, C. M. (1940). *Thescelosaurus edmontonensis*, n. sp., and classification of the Hypsilophodontidae. *Journal of Paleontology Memoir*, *14*, 481–494.

Suarez, C. A., González, L. A., Ludvigson, G. A., Cifelli, R. L., & Tremain, E. (2012). Water utilization of the Cretaceous Mussentuchit Member local vertebrate fauna, Cedar Mountain Formation, Utah, USA: Using oxygen isotopic composition of phosphate. *Palaeogeography, Palaeoclimatology, Palaeoecology*, *313*, 78–92.

Sues, H.-D. (1980). Anatomy and relationships of a new hypsilophodontid dinosaur from the Lower Cretaceous of North America. *Palaeontographica Abt A*, *169*, 51–72.

Sues, H.-D., Evans, D. C., Galton, P. M., & Brown, C. M. (2023). Anatomy of the neornithischian dinosaur *Parksosaurus warreni* (Parks, 1926) from the Upper Cretaceous (Lower Maastrichtian) Horseshoe Canyon Formation of Alberta, Canada. *Cretaceous Research*, *141*, 105369.

Thomas, D. A. (2015). The cranial anatomy of *Tenontosaurus tilletti* Ostrom, 1970 (Dinosauria, Ornithopoda). *Palaeontologia Electronica*, *18*, 1–99.

Trayler, R. B., Schmitz, M. D., Cuitiño, J. I., Kohn, M. J., Bargo, M. S., Kay, R. F., Strömberg, C. A., & Vizcaíno, S. F. (2020). An improved approach to age-modeling in deep time: Implications for the Santa Cruz Formation, Argentina. *GSA Bulletin*, *132*, 233–244.

Tucker, R. T., Crowley, J. L., Mohr, M. T., Renaut, R. K., Makovicky, P. J., & Zanno, L. E. (2023). Exceptional age constraint on a fossiliferous sedimentary succession preceding the Cretaceous thermal maximum. *Geology*, *51*, 962–967.

Tucker, R. T., King, M. R., Mohr, M. T., Renaut, R. K., Fekete, J. W., Makovicky, P. J., & Zanno, L. E. (Accepted). Tectonosedimentation history of the Upper Cedar Mountain Formation, Central Utah, USA. Sedimentology (SED-2023-104).

Tucker, R. T., Suarez, C. A., Makovicky, P. J., & Zanno, L. E. (2022). Paralic sedimentology of the Mussentuchit Member coastal plain, Cedar Mountain Formation, central Utah, USA. *Journal of Sedimentary Research*, *92*, 546–569.

VanBuren, C. S., & Evans, D. C. (2017). Evolution and function of anterior cervical vertebral fusion in tetrapods. *Biological Reviews*, *92*, 608–626.

Varricchio, D. D., Martin, A. J., & Katsura, Y. (2007). First trace and body fossil evidence of a burrowing, denning dinosaur. *Proceedings of the Royal Society B*, *274*, 1–7.

Vernygora, O. V., Simões, T. R., & Campbell, E. O. (2020). Evaluating the performance of probabilistic algorithms for phylogenetic analysis of big morphological datasets: A simulation study. *Systematic Biology*, *69*, 1088–1105.

Voorhies, M. (1975a). A new genus and species of fossil kangaroo rat and its burrow. *Journal of Mammalogy*, *56*, 160–176.

Voorhies, M. R. (1975b). Vertebrate burrows. In *The study of trace fossils* (pp. 325–350). Springer.

Weaver, L. N., Varricchio, D. J., Sargis, E. J., Chen, M., Freimuth, W. J., & Mantilla, G. P. W. (2020). Early mammalian social behaviour revealed by multituberculates from a dinosaur nesting site. *Nature Ecology & Evolution*, *5*, 1–6.

Weishampel, D. B. (2004). Ornithischia. In D. B. Weishampel, P. Dodson, & H. Osmólska (Eds.), *The Dinosauria* (2nd ed., pp. 323–324). University of California Press.

Weishampel, D. B., Jianu, C. M., Csiki, Z., & Norman, D. B. (2003). Osteology and phylogeny of *Zalmoxes* (ng), an unusual euornithopod dinosaur from the latest Cretaceous of Romania. *Journal of Systematic Palaeontology*, *1*, 65–123.

Whitaker, R. (1982). Status of Asian crocodilians. In: Crocodiles: Proceedings of the 5th working meeting of the crocodile specialist Group of the Species Survival Commission of the International Union for Conservation of nature and natural resources convened at the Florida state museum, Gainesville, Florida, USA, 12 to 16 August 1980: IUCN. p. 237.

Wiens, J. J., & Morrill, M. C. (2011). Missing data in phylogenetic analysis: Reconciling results from simulations and empirical data. *Systematic Biology*, *60*, 719–731.

Woodruff, D. C., & Varricchio, D. J. (2011). Experimental modeling of a possible *Oryctodromeus cubicularis* (Dinosauria) burrow. *PALAIOS*, *26*, 140–151.

Xu, X., Makovicky, P. J., Wang, X.-l., Norell, M. A., & You, H.-l. (2002). A ceratopsian dinosaur from China and the early evolution of Ceratopsia. *Nature*, *416*, 314–317.

Yang, J.-S., Yi, J., Dong, L.-Y., Liu, J., & PalAsiatica, V. (2018). Tetrapod burrows from the Triassic Ermaying Formation of shaanxi, China. *Vertebrata PalAsiatica*, *56*, 147–156.

Yang, Y., Wu, W., Dieudonné, P.-E., & Godefroit, P. (2020). A new basal ornithopod dinosaur from the Lower Cretaceous of China. *PeerJ*, *8*, e9832.

Zan, S., Chen, J., Jin, L., & Li, T. (2005). A primitive ornithopod from the Early Cretaceous Quantou Formation of central Jilin, China. *Vertebrata pal Asiatica*, *43*, 182–193.

Zanno, L. E., Avrahami, H. M., Gates, T., Tucker, R. T., & Mackovicky, P. J. (2019). Preliminary Data On Elongatoolithid Clutches And Associated Fauna From The Cenomanian Mussentuchit Member, Cedar Mountain Formation Of Utah. VII International Symposium on Dinosaur Eggs and Babies, Shiyan, China.

Zanno, L. E., Gates, A. E., Avrahami, H. M., Tucker, R. T., & Makovicky, P. (2023). An early-diverging iguanodontian (Dinosauria: Rhabdodontomorpha) from the Late Cretaceous of North America. *PLoS One*, *18*, e0286042.

Zanno, L. E., & Makovicky, P. J. (2013). Neovenatorid theropods are apex predators in the Late Cretaceous of North America. *Nature Communications*, *4*, 2827.

Zanno, L. E., Tucker, R. T., Canoville, A., Avrahami, H. M., Gates, T. A., & Makovicky, P. J. (2019). Diminutive fleet-footed tyrannosauroid narrows the 70-million-year gap in the North American fossil record. *Communications Biology*, *2*, 64.

Zanno, L. E., Tucker, R. T., Suarez, C., Avrahami, H. M., Herzog, L., Hedge, J., Gates, T. A., Suarez, M., Lund, E. K., Freimuth, W. J., Beguesse, K., King, M. R., Cifelli, R. L., & Makovicky, P. J. (2023). Paleobiodiversity of the Mussentuchit Member, Cedar Mountain Formation (Utah): New discoveries enhance and contextualize an exceptional window into Mid-Cretaceous terrestrial ecosystems. 14th Conference on Mesozoic Terrestrial Ecosystems. The Anatomical Record.

Zheng, W., Jin, X., Shibata, M., Azuma, Y., & Yu, F. (2012). A new ornithischian dinosaur from the Cretaceous Liangtoutang Formation of Tiantai, Zhejiang Province, China. *Cretaceous Research*, *34*, 208–219.

Zheng, X.-T., You, H.-L., Xu, X., & Dong, Z.-M. (2009). An Early Cretaceous heterodontosaurid dinosaur with filamentous integumentary structures. *Nature*, *458*, 323–336.

SUPPORTING INFORMATION

Additional supporting information can be found online in the Supporting Information section at the end of this article.

How to cite this article: Avrahami, H. M., Makovicky, P. J., Tucker, R. T., & Zanno, L. E. (2024). A new semi-fossorial thescelosaurine dinosaur from the Cenomanian-age Mussentuchit Member of the Cedar Mountain Formation, Utah. *The Anatomical Record*, *307*(12), 3717–3781. https://doi.org/10.1002/ar.25505